UNIVERSITY OF CALIFORNIA, SAN DIEGO

Defining the Relationship Between Kinetochore Structure and Spindle Checkpoint Signaling

A dissertation submitted in partial satisfaction of the

requirements for the degree Doctor of Philosophy

in

Biomedical Sciences

by

Anthony W. Essex

Committee in charge:

Professor Arshad Desai, Chair
Professor Don Cleveland
Professor Andy Dillin
Professor Steve Dowdy
Professor Karen Oegema

2009

The dissertation of Anthony W. Essex is approved, and it is acceptable in quality and form for publication of microfilm and electronically:

_____

_____

_____

_____

_____

Chair

University of California, San Diego

2009

Table of Contents

List of Figures

List of Tables

Acknowledgements

I would first like to thank my beautiful wife Laura, who has encouraged and supported me through every step of graduate school. Arshad and Karen have been outstanding mentors who have provided me with excellent guidance and I thank them wholeheartedly for everything, including their patience and encouragement. The rest of my thesis committee (Don, Steve and Andy) have also been terrific, having provided needed guidance and expert advice along the way. I would also like to thank my family and friends, including Betty, for reminding me that every day should include fun of some kind.

Chapter 2, in full, was published under the following citation: *Mol. Biol. Cell*, 2009(4):1252-67, Essex A, Dammermann A, Lewellyn L, Oegema K, and Desai A. The dissertation author was the primary researcher and author of this paper.

Chaper 3, in full, was published under the following citation: *Genes Dev*., 2008 Sep. 1;22(17):2385-99, Gassmann R, Essex A, Hu JS, Maddox PS, Motegi F, Sugimoto A, O'Rourke SM, Bowerman B, McLeod I, Yates JR 3rd, Oegema K, Cheeseman IM, and Desai A. The dissertation author was co-second author of this paper and created figure 4, including performing the experiments and data analysis.

Vita

1999 BS, Biomedical Technologies, University of Vermont

2009 PhD, Biomedical Sciences, University of California, San Diego

Publications

Essex A, Dammermann A, Lewellyn L, Oegema K, Desai A. *Systematic analysis in C. elegans reveals that the spindle checkpoint is comprised of two largely independent branches.* Mol Biol Cell. 2009 Feb;20(4): 1252-67.

Yamamoto TG, Watanabe S, **Essex A**, Kitagawa R. *SPDL-1 functions as a kinetochore receptor for MDF-1 in Caenorhabditis elegans*. J Cell Biol. 2008 Oct 20:183(2):187-94.

Gassman R, **Essex A***, Hu JS*, Maddox PS, Motegi F, Sugimoto A, O'Rourke SM, Bowerman B, McLeod I, Yates JR 3rd, Oegema K, Cheeseman IM, Desai A. *A new mechanism controlling kinetochore-microtubule interactions revealed by comparison of two dynein-targeting components: SPDL-1 and the Rod/Zwilch/Zw10 complex.* Genes Dev. 2008 Sep 1;22(17):2385-99. * *Denotes equal contribution by these authors*

Liu GY, **Essex A**, Buchanan JT, Datta V, Hoffman HM, Bastian JF, Fierer J, Nizet V. *Staphylococcus aureus golden pigment impairs neutrophil killing and promotes virulence through its antioxidant activity.* J Exp Med. 2005 Jul 18;202(2):209-15.

Ma JN, Currier EA, **Essex A**, Feddock M, Spalding TA, Nash NR, Brann MR, Burstein ES. *Discovery of novel peptide/receptor interactions: identification of*

PHM-27 as a potent agonist of the human calcitonin receptor. Biochem Pharmacol. 2004 Apr 1;67(7):1279-84.

Weissman JT, Ma JN, **Essex A**, Gao Y, Burstein ES. *G-protein-coupled receptor-mediated activation of rap GTPases: characterization of a novel Galphai regulated pathway.* Oncogene. 2004 Jan 8;23(1):241-9.

Ford DJ, **Essex A**, Spalding TA, Burstein ES, Ellis J. *Homologous mutations near the junction of the sixth transmembrane domain and the third extracellular loop lead to constitutive activity and enhanced agonist affinity at all muscarinic receptor subtypes.* J Pharmacol Exp Ther. 2002 Mar;300(3):810-7.

ABSTRACT OF THE DISSERTATION

Defining the Relationship Between Kinetochore Structure and Spindle Checkpoint Signaling

by

Anthony W. Essex

Doctor of Philosophy in Biomedical Sciences

University of California, San Diego, 2009

Professor Arshad Desai, Chair

In this dissertation, I use the early embryo of the nematode *Caenorhabditis elegans* to probe the relationships between kinetochore formation and spindle checkpoint signaling. The spindle checkpoint is a conserved signaling pathway that delays cell cycle progression in mitosis until all chromosomes have properly attached to microtubules emanating from opposing spindle poles. To trigger checkpoint activation, I undertook a strategy

of inhibiting centriole duplication, using RNAi specific for components of the centriole duplication machinery. Such depletions result in bipolar spindles in the first mitotic division (serving as useful internal controls), while leading to monopolar spindle formation in the second and third divisions. Monopolar spindles are known to trigger checkpoint activation, as kinetochores lack both full attachment and tension. By performing live imaging video microscopy on these embryos, I was able to quantitatively assess checkpoint status by timing cell cycle progression. I found that cells with monopolar spindles exhibited cell cycle delays that were dependent on each of the conserved checkpoint proteins in *C. elegans.* Kinetochores are proteinaceus organelles that connect DNA to microtubules, and are essential for chromosome segregation in mitosis. Using the timing assay described above, I set out to comprehensively determine the contribution of kinetochore proteins for checkpoint signaling, and found that these proteins could be placed into one of three categories based on their phenotypes in the timing assay; required for checkpoint signaling, not required, or those that trigger checkpoint activation when depleted. Checkpoint activation is correlated with enrichment of specific components of the pathway on unattached kinetochores. To correlate checkpoint protein recruitment with the functional analysis of checkpoint signaling, I generated worm strains stably expressing fluorescently tagged checkpoint proteins Mad2^{MDF-2}, Mad3^{SAN-1}, and BUB-3, and systematically determined the requirements for their localization and enrichment at

kinetochores. I also used these assays to characterize the roles of the recently discovered kinetochore protein SPDL-1 in checkpoint activation and signaling. Taken together, my results indicate that checkpoint activation is coordinately directed by three key kinetochore components – the NDC-80 complex, the Rod/Zwilch/Zw10 complex, and BUB-1 – that are targeted independently of one another by the outer kinetochore scaffold protein KNL-1. Surprisingly, I found that Mad3^{SAN-1}, unlike other checkpoint proteins, does not enrich at unattached kinetochores, and that subtly elevating Mad2^{MDF-2} levels bypasses the requirement for BUB-3 and Mad3^{SAN-1} in kinetochore-dependent checkpoint activation. I propose that a core kinetochore-generated Mad1^{MDF-1}/ Mad2^{MDF-2} signal is integrated with a largely independent cytoplasmic Mad3^{SAN-1}/BUB-3-based signal to coordinately regulate checkpoint activation, possibly in response to different checkpoint-activating states. I discuss the rationale for the partitioning of the checkpoint signaling pathway into two branches, and the newly elucidated relationships between kinetochore assembly and checkpoint signaling.

Chapter 1: Introduction

1.1 Chromosome Segregation in Mitosis

Mitosis is the process of cell division, the ultimate goal of which is the generation of two new (daughter) cells with genetic complements identical to the parental cell. The physical segregation of duplicated parental DNA is mediated by the mitotic spindle, a dynamic array of microtubules and motor proteins. Microtubules, 25-nm diameter polymers of α/β-tubulin dimers, are anchored by two microtubule organizing centers (centrosomes, a.k.a. spindle poles), and attach to chromosomes to facilitate their segregation. Connecting DNA to microtubules are kinetochores, proteinaceus organelles essential for chromosome segregation (Cheeseman and Desai, 2008). The first accurate depictions of mitosis came from the work of Walther Flemming in 1882 [reprinted in (Flemming, 1965)]. Since that time, mitosis has traditionally been sub-divided into several phases based on cellular morphology. Having duplicated the genome in S-phase, mitosis begins in prophase, in which the chromosomes (as sister chromatids) begin to condense and become highly compacted. In prometaphase, the nuclear envelope disassembles and microtubule organization at centrosomes increases as a recognizable spindle shaped array of microtubules forms. Microtubules begin to attach to DNA via kinetochores, and chromosomes start oscillate back and forth along the spindle axis as they attach first to microtubules emanating from one spindle

pole, then the other. In metaphase, all of the sister chromatid pairs have attached to microtubules originating from opposing spindle poles, a state known as biorientation. As chromosomes become bioriented, they congress to form a metaphase plate in the middle of the mitotic spindle, with their long axes perpendicular to the plane of cell division. In anaphase, the sister chromatids separate towards opposite spindle poles. In telophase, the chromatids decondense, the nuclear envelope reforms, and a cortical actomyosin ring cleaves the one parental cell in half, resulting in two daughter cells (Cheeseman and Desai, 2008).

1.2 The Kinetochore

Kinetochores are dynamic organelles, containing over 80 individual protein components identified to date in vertebrates. (Cheeseman and Desai, 2008). Studies using electron microsocopy reveal kinetochores as trilaminar structures, consisting of an inner plate forming the chromatin interface, a middle (or linker) layer, and an outer layer that forms the microtubule interface (Brinkley and Stubblefield, 1966; Dong et al., 2007; McEwen et al., 2007). Kinetochore proteins perform a diverse array of tasks, from building a foundation on centromeric chromatin, to forming load-bearing connections with microtubules, as well as monitoring the status of those attachments. Key proteins implicated in each of these processes will be outlined in the following sections, starting from their localization to the inner plate and moving outward.

1.3 The Centromere

Centromeres are specialized regions of chromatin which form the foundation of kinetochore assembly. Morphologically, they are defined as the primary constriction point on metaphase chromosomes. Chromosomes consist of DNA wrapped tightly around a core octamer of histones, forming the nucleosome. The nucleosome in turn is comprised of 2 copies each of Histone-H2A, Histone-H2B, Histone-H3, and Histone-H4. A distinctive feature of centromeres is the presence of a specialized histone variant CENP-A in place of Histone-H3 (Blower et al., 2002; Palmer et al., 1991; Sullivan et al., 1994). The presence of CENP-A itself is absolutely necessary for kinetochore formation in every system examined to date; without it, kinetochores fail to form, and the resulting absence of chromosome segregation leads to aneuploidy and cell death (Collins et al., 2005; Howman et al., 2000; Kalitsis et al., 1998; Meluh et al., 1998; Oegema et al., 2001; Sullivan et al., 2001; Takahashi et al., 2000). How the centromere is specified, and by extension how CENP-A is targeted to centromeres remain open areas of investigation. In all organisms apart from budding yeast, which possess a sequence-specific 125 base pair region required for $Cse4^{CENP-A}$ loading (Tanaka et al., 1999) the centromere is not defined by a specific nucleotide sequence. A conserved feature of the centromere in vertebrates include repetitive AT rich regions of α-satellite DNA. However, α-satellite DNA is neither necessary nor sufficient for centromere formation (Amor and Choo, 2002). The prevailing theory in the

field is that centromeres are specified not by sequence-specific, but rather by epigenetic mechanisms, and CENP-A itself has been postulated to act as this epigenetic mark (Cleveland et al., 2003). Recently, two proteins required for CENP-A loading at centromeres have been identified. These proteins, KNL-2 and Mis18, have been shown to localize transiently to centromeres from telophase throught G1, coincident with the timing of new CENP-A deposition. Furthermore, depletions of either of these proteins cause CENP-A mislocalization in *C. elegans* and in human cells. KNL-2 contains a myb domain, a common feature of DNA-binding proteins and chromatin remodeling complexes (Fujita et al., 2007; Hayashi et al., 2004; Maddox et al., 2007). However, a direct interaction of either protein with CENP-A has yet to be shown, leaving the mechanism by which they affect CENP-A loading open to speculation.

1.4 Kinetochore Microtubule Binding

The core microtubule binding site of the kinetochore is likely composed of a multiprotein complex called the KMN network (KNL-1, Mis12 complex, Ndc80 complex)(Cheeseman et al., 2006). The Ndc80 complex is conserved throughout eukaryotes, and is essential for kinetochore-microtubule interactions (Cheeseman and Desai, 2008). The Ndc80 complex contains four proteins and forms a rod-like structure with globular heads of the proteins Spc24 and Spc25 at one end (facing the centromere), and the heads of Ndc80 and Nuf2 proteins oriented outward (away from the centromere) (Ciferri et al.,

2005; Wan et al., 2009; Wei et al., 2005). Both the Ndc80 complex and the protein KNL-1 exhibit weak microtubule binding activity; while the Mis12 complex alone does not bind microtubules, it increases the microtubule binding affinity of KNL-1, and a synergistic increase in microtubule binding activity was observed in the presence of all three members of the KMN network *in vitro* (Cheeseman et al., 2006). The crystal structure of the globular region of the Ndc80 subunit revealed a calponin homology (CH) domain fold, which resembles the microtubule binding domain of the microtubule plus-end binding protein EB1 (Wei et al., 2007). The N-terminal amino acid tail of Ndc80 also makes a positive contribution to microtubule binding (Wei et al., 2007), and contains a region important for phosphoregulation by the Aurora B kinase (Cheeseman et al., 2006). The functional significance of these domains for microtubule binding has been demonstrated *in vivo* (Guimaraes et al., 2008; Miller et al., 2008), and *in vitro* work has shown that the Ndc80 complex can form load bearing attachments to dynamic microtubules (McIntosh et al., 2008; Powers et al., 2009). Crystallization of Ndc80 with Nuf2 revealed an additional CH domain present on Nuf2, leading to the proposal of a “two-headed” model postulating that the conserved faces of the Ndc80 and Nuf2 CH domains bind microtubules by docking onto adjacent tubulin-tubulin interfaces (Ciferri et al., 2008). However, combining crystal structure data with cryo-EM data led to an alternate model in which the globular domain of the Ndc80 subunit binds strongly at the interface between tubulin dimers and weakly at the adjacent

interdimer interface of microtubules, along the protofilament axis (Wilson-Kubalek et al., 2008).

While the KMN network is of central importance, a number of other proteins including CLIP-170, dynein, CENP-E, CENP-F and the Ska1 complex may work in parallel or synergistically with the KMN network to bind microtubules. CLIP-170 is a microtubule plus-end tracking protein, and in its absence, chromosomes cannot align properly resulting from lack of robust chromosome-microtubule interactions (Dujardin et al., 1998; Tanenbaum et al., 2006). Disruption of the minus end-directed motor protein dynein or its activator complex dynactin causes defects in the stability of kinetochore-microtubule interactions, as well as defective chromosome alignment and segregation (Howell et al., 2001; Yang et al., 2007). Kinetochores in cells depleted of CENP-E, a kinesin-7 family member, exhibit fewer bound microtubules than controls (McEwen et al., 2001; Putkey et al., 2002). CENP-F has two microtubule binding domains, and may contribute to the stability of kinetochore-microtubule interactions (Bomont et al., 2005; Feng et al., 2006; Holt et al., 2005). Finally, the Ska1 complex has recently been shown to be important for robust binding of kinetochores to microtubules (Gaitanos et al., 2009; Hanisch et al., 2006; Wan et al., 2009; Welburn et al., 2009).

1.5 Chromosome Segregation and the Spindle Checkpoint

Two key events mark the transition from metaphase to anaphase: inactivation of the master mitotic kinase Cdk1 via the destruction of cyclin B,

and the cleavage of cohesin holding sister chromatids together (Peters, 2002).The timing of these events is carefully coordinated to ensure that it begins only after all chromatids are properly bioriented on the mitotic spindle. Should either occur prior to biorientation, aneuploidy may result (cells with an abnormal number of chromosomes), which may promote tumorigenesis or apoptosis (Rajagopalan and Lengauer, 2004). To prevent this, kinetochores serve as platforms for a conserved signaling pathway called the spindle checkpoint (or mitotic checkpoint) which functions from prometaphase until metaphase to monitor kinetochore-microtubule attachments and inhibit mitotic progression until all chromosomes have bioriented (Musacchio and Salmon, 2007). The checkpoint negatively regulates the anaphase promoting complex/cyclosome (APC/C), an E3 ubiquitin ligase, from inducing the destruction of securin and cyclin B. Securin binds separase, keeping it inactive; following securin degradation separase cleaves the cohesin holding sister chromatids together. The checkpoint sequesters or inhibits Cdc20 (Hwang et al., 1998; Kim et al., 1998), which is essential for APC/C activation and substrate recognition (Yu, 2007). Thus, by temporally restricting APC/C activation, the checkpoint ensures accurate chromosome segregation in every cell division.

1.6 Checkpoint Proteins and Kinetochores

The first insights into the molecular components of the checkpoint arose from budding yeast screens for mutants unable to arrest in mitosis in the

presence of spindle poisons. These screens identified mutations in the canonical checkpoint proteins Mad1 (*m*itotic *a*rrest *d*eficient), Mad2 and Mad3 (BubR1 in vertebrates, which contains a kinase domain absent in fungi or nematodes), as well Bub1 and Bub3 (*b*udding *u*ninhibited by *b*enzimidazole) (Hoyt et al., 1991; Li and Murray, 1991). Other "core" checkpoint constituents include Mps1 (Weiss and Winey, 1996), CENP-E (Abrieu et al., 2000), and RZZ (*R*od, *Z*wilch and *Z*w10), which copurify as a complex and are interdependent for their kinetochore localization. (Buffin et al., 2005; Karess, 2005; Kops et al., 2005; Williams et al., 2003). Several early lines of evidence converged to implicate the kinetochore as the source of a cell cycle checkpoint. First, was the observation that the timing of anaphase onset was tightly linked to the timing of biorientation of the last chromatid pair (Rieder et al., 1994). Additionally, the presence of a single unattached chromosome was sufficient to delay anaphase entry (Rieder et al., 1995). The fact that checkpoint proteins were observed to concentrate at kinetochores beginning in prometaphase and were depleted following chromosome biorientation lent more credence to the hypothesis (Chen et al., 1998; Chen et al., 1996; Li and Benezra, 1996; Taylor et al., 1998; Taylor and McKeon, 1997). This enrichment is now generally accepted as reflecting the local kinetochore-catalyzed reaction that generates the inhibitor of the APC/C (Musacchio and Salmon, 2007). It has recently been directly demonstrated that the presence of

unattached kinetochores accelerates the production of the “wait-anaphase” signal (Kulukian et al., 2009).

At the molecular level, how the status of kinetochore-microtubule interactions are translated to generate inhibitors of Cdc20 and APC/C activation is an open area of investigation. One leading candidate such an inhibitor is Mad2, which requires Mad1 for kinetochore targeting (Chen et al., 1998). *In vitro*, Mad2 directly inhibits the ubiquitin ligase activity of purified APC/C (Fang et al., 1998; Li et al., 1997). *In vivo*, Mad2 exists in two roughly equal size populations, one which is stably kinetochore bound to Mad1 and one which is turning over rapidly at unattached kinetochores (Howell et al., 2000; Shah et al., 2004). Structural and *in vitro* experiments reveal that when bound to either Mad1 or Cdc20, Mad2 adopts a conformation called closed-Mad2 (or Mad2-C) while unbound cytosolic Mad2 is called open-Mad2 (or Mad2-O). Mad2-O interacts with Mad2-C on the kinetochore Mad1-Mad2-C heterodimer, inducing a conformational change from Mad2-O to Mad2-C. Mad2-C then either dissociates from Mad1 to form a transient dimeric intermediate that then binds (and inhibits) Cdc20, or alternatively is directly passed on to Cdc20 from Mad1. An alternative model proposes that the Mad1-Mad2-C/Mad2-O interaction merely primes Mad2-O, and it converts to Mad2-C only after interacting with Cdc20 in the cytosol. Mad2-C-Cdc20 then acts as an amplifier of the checkpoint independently of kinetochores, catalyzing the conversion of more cytosolic Mad2-O to Mad2-C-Cdc20 (De Antoni et al.,

2005; Luo et al., 2002; Luo et al., 2004; Mapelli et al., 2007; Simonetta et al., 2009; Sironi et al., 2002; Vink et al., 2006; Yang et al., 2008). An attractive element of this last model is that it provides a potential explanation for how a single unattached kinetochore in a cell can inhibit progression into anaphase. However, Mad2 is unlikely to be the sole inhibitor of Cdc20 and the APC/C. BubR1 also binds Cdc20 and inhibits APC/C activity *in vitro* and appears to do so synergistically with Mad2, independently of its kinase activity. (Fang, 2002; Tang et al., 2001). In human cells, phosphorylation of Cdc20 by Bub1 inhibits APC/C activity *in vitro* (Tang et al., 2004a). Adding another layer of complexity to the story is the presence of a *M*itotic *C*heckpoint *C*omplex (MCC) containing BubR1 (Mad3 in yeast and nematodes), Bub3, Mad2 and Cdc20 (Fraschini et al., 2001; Hardwick et al., 2000; Sudakin et al., 2001). *In vitro*, MCC isolated from human cells displays ~3000-fold higher inhibitory activity towards APC/C compared to recombinant Mad2 alone but (surprisingly) is detectable in interphase, although it appears active only on APC/C isolated from mitotic cells (Sudakin et al., 2001). Furthermore, MCC can be isolated from budding yeast strains containing mutant Ndc10, a protein necessary for kinetochore formation and therefore checkpoint activation (Fraschini et al., 2001). This indicates that MCC may exist throughout the cell cycle and independently of checkpoint activation, which begs the question of how unattached kinetochores contribute to its formation or modulate its activity. The regulation of APC/C activity is complex and likely involves multiple mechanisms; in

budding yeast, conserved KEN-box motifs (commonly found in APC/C substrates) in Mad3 are required for Mad3-Cdc20 binding and thus Mad3 competes with APC/C substrates, acting as a “pseudosubstrate” inhibitor of the APC/C (Burton and Solomon, 2007; King et al., 2007b). Another paper reached a similar conclusion regarding the vertebrate orthologue of Mad3 (BubR1), although their data imply that the APC/C inhibition occurs during interphase, not mitosis (Malureanu et al., 2009). Regulation of Cdc20 also goes beyond simply binding to the MCC and APC/C, as Cdc20 itself has recently been shown to be ubiquitinylated by the APC/C, and this ubiquitinylation is necessary for maintaining checkpoint arrest in human cells (Nilsson et al., 2008). Structural studies have now shed more light on how MCC may inhibit APC/C, from the findings that when the checkpoint is active, MCC components bound to APC/C partially overlap with the Cdc20 binding site, keeping the APC/C in a structurally “closed” conformation and preventing binding and ubiquitinylation of cyclin B and securin (Herzog et al., 2009). Thus, it is now clear that inhibition of APC/C activity is not simply due to checkpoint proteins binding and sequestering Cdc20.

1.7 Sensing Kinetochore-Microtubule Interactions

What specific features of kinetochore-microtubule interactions activate the checkpoint? Centromeres of properly bioriented sister kinetochores are under tension prior to cohesin cleavage, as they experience microtubule pulling forces emanating from opposing spindle poles. Early work suggested

that the lack of tension that exists prior to chromosome biorientation was the primary factor sensed by the checkpoint (Li and Nicklas, 1995). It is clear that unattached kinetochores activate the checkpoint, but they also lack tension between centromeres. The Aurora B kinase, a component of the chromosomal passenger complex, may be a specialized component of the checkpoint adapted specifically to sense lack of tension, as when one kinetochore binds microtubules while its sister is unattached or when both sister kinetochores bind microtubules emanating from the same spindle pole (syntelic attachment). Aurora B localizes between sister kinetochores at the inner centromere, where in response to the absence of tension it phosphorylates substrates such as the Ndc80 complex and MCAK, promoting detachment of bound microtubules and creating unattached kinetochores which subsequently activate the checkpoint (Biggins and Murray, 2001; Cheeseman et al., 2006; Ciferri et al., 2008; DeLuca et al., 2006; Hauf et al., 2003; Lampson et al., 2004; Pinsky and Biggins, 2005; Sandall et al., 2006; Tanaka et al., 2002). In this capacity, the principal state sensed by the checkpoint is unattached kinetochores, and Aurora B contributes to this state directly but does not directly modulate APC/C inhibition. However, this may not be the whole story at least in human cells, where a direct requirement for Aurora B in checkpoint signaling has been proposed given the reduction in kinetochore localization of checkpoint components such as BubR1 and Mad2 following depletion or chemical inhibition of Aurora B (Ditchfield et al., 2003; Morrow et al., 2005).

While the necessity of Aurora B in response to lack of tension is firmly established, the longstanding model that the distance between sister centomeres is the critical determinant in tension sensing has recently been challenged by two studies suggesting that intrakinetochore stretch or tension satisfies the checkpoint (Maresca and Salmon, 2009; Uchida et al., 2009).

1.8 Silencing the Checkpoint

Relative to checkpoint activation and signaling, little attention has been focused on how the checkpoint signal is extinguished once proper kinetochore microtubule interactions have formed. A Mad2 binding protein, $p31^{comet}$, has been identified in vertebrates as an important factor in silencing the checkpoint. $p31^{comet}$ specifically binds the Mad2-C conformer (whether Mad2-C is bound to Mad1 or Cdc20) without displacing Cdc20, and in doing so blocks Mad2 from inhibiting APC/C (Vink et al., 2006; Xia et al., 2004). It also prevents Mad2-O from binding Mad2-C (Mapelli et al., 2006; Vink et al., 2006). If and how kineteochores modulate $p31^{comet}$ remain completely unknown, and it is important to note that no orthologues of this protein have been identified outside of vertebrates. Besides $p31^{comet}$, microtubule dependent dynein-mediated transport of checkpoint proteins (including Mad2 and Rod) off of kinetochores has received much attention as a potential mechanism for silencing the checkpoint following proper chromosome biorientation (Howell et al., 2001; Wojcik et al., 2001). Interestingly, the RZZ complex itself is required for Mad1 and Mad2 to localize to kinetochores (Buffin et al., 2005; Kops et al.,

2005), as well as dynein through its cofactor dynactin (Starr et al., 1998). A caveat to the dynein checkpoint silencing hypothesis is the absence of a nuclear dynein homologue in *S. Cerevisiae.*

1.9 Holocentric Chromosomes

Two chromosome architectures are prevalent in eukaryotes, termed monocentric and holocentric. These terms reflect the nature of the centromere; in monocentrics, the more prevalent form seen from yeast to humans, the centromere is the primary constriction on a metaphase chromosome upon which the kinetochore forms. Many eukaryotes display an alternate chromosome architecture called holocentric or holokinetic, in which no primary constriction is present but rather spindle microtubules attach to kinetochores along the entire length of the chromosome. Thus, the entire outer surface of the chromosome serves as the centromere upon which the kinetochore forms. Kinetochores in holocentrics are described as diffuse (Maddox et al., 2004). Holocentric chromosome architecture appears to have arisen multiple times during evolution since it is present in independent eukaryotic lineages including all nematodes, hemipteran insects and numerous plant species (Pimpinelli and Goday, 1989). Despite their morphological differences, the proteins comprising centromeres and kinetochores, as well as the mechanisms of centromere specification and chromosome segregation are highly conserved between monocentrics and holocentrics, and the nematode *Caenorhabditis elegans* has emerged as an important model system for

studying kinetochore assembly and function (Cheeseman et al., 2004; Desai et al., 2003; Maddox et al., 2004; Moore et al., 1999; Moore and Roth, 2001; Oegema et al., 2001).

1.10 *Caenorhabditis elegans*

The nematode *Caenorhabditis elegans* has emerged as a powerful model system in modern scientific research. This worm has many attractive attributes as a model organism; they are eukaryotes with a completely sequenced genome, they are small (approximately 1 mm long as adults), fast growing (~2.5 days from hatching to adulthood) are transparent, and easy to grow in the laboratory on an *E. coli* diet in petri dishes. The developmental pattern of all 959 somatic cells has been traced. They are hermaphrodites, and a single organism can yield up to 300 progeny. They are a diploid organism, possessing five pairs of autosomes (I, II, III, IV and V) and one pair of sex chromosomes (XX). Males arise spontaneously at a low frequency due to X-chromosome nondisjunction in meiosis and are (XO), and can then be maintained indefinitely by mating to hermaphrodites, which will preferentially utilize the male sperm in embryo fertilization. Males are exceptionally useful for performing genetic crosses. Several features of the organism make it particularly amenable to studying cell division using the early embryo. Of note are the rapid and highly stereotypical mitotic divisions, which are each approximately 20 minutes long. The invariant nature of the first several mitotic divisions allows for easy quantification of defects or changes following

molecular perturbations, and the relatively weak DNA damage (Brauchle et al., 2003) and spindle checkpoints (Encalada et al., 2005) allows the cell cycle to proceed despite the presence of massive defects. Transgenic strains stably expressing fluorescently tagged proteins driven by germline-expressed promoters allow for real-time quantitative visualization of protein dynamics in the early embryo, when combined with live imaging video microscopy. Arguably one of the most useful features of this organism is the effectiveness of RNAi to deplete gene products in the early embryo. In other systems, RNA-mediated depletion of targeted mRNA is rapid, but any pre-existing protein product is subject to the half-life of that protein, which may be considerably long. The unique assembly-line architecture of the *C. elegans* gonad ensures that any pre-existing protein present when the dsRNA is introduced is depleted by the continual packaging of maternal cytoplasm into oocytes. Thus, depletion rates of pre-existing proteins depend on the rate of embryo production instead of protein half-life, so depletion kinetics tend to be similar for different targets. As At 36 to 48 hours following introduction of dsRNA, embryos are typically 95-99% depleted of the target protein.

Chapter 2: Systematic Analysis in *Caenorhabditis elegans* Reveals that the Spindle Checkpoint Is Composed of Two Largely Independent Branches

2.1 Summary

Kinetochores utilize the spindle checkpoint to delay anaphase onset until all chromosomes have formed bipolar attachments to spindle microtubules. Here, we use controlled monopolar spindle formation to systematically define the requirements for spindle checkpoint signaling in the *C. elegans* embryo. The results, when interpreted in light of kinetochore assembly epistasis analysis, indicate that checkpoint activation is coordinately directed by the NDC-80 complex, the Rod/Zwilch/Zw10 complex, and BUB-1—three components independently targeted to the outer kinetochore by the scaffold protein KNL-1. These components orchestrate the integration of a core Mad1^{MDF-1}/Mad2^{MDF-2}-based signal with a largely independent Mad3^{SAN-1}/BUB-3 pathway. Evidence for independence comes from that fact that subtly elevating Mad2^{MDF-2} levels bypasses the requirement for BUB-3 and Mad3^{SAN-1} in kinetochore-dependent checkpoint activation. Mad3^{SAN-1} does not accumulate at unattached kinetochores and BUB-3 kinetochore localization is independent of Mad2^{MDF-2}. We discuss the rationale for a bipartite checkpoint mechanism in which a core Mad1^{MDF-1}/Mad2^{MDF-2} signal generated at

kinetochores is integrated with a separate cytoplasmic Mad3^{SAN-1}/BUB-3-based pathway.

2.2 Introduction

Kinetochores assemble on centromeric DNA to connect spindle microtubules to sister chromatids and enable their segregation (Cheeseman and Desai, 2008). Improper segregation can generate aneuploid daughter cells, which in turn may promote apoptosis or tumorigenesis (Rajagopalan and Lengauer, 2004). To prevent aneuploidy, a kinetochore-based signaling pathway called the spindle checkpoint monitors chromosome-microtubule attachments and inhibits anaphase onset until all chromosomes have successfully bioriented, i.e. the two sister chromatids have attached to spindle microtubules emanating from opposing spindle poles (Musacchio and Salmon, 2007). The presence of even a single unattached kinetochore is sufficient to inhibit progression into anaphase in somatic cells (Rieder et al., 1995).

Screens for budding yeast mutants unable to arrest in the presence of microtubule depolymerizing drugs identified Mad1, Mad2 and Mad3 (for mitotic arrest deficient) and Bub1, and Bub3 (for budding uninhibited by benzimidazole) as molecular components of the checkpoint (Hoyt et al., 1991; Li and Murray, 1991). Mps1, a kinase essential for spindle pole body duplication, was subsequently also shown to be required for the checkpoint (Weiss and Winey, 1996). Vertebrates and flies have additional proteins essential for checkpoint signaling including Rod, Zwilch, and Zw10 (RZZ),

which co-purify as a complex and are interdependent for their kinetochore localization (Buffin et al., 2005; Karess, 2005; Kops et al., 2005; Williams et al., 2003), and the kinesin-like motor protein CENP-E (Abrieu et al., 2001). Another difference between vertebrates and yeast is that the Mad3-like vertebrate protein BubR1 contains a C-terminal Bub1-like kinase domain (Murray and Marks, 2001). Localization interdependencies, turnover dynamics and biochemical interactions among the checkpoint proteins have been primarily studied in vertebrates and yeast and indicate that Bub1 is at the top of the checkpoint protein kinetochore localization hierarchy (Gillett et al., 2004; Johnson et al., 2004; Meraldi et al., 2004; (Rischitor et al., 2007; Sharp-Baker and Chen, 2001) and that downstream components such as Mad2 are rapidly exchanging at unattached kinetochores to communicate the checkpoint signal to the cytoplasm (Musacchio and Salmon, 2007).

Checkpoint activation delays sister chromatid separation and mitotic exit by preventing the APC/C (anaphase-promoting complex/cyclosome), an E3-ubiquitin ligase, from inducing the destruction of securin and cyclin B (Peters, 2002; Yu, 2002). The checkpoint sequesters or inhibits Cdc20 (Hwang et al., 1998; Kim et al., 1998), which is essential for APC/C activation and substrate recognition (Yu, 2007). The precise mechanism of Cdc20 inhibition by the checkpoint is a current topic of investigation. Recent structural and *in vitro* studies have shown that a kinetochore bound Mad1-Mad2 complex interacts with free Mad2 and modifies its conformation to make

it a more potent inhibitor of APC-Cdc20 (De Antoni et al., 2005; Luo et al., 2004; Mapelli et al., 2007; Sironi et al., 2002; Vink et al., 2006; Yang et al., 2008). However, Mad2 is unlikely to be the sole Cdc20 inhibitor. BubR1 has been shown to directly bind Cdc20 and subunits of the APC/C (Sironi et al., 2002; Tang et al., 2001). Bub1 has also been shown to bind and phosphorylate Cdc20 (Tang et al., 2004a). Finally, a complex named MCC (for mitotic checkpoint complex) containing BubR1 (Mad3 in yeast and worms), Bub3, Mad2 and Cdc20 that displays much higher APC/C inhibitory activity than purified Mad2 *in vitro* has been purified from HeLa cells as well as budding yeast (Fraschini et al., 2001; Hardwick et al., 2000; Sudakin et al., 2001).

The early *C. elegans* embryo has emerged as an important model for studying kinetochore assembly and function. *In vivo* assembly epistasis analysis has comprehensively defined the relationships between kinetochore constituents, including proteins that direct assembly of centromeric chromatin (Maddox et al., 2007) and proteins that provide the core microtubule-binding activity of the kinetochore (Cheeseman et al., 2006; Cheeseman et al., 2004; Desai et al., 2003). These studies revealed a central role for the scaffold-like protein KNL-1 in outer kinetochore assembly, including the targeting of Bub1, the upstream kinase involved in spindle checkpoint activation (Desai et al., 2003). The role of KNL-1 family proteins in checkpoint signaling is conserved in vertebrates (Kittler et al., 2007; Kiyomitsu et al., 2007). A delay in mitosis

following treatment with microtubule-depolymerizing drugs has been documented in the gonad and in embryos (Encalada et al., 2005; Hajeri et al., 2008; Kitagawa and Rose, 1999; Nystul et al., 2003; Stein et al., 2007; Tarailo et al., 2007), and spindle checkpoint proteins have been implicated in cessation of activity under anoxia (Nystul et al., 2003) and starvation-induced arrest of germ cell precursors (Watanabe et al., 2008).

Here, we develop a controlled monopolar spindle formation-based assay in the early *C. elegans* embryo to systematically analyze the relationship between kinetochore structure and checkpoint activation. Our results indicate that checkpoint activation is coordinately directed by three components — the NDC-80 complex, the Rod/Zwilch/Zw10 complex, and BUB-1 — that are targeted independently of one another by the outer kinetochore scaffold protein KNL-1. Mad3^{SAN-1}, unlike the other checkpoint proteins, does not enrich at unattached kinetochores. Surprisingly, a subtle (2.5-fold) increase in Mad2^{MDF-2} levels can bypass the requirement of Mad3^{SAN-1} as well as BUB-3 for checkpoint activation. We propose that a core Mad1^{MDF-1}/Mad2^{MDF-2} signal generated at kinetochores is integrated with a largely independent cytoplasmic Mad3^{SAN-1}/BUB-3-based signal to achieve APC/C inhibition.

2.3 Results

2.3.1 Controlled Monopolar Spindle Formation in the C. elegans Embryo Elicits a Cell Cycle Delay that Requires Conserved Spindle Checkpoint Components

To quantitatively monitor spindle checkpoint signaling in *C. elegans* embryos, we triggered checkpoint activation by generating monopolar spindles. In *C. elegans*, RNAi-mediated depletion of proteins required for centriole duplication results in a bipolar first division, which serves as a useful internal control, followed by subsequent monopolar divisions (Fig. 2.1A; (O'Connell *et al.*, 2001). Monopolar spindles have both unattached kinetochores and kinetochores not under tension and have been shown to activate the checkpoint in other organisms (Kapoor et al., 2000). This approach avoids drug treatments, which are difficult due to the impermeable egg-shell surrounding the embryos.

We quantified the time from nuclear envelope breakdown (NEBD) to chromosome decondensation (DCON) in embryos expressing GFP-histone H2b (to mark the chromosomes) and GFP-γ-tubulin (to mark the spindle poles). NEBD was defined by diffusion of free GFP-histone H2b out of the nucleoplasm and DCON as the disappearance of fluorescent punctae throughout the decondensing chromatin (Fig. 2.1B). Monopolar spindles were generated by depleting the kinase ZYG-1 or the centriole structural protein SAS-6 (Bettencourt-Dias and Glover, 2007). In both control and centriole

duplication-inhibited embryos, the timing of NEBD – DCON was unaltered in the first mitotic division. By contrast, the same interval in the subsequent monopolar mitotic divisions was significantly elongated in both the anterior AB cell (Fig. 2.1C) and the posterior P1 cell (not shown). In all subsequent experiments, we only present analysis of mitotic timing in the first embryonic division and in the AB cell.

To determine if the delay in cells with monopolar spindles was due to spindle checkpoint activation, we co-depleted the conserved checkpoint protein Mad2^{MDF-2}. Mad2^{MDF-2} co-depletion did not affect the timing of the first bipolar division (Fig. 2.1C; Movie S2.1), but abolished the cell cycle delay triggered by monopolar spindle formation (Fig. 2.1B, C; Movie S2.2). Mad2^{MDF-2} depletion on its own did not affect the NEBD-DCON interval in either division (Fig. S2.1A). Similar results were obtained for both ZYG-1 and SAS-6 depleted embryos, establishing that the delay in mitotic exit is due to the presence of monopolar spindles and not due to a specific role for the targeted proteins in cell cycle progression. We conclude that controlled generation of monopolar spindles elicits a Mad2^{MDF-2} dependent cell cycle progression delay in the *C. elegans* embryo.

The *C. elegans* homologs of proteins implicated in checkpoint signaling are indicated in Figure 2.1D together with the consequences of their RNAi-mediated depletion. *C. elegans* has a Mad3-like protein (Mad3^{SAN-1}) instead of a BubR1-like kinase and lacks an Mps1-like kinase, which is also absent in

other related nematodes with sequenced genomes. Unlike depletion of other checkpoint proteins, depletion of BUB-1, ROD-1 or Zwilch^{ZWL-1} resulted in penetrant embryonic lethality, reflecting functions for these proteins in chromosome segregation in addition to their role in checkpoint signaling. Depletion of Zw10^{CZW-1} resulted in penetrant sterility consistent with a previously described non-mitotic function for Zw10 (independently of Rod and Zwilch) in membrane trafficking (Hirose et al., 2004), which is required for oocyte production.

We next examined the consequences of depleting components of the spindle checkpoint pathway in the monopolar spindle assay. Individual depletions of each protein abolished the monopolar spindle-induced mitotic delay (Fig. 2.1E**).** By contrast, none of the depletions affected the timing of the first bipolar division (Fig. 2.1E). Abolishing checkpoint signaling by depletion of Mad1^{MDF-1} also did not alter kinetochore-spindle microtubule interactions, as assessed by quantitative analysis of spindle pole separation (Fig. S2.1B; (Oegema *et al.*, 2001). We conclude that controlled monopolar spindle formation generates a reproducible spindle checkpoint-mediated cell cycle delay in the early *C. elegans* embryo.

2.3.2 Systematic Analysis Subdivides the Protein Constituents of the Kinetochore into Three Classes Based on Their Roles in Spindle Checkpoint Activation

The protein components of the *C. elegans* kinetochore can be partitioned into different functional groups. A set of three proteins (CENP-A^{HCP-3}, CENP-C^{HCP-4} and KNL-2) form the centromeric chromatin foundation for kinetochore assembly (Buchwitz et al., 1999; Maddox et al., 2007; Moore and Roth, 2001; Oegema et al., 2001). The conserved KNL-1/Mis12 complex/Ndc80 complex (KMN) network assembles on this foundation to form the core microtubule-binding site of the kinetochore (Cheeseman et al., 2006; Cheeseman et al., 2004; Desai et al., 2003). KNL-1 serves as a scaffold that recruits not only the microtubule-binding NDC-80 complex but also other outer kinetochore proteins such as the RZZ complex, the kinase BUB-1, the CENP-F-like proteins HCP-1/2, and the microtubule-binding protein $CLASP^{CLS-2}$ (Desai et al., 2003).

To investigate their role in spindle checkpoint activation, we systematically analyzed the consequences of depleting kinetochore components on the monopolar spindle-induced cell cycle delay. As the chromosome missegregation associated with several of these depletions made chromosome decondensation difficult to score, we used an alternative method to time cell cycle progression by measuring the interval from NEBD to onset of cortical contractility (OCC) in a strain co-expressing mCherry-Histone

H2b and a GFP-tagged plasma membrane marker (Fig. 2.2B; Movies S2.3 and S2.4). Cortical contractility is tightly linked to mitotic exit and is a frequently utilized visual marker in live imaging studies (Canman et al., 2000; Kurz et al., 2002). We defined OCC as the transition of the membrane from a roughly circular conformation to a rectangular one (in embryos with bipolar spindles), or to the appearance of membrane "blebs" (in embryos with monopolar spindles; Fig. 2.2B, arrowheads). Using this assay, we confirmed that monopolar spindles trigger a Mad2^{MDF-2} dependent increase in the NEBD-OCC interval relative to controls (Fig. 2.2C; Movie S2.4).

Next, we depleted each of the kinetochore components on their own and in conjunction with ZYG-1 and measured the NEBD-OCC intervals for the first two mitotic divisions. None of the tested proteins affected the NEBD to OCC interval during the first bipolar mitotic division (Fig. 2.2C; Movie S2.3**).** By contrast, analysis of cell cycle timing in the AB cell partitioned the targeted kinetochore components into three classes. The first class (I), which includes CENP-A^{HCP-3}, CENP-C^{HCP-4}, KNL-3 (not shown), KNL-1, and NDC-80, is comprised of proteins required for the monopolar spindle-induced delay; depletions of proteins in this class did not result in a significant cell cycle delay relative to controls (Fig. 2.2C**).** The second class (II), which includes MCAK^{KLP-7} and the non-essential kinetochore protein KBP-5 (Fig. 2.2C & not shown**)**, was dispensable for the monopolar spindle-induced delay. The third class (III) includes proteins whose depletion induces a cell cycle delay on their

own, regardless of whether spindles were bipolar or monopolar; HCP-1/2, which are functionally analogous to CENP-F in vertebrates (Cheeseman et al., 2005; Encalada et al., 2005; Hajeri et al., 2008; Moore and Roth, 2001; Tarailo et al., 2007), fell into this class (Fig. 2.2C). The delay in HCP-1/2-depleted embryos was abolished by Mad2^{MDF-2} or Mad3^{SAN-1} co-depletion, but was of lower magnitude compared to the delay induced by monopolar spindles (Fig. 2.2C). Co-depletion of ZYG-1 did not increase the delay resulting from HCP-1/2 depletion, indicating that in addition to performing a function that prevents checkpoint activation, HCP-1/2 also make a positive contribution that increases the magnitude of the checkpoint signal.

In addition to the systematic analysis of kinetochore proteins described above, we also analyzed whether the inner centromere-localized Aurora B^{AIR-2} kinase subunit of the chromosomal passenger complex or the putative single Shugoshin family protein SGO-1 in *C. elegans* (C33H5.15; Kitajima et al., 2004) are required for checkpoint signaling. We did not observe abrogation of the monopolar-spindle induced cell cycle delay following inactivation of Aurora B^{AIR-2} using a temperature sensitive mutant allele (*or707ts*; (Severson *et al.*, 2000); or following *sgo-1(RNAi)* (Fig. S2.2B).

When considered in light of the assembly hierarchy of the kinetochore (Fig. 2.2A), the above data confirm that checkpoint signaling requires a core kinetochore scaffold. In addition, the results suggest that recruitment of 3

different components (the NDC-80 complex, the RZZ complex and BUB-1) by KNL-1 is critical for checkpoint activation.

2.3.3 Checkpoint Signaling Status Following Inhibition of the Three Classes of Kinetochore Constituents Correlates with GFP::Mad2^{MDF-2} Enrichment at Unattached Kinetochores

Checkpoint activation correlates with the enrichment of specific components of the pathway, most prominently Mad2, on unattached kinetochores (Musacchio and Salmon, 2007). This enrichment is thought to reflect the local kinetochore-catalyzed reaction that generates the inhibitor of the APC/C. To correlate Mad2 recruitment with the functional analysis of checkpoint signaling, we generated a strain stably co-expressing GFP::Mad2^{MDF-2} and mCherry-Histone H2b. In the early mitotic divisions of control embryos, GFP::Mad2^{MDF-2} fluorescence is detected at the nuclear envelope/nucleoplasm beginning in prophase. After NEBD, GFP::Mad2^{MDF-2} remains present as a “cloud” of diffuse fluorescence surrounding the chromatin until anaphase onset, at which point it rapidly dissipates (Fig. 2.3A; Movie S2.5). Thus, no significant kinetochore localization of GFP::Mad2^{MDF-2} is observed in control embryos. In embryos depleted of ZYG-1 or SAS-6, GFP::Mad2^{MDF-2} localization was indistinguishable from controls during the first bipolar mitotic division (not shown). However, during the second monopolar division, GFP::Mad2^{MDF-2} accumulated on the away-from-pole side of the chromatin after NEBD, reaching its peak intensity within 2 minutes (Fig.

2.3A,C; Movie S2.5) followed by decay of the signal. Thus, the accumulation of GFP::Mad2^{MDF-2} at kinetochores correlates with functional checkpoint signaling.

Immunoblotting indicated that the GFP::Mad2^{MDF-2} transgene was expressed at ~1.5 times the level of endogenous Mad2^{MDF-2} (Fig. 2.3B) and it caused a monopolar spindle-induced delay in the Mad2^{MDF-2} deletion strain *mdf-2(tm2190)* (Fig. S2.3A). GFP::Mad2^{MDF-2} localization was qualitatively similar on monopolar spindles generated in the deletion mutant strain. We also observed partial rescue of the variable and low brood size phenotype of the *mdf-2(tm2190)* strain (not shown). As the transgene is expressed under the *pie-1* promoter (Green et al., 2008), a lack of full rescue may reflect restricted expression.

We next analyzed the recruitment of GFP::Mad2^{MDF-2} to unattached kinetochores following depletion of the three classes of kinetochore components (Fig. 2.3D). GFP::Mad2^{MDF-2} failed to accumulate on monopolar spindle-associated chromosomes following depletion of class I components, which are essential for checkpoint signaling. By contrast, depletion of class II components, which are not required for the monopolar spindle induced delay, did not affect the kinetochore accumulation of GFP::Mad2^{MDF-2}. AuroraB^{AIR-2} inhibition, which does not abrogate the checkpoint-induced delay, also did not affect kinetochore accumulation of GFP::Mad2^{MDF-2} (Fig. S2.2C). Consistent with the fact that their depletion triggers the checkpoint even in the absence of

monopolar spindles, depletion of the class III components HCP-1/2 induced GFP::Mad2^{MDF-2} accumulation both in the presence and absence of monopolar spindles (Fig. 2.3D). These results support a strict correlation between the ability of unattached kinetochores to induce a cell cycle delay and their ability to recruit GFP::Mad2^{MDF-2}, providing strong support for the model that the kinetochore scaffold-based local recruitment of Mad2^{MDF-2} is required to generate the signal that inhibits APC/C activity.

2.3.4 GFP::Mad2^{MDF-2} Accumulation At Kinetochores is Unaffected By Depletion of Mad3^{SAN-1} and is Reduced, but not Eliminated, by Depletion of BUB-3

We next investigated GFP-Mad2^{MDF-2} localization at unattached kinetochores following depletion of conserved checkpoint pathway proteins (Fig. 2.1D). We expected that since all of these proteins are required for the monopolar spindle-induced delay (Fig. 2.1E), their depletion would eliminate GFP::Mad2^{MDF-2} localization, as observed for class I kinetochore components. This was indeed the case following depletion of Mad1^{MDF-1}, BUB-1 or ROD-1 (Fig. 2.3E). However, depletion of Mad3^{SAN-1} had no significant effect on GFP::Mad2^{MDF-2} localization at unattached kinetochores (Fig. 2.3E; Fig. S2.3B; Movie S2.8). To confirm this result, we repeated the analysis using a viable null mutant of *san-1* (*san-1(ok1580)*; referred to subsequently as Mad3$^{san-1}\Delta$) that, similar to Mad3^{SAN-1} depletion by RNAi, is unable to generate a monopolar spindle-induced cell cycle delay (Fig. S2.4A). Even in the Mad3^{san-}

*1*Δ strain, we did not see a significant reduction in the accumulation of GFP::Mad2^{MDF-2} at unattached kinetochores compared to controls (Fig 2.3F; Movie S2.9). Depletion of BUB-3 reduced the accumulation of GFP::Mad2^{MDF-2} but did not eliminate its kinetochore localization (Fig. 2.3E; Movie S2.7). Quantitative analysis of the peak GFP::Mad2^{MDF-2} fluorescence on chromosomes of monopolar spindles confirmed these observations **(**Fig. S2.3B**)**. We conclude that Mad3^{SAN-1} and BUB-3 are not essential for the accumulation of GFP::Mad2^{MDF-2} at unattached kinetochores.

2.3.5 Mad3^{SAN-1} Does Not Enrich at Unattached Kinetochores When the Spindle Checkpoint is Active

Mad3^{SAN-1} is not required for Mad2^{MDF-2} to accumulate at unattached kinetochores. To determine if the converse is also true, we generated a strain co-expressing mCherry-Histone H2b and GFP::Mad3^{SAN-1}. Expression of the Mad3^{SAN-1} transgene restored a monopolar spindle-induced cell cycle delay in the Mad3^{san-1}Δ strain (Fig. S2.4A). In control embryos, GFP::Mad3^{SAN-1} showed diffuse localization in the vicinity of chromatin at prometaphase, which appeared significantly reduced by metaphase; there was no signal above background in other stages of mitosis (Fig. 2.4A; Movie S2.10). Surprisingly, we did not detect enrichment of GFP::Mad3^{SAN-1} at kinetochores of monopolar spindle-associated chromosomes; instead, we observed a diffuse localization pattern similar to that in control embryos with bipolar spindles (Fig. 2.4B; Movie S2.10). This localization pattern was unchanged in the absence of a

wild-type Mad3^{SAN-1} allele (Fig. 2.4C; Movie S2.11) and was eliminated by RNAi-mediated depletion of Mad3^{SAN-1} (Fig. S2.4B). Co-depletion of Mad2^{MDF-2}, Mad1^{MDF-1}, or BUB-1 had no significant effect on this diffuse localization; by contrast, in BUB-3 depleted embryos, the GFP signal was significantly diminished (Fig. 2.4B; Movies S2.12 & S2.13). The latter observation suggests that Mad3^{SAN-1} protein may be destabilized following depletion of BUB-3; we were unable to confirm this due to lack of a suitable anti-Mad3^{SAN-1} antibody. We conclude that Mad3^{SAN-1} is not co-enriched on unattached kinetochores and that its stability may be dependent on BUB-3.

2.3.6 BUB-3 Exhibits Basal Kinetochore Localization that is Enriched at Unattached Kinetochores in a BUB-1-Dependent but Mad1^{MDF-1}/Mad2^{MDF-2}-Independent Manner

We next generated a strain co-expressing GFP::BUB-3 and mCherry-Histone H2b and performed experiments similar to those performed for Mad3^{SAN-1}. Both endogenous BUB::3 (Fig. S2.5A) and GFP::BUB-3 (Fig. 2.4D) were detected at kinetochores of control embryos. BUB::3 is first detectable on condensing chromosomes in late prophase, and reaches maximal fluorescence intensity as paired lines on kinetochores at metaphase (Fig. 2.4D; Movie S2.14). It rapidly dissipates from kinetochores in early anaphase, and is no longer detectable by late anaphase/early telophase. In cells with monopolar spindles, GFP::BUB-3 becomes enriched on the unattached kinetochores on the chromosomal face away from the pole (Fig.

2.4E; Movie S2.14). We conclude that BUB-3 has a basal kinetochore localization that is amplified when the checkpoint is active.

We next wanted to investigate the relationship between BUB-3 enrichment and Mad2^{MDF-2} enrichment at unattached kinetochores. We did not observe an effect of depleting either Mad1^{MDF-1} or Mad2^{MDF-2} on the enrichment of BUB-3 at unattached kinetochores (Fig. 2.4E). We also did not observe an effect of depleting Mad3^{SAN-1} (Fig. 2.4E), indicating that BUB-3 levels and localization are independent of Mad3^{SAN-1}. By contrast, depletion of BUB-1 eliminated BUB-3 localization on both control bipolar (not shown) and monopolar spindles (Fig. 2.4E; Movie S2.15); depletion of the RZZ complex subunit ROD-1, reduced the level of BUB-3 at unattached kinetochores although localization was still evident (Fig. 2.4E; Movie S2.16) but depletion of the Ndc80 complex did not have a significant effect (Fig. S2.5C).

In converse experiments, BUB-3 depletion had no effect on BUB-1 (Figure 2.4F) or RZZ complex kinetochore localization (data not shown). Because BUB-3 depletion does not lead to embryonic lethality, these results suggest that BUB-3 is not essential for the other chromosome segregation functions of BUB-1 and the RZZ complex. We conclude that BUB-3 exhibits basal kinetochore localization and accumulates at checkpoint-signaling kinetochores in a BUB-1-dependent manner.

2.3.7 The NDC-80 complex, the RZZ complex and BUB-1 converge downstream of KNL-1 to direct the accumulation of Mad2^{MDF-2} and BUB-3 and checkpoint activation

The NDC-80 complex, BUB-1, and the RZZ complex are all dependent on KNL-1 for their kinetochore localization (Cheeseman et al., 2004; Desai et al., 2003) and are all essential for checkpoint activation. Previous work has shown that NDC-80 complex is recruited to kinetochores independently of BUB-1 and the RZZ complex (Desai *et al.*, 2003; Gassmann *et al.*, 2008). Consistent with this, localization of BUB-3, which depends on BUB-1, is independent of the NDC-80 complex (Fig. S2.5C). We extended this analysis to show that BUB-1 and the RZZ complex also target to kinetochores independently of each other (Fig. 2.4G). Thus, three components with distinct functions that are independently targeted to kinetochores by KNL-1 are integrated to direct Mad2^{MDF-2} and BUB-3 recruitment and checkpoint activation (Fig. 2.4H). Interestingly, the kinetochore targeting of Mad2^{MDF-2} and BUB-3 reflect different, largely independent, pathways downstream of NDC-80, BUB-1, and the RZZ complex (Fig. 2.4H). The kinetochore accumulation of Mad2^{MDF-2} (and presumably also Mad1^{MDF-1}) requires NDC-80, BUB-1, and the RZZ complex and is enhanced by (but does not require) BUB-3. The kinetochore localization of BUB-3 requires BUB-1 and is enhanced by the presence of the RZZ complex, but does not require Mad1^{MDF-1} or Mad2^{MDF-2}. The existence of distinct pathways for the recruitment of

Mad2^{MDF-2} and BUB-3 may facilitate the integration of different inputs during spindle checkpoint activation.

2.3.8 A Subtle Increase in Mad2^{MDF-2} Levels Bypasses the Requirement for Mad3^{SAN-1} and BUB-3 to Elicit a Kinetochore-Dependent Monopolar Spindle-Induced Cell Cycle Delay

In the strain expressing both endogenous and GFP::Mad2^{MDF-2}, basal cell cycle timing was unaffected and monopolar spindles increased the NEBD-DCON interval (Fig. 2.5A). As this increase was dependent on Mad1^{MDF-1} (Fig. 2.5A) and KNL-1 (not shown), it reflects kinetochore-dependent signaling and excludes the trivial possibility that overexpression of Mad2^{MDF-2} is causing a cell cycle delay by general cytoplasmic inhibition of the APC/C. Strikingly, depletion of Mad3^{SAN-1} or BUB-3 did not eliminate the monopolar spindle-induced delay in this strain (Fig. 2.5A). The same result was obtained after crossing the GFP::Mad2^{MDF-2} transgene into the Mad3$^{\textit{san-1}}\Delta$ strain background (Fig. 2.5B). Importantly, the monopolar spindle-induced delay in the Mad3$^{\textit{san-1}}\Delta$ strain expressing the GFP::Mad2^{MDF-2} transgene required Mad1^{MDF-1} (Fig. 2.5B), indicating that the Mad3^{SAN-1}-independent delay was kinetochore-dependent. We did not observe a bypass of the requirement for Mad1^{MDF-1} in the strain expressing GFP::BUB-3 (Fig. S2.5D), indicating that kinetochore-localized Mad1^{MDF-1}/Mad2^{MDF-2} is indispensable for checkpoint signaling and that the bypass only works one-way.

Since GFP::Mad2^{MDF-2} was expressed from the transgene at 1.5 times the level of endogenous Mad2^{MDF-2} (Fig. 2.3B) the total level of Mad2^{MDF-2} in the GFP::Mad2^{MDF-2} strain was ~2.5 times that in controls. These results suggest that a subtle increase in Mad2^{MDF-2} levels is sufficient to bypass the requirement for Mad3^{SAN-1} or BUB-3 to elicit a monopolar spindle-induced kinetochore-dependent cell cycle delay. If this were true, then restoring Mad2^{MDF-2} expression to endogenous levels should reverse this effect. To test this prediction, we used dsRNAs targeting GFP and ZYG-1 to simultaneously eliminate expression of the GFP-Mad2^{MDF-2} transgene and generate monopolar spindles. In this condition, a delay in the NEBD-DCON interval was observed that was not significantly different from ZYG-1 depletions alone (Fig. 2.5A); the lack of any GFP signal on the chromosomes confirmed the efficacy of the GFP dsRNA (Fig. 2.5C). When we then additionally co-depleted Mad3^{SAN-1} or BUB-3, the monopolar-spindle induced delay in the NEBD-DCON interval was eliminated, indicating that the bypass of the requirement for Mad3^{SAN-1} and BUB-3 is dependent on the expression of the GFP-Mad2^{MDF-2} transgene (Fig. 2.5A).

It is possible that the GFP::Mad2^{MDF-2} fusion is functionally altered in terms of APC/C inhibitory activity – however, neither basal cell cycle timing nor the extent of the kinetochore-dependent delay, both of which are sensitive to APC/C inhibition, were significantly affected by its presence. We conclude

that a subtle increase in Mad2^{MDF-2} levels bypasses the requirement for Mad3^{SAN-1} and BUB-3 in kinetochore-dependent spindle checkpoint signaling.

2.4 Discussion

2.4.1 Systematic Analysis of the Requirements for Spindle Checkpoint Activation Indicates a Central Role for the KMN Network

Here, we use controlled monopolar spindle formation to perform a systematic analysis of the requirements for checkpoint activation and Mad2^{MDF-2} recruitment in the *C. elegans* embryo. Our analysis comparing the classification of kinetochore proteins into functional groups based on phenotypic analysis and their position in the kinetochore assembly hierarchy to their role in checkpoint activation (Figure 2.6A), strongly supports the model that a kinetochore-triggered reaction is central to checkpoint activation. Specifically, all tested inhibitions that abrogate outer kinetochore assembly, including depletion of the centromeric histone CENP-A, prevented checkpoint activation. This result appears contradictory to checkpoint-dependent mitotic delays reported following inhibition of the centromeric histone CENP-A in *Drosophila* embryos and vertebrate cells (Blower et al., 2006; Regnier et al., 2005). It is possible that this reflects a difference in kinetochore assembly pathways between these systems. Alternatively, the high stability of CENP-A, which does not affect intrinsic turnover-independent RNAi-mediated depletion in *C. elegans* (Oegema and Hyman, 2006) but does affect depletion efficacy in

mutant *Drosophila* embryos that contain maternal product (Blower et al., 2006) or in chicken cells where expression of a rescuing transgene is turned off (Regnier et al., 2005), may account for the difference.

Our systematic analysis identifies the core microtubule-binding site of the kinetochore, the KMN network, as the most downstream stably kinetochore-localized protein group required for checkpoint activation. Specifically, three components with distinct functions that are independently targeted to kinetochores by the scaffold protein KNL-1 — the NDC-80 complex, the RZZ complex and BUB-1 — are all critical for checkpoint activation. The NDC-80 complex directly associates with KNL-1 in the KMN network (Cheeseman et al., 2004) and has been implicated in checkpoint signaling in other systems (Gillett et al., 2004; McCleland et al., 2003; Meraldi et al., 2004). Based on work in human cells, the association of KNL-1 with BUB-1 is also likely to be direct (Kiyomitsu et al., 2007). At least in *C. elegans*, where a Zwint-like intermediate protein bridging KNL-1 and the RZZ complex is not present, the RZZ complex may also directly associate with KNL-1. Taken together, these findings suggest an analogy to signaling networks where different inputs integrated by scaffold proteins control signaling reactions. In the case of the spindle checkpoint, mechanical inputs from two independently targeted microtubule-binding activities of distinct functions, one resident in the Ndc80 complex and the second in the dynein/dynactin motor complex targeted by the RZZ complex, are likely

integrated with BUB-1 in the context of the KNL-1 scaffold. Investigating the mechanism of integration will require developing a means to model the checkpoint reaction *in vitro* with a faithful facsimile of the activation base provided by the kinetochore – such an effort should be facilitated by the reconstitution of the *C. elegans* KMN network (Cheeseman et al., 2006).

2.4.2 The Core Checkpoint Pathway in *C. elegans*

In *C. elegans*, the core checkpoint pathway is simplified relative to other metazoan systems – no Mps1-like kinase exists and a Mad3- instead of a BubR1-like protein is present. It is possible that this simplification is linked to weakening of the checkpoint to accommodate the large diffuse kinetochores on the holocentric chromosomes of this organism. At least in the second embryonic division, which is the focus of our work, monopolar spindles are only able to extend the mitotic phase of the cell cycle 2-fold. Alternatively, the relatively small magnitude of the delay at the two-cell stage may reflect the large cytoplasm-to-nuclear ratio in the blastomeres at two-cell stage, consistent with the previously established relationship between the checkpoint signal efficacy and the nuclear-cytoplasmic ratio observed in *Xenopus* embryos (Minshull et al., 1994). A fast acting temperature-sensitive mutant that permits generation of monopolar spindles in later embryonic cell divisions, where the cells are smaller, should help distinguish between these possibilities in future work.

Depletion of the core checkpoint proteins had no effect on basal cell cycle timing, but all were essential for the monopolar spindle-induced cell cycle delay. In addition, recruitment of Mad2^{MDF-2} to kinetochores was observed only when the checkpoint was activated — no significant accumulation at kinetochores was evident in control embryos. By contrast, both BUB-1 and BUB-3 localized to kinetochores even without checkpoint activation. This is consistent with the idea that BUB-1 provides an essential function in chromosome segregation that is required for embryonic viability. These results are generally analogous to what has been reported in budding yeast, where Mad1 and Mad2 localization is only observed following drug-induced microtubule depolymerization and where Bub1 and Bub3 mutants are significantly more sick than Mad1 and Mad2 mutants (Gillett et al., 2004; Warren et al., 2002). Several non-checkpoint functions for Bub1 family kinases have been reported in yeast and vertebrates (Boyarchuk et al., 2007; Johnson et al., 2004; Kitajima et al., 2005; Tang et al., 2004b; Vaur et al., 2005) and at least one of these (targeting of CENP-F-like proteins HCP-1/2 to kinetochores) is conserved in *C. elegans* embryos ((Encalada et al., 2005); not shown).

In addition to the core checkpoint proteins and the KMN network, we also observed a positive contribution to checkpoint signaling from HCP-1/2. Depletion of these proteins in cells with either bipolar or monopolar spindles triggers a Mad2^{MDF-2}/ Mad3^{SAN-1}-dependent cell cycle delay, but the magnitude

of this delay is less than that when HCP-1/2 are present. Synthetic genetic screens have identified HCP-1, but not HCP-2, as a contributor to checkpoint signaling in *C. elegans* (Hajeri et al., 2008; Tarailo et al., 2007) – our results extend these studies by showing that HCP-1/2 are not required for $Mad2^{MDF-2}$ enrichment at kinetochores; HCP-1/2 may control the extent of $Mad2^{MDF-2}$ accumulation or they may act at a different step that affects the potency of the inhibitory signal. Analogous conclusions have been made from studies on vertebrate CENP-F (for discussion, see (Hajeri et al., 2008; Tarailo et al., 2007)). Finally, $MCAK^{KLP-7}$ was dispensable for both checkpoint activation and $Mad2^{MDF-2}$ kinetochore localization. This result is in contrast to a previous report that $MCAK^{KLP-7}$ is required for the checkpoint based on differential interference-contrast imaging of nocodazole-treated embryos (Encalada et al., 2005). The reason for this discrepancy is currently unclear; we note that inhibition of kinesin-13s in vertebrates has not suggested an involvement in checkpoint activation (e.g. see (Manning *et al.*, 2007).

2.4.3 Mad3 versus BubR1 in the Core Checkpoint Pathway

C. elegans is the only metazoan analyzed to date that lacks a BubR1-like kinase and instead has a truncated Mad3-like protein. An interesting emerging pattern is that the presence of a BubR1-like kinase correlates with the presence of a CENP-E-like kinetochore-localized kinesin motor (Abrieu et al., 2000; Chan et al., 1999). Worms and fungi, which have Mad3 instead of BubR1, lack CENP-E. The described functional links between CENP-E and

the BubR1 kinase during checkpoint signaling in vertebrates are consistent with this pattern (Mao et al., 2005).

The most significant difference between Mad3^{SAN-1} in *C. elegans* and BubR1 in other metazoans is with respect to kinetochore localization. The BubR1-like proteins in *Drosophila* and vertebrates localize to kinetochores, whereas we find that a functional *C. elegans* GFP:Mad3^{SAN-1} does not. Interestingly, chromatin immunoprecipitation and microscopy failed to detect budding yeast Mad3 at kinetochores under spindle depolymerization conditions that significantly enriched Mad1 and Mad2 at kinetochores (Gillett et al., 2004). This similarity suggests that Mad3-like proteins, as compared to BubR1-like protein kinases, are not enriched at kinetochores and, by inference, act primarily in the cytoplasm/nucleoplasm. However, contrary to this suggestion, fission yeast Mad3 localizes to kinetochores (Millband and Hardwick, 2002). Experiments in which the Mad3s are switched between the two yeasts and *C. elegans* may help define the signals that control Mad3 localization and elucidate its site of action with respect to checkpoint signaling. Whether the kinetochore localization of Mad3 in fission yeast or BubR1 in vertebrate cells is essential for checkpoint signaling has not been established. Recent studies in vertebrates are leading to the conclusion that, similar to our findings in *C. elegans* for Mad3^{SAN-1}, the checkpoint signaling function of BubR1 is independent of kinetochores (A. Kulukian and D. Cleveland, personal communication); the kinetochore localization of BubR1 may

contribute to a distinct non-checkpoint role in chromosome segregation (Lampson and Kapoor, 2005).In *C. elegans*, Mad3^{SAN-1} and Mad2^{MDF-2} are both required for the monopolar spindle-induced cell cycle delay in the early embryo. However, the fact that subtle overexpression of Mad2^{MDF-2} bypasses the requirement for Mad3^{SAN-1} as well as BUB-3 indicates that Mad2^{MDF-2} is functionally more important. Consistent with this idea, the developmental phenotypes associated with deletion of Mad3^{SAN-1} are significantly weaker than those resulting from mutations in Mad1^{MDF-1} and Mad2^{MDF-2}, which lead to pronounced defects in germline development and embryo production (Kitagawa and Rose, 1999; Stein et al., 2007). We speculate that in the germline, the core Mad1-Mad2 mechanism may be upregulated independently of Mad3 to protect against aneuploidy. It is also possible that, similar to meiosis in budding yeast (Shonn *et al.*, 2003), the Mad1-Mad2 mechanism may provide an additional function important for chromosome segregation. Further work on these two interacting branches of the checkpoint pathway in the context of developmental regulation may provide insights into both the basal checkpoint signaling mechanism and its adaptation in different contexts.

2.4.4 Mad1^{MDF-1}/Mad2^{MDF-2} versus Mad3^{SAN-1}/BUB-3: Two Branches of the Checkpoint Signaling Pathway

The most interesting theme emerging from our systematic analysis was the partitioning of the kinetochore-dependent checkpoint signaling pathway into two largely independent branches. Mad2^{MDF-2} (and presumably also

Mad1^{MDF-1}) accumulate at kinetochores and, in the situation where Mad2^{MDF-2} levels are elevated, support kinetochore-dependent checkpoint activation independently of BUB-3 and Mad3^{SAN-1}. Conversely, BUB-3 targets to and become enriched at kinetochores in the absence of Mad2^{MDF-2}, although in this case no checkpoint signal is generated. The independence of Mad1/Mad2 kinetochore localization from Mad3^{SAN-1} is supported by work in yeast (Gillett et al., 2004; Vanoosthuyse et al., 2004) and by BubR1 depletion in human cells (Johnson *et al.*, 2004; Meraldi *et al.*, 2004). Although Mad3^{SAN-1} does not localize to kinetochores upon checkpoint activation, two lines of evidence support a functional link to BUB-3. First, subtle overexpression of Mad2^{MDF-2} bypassed depletion of either BUB-3 or Mad3^{SAN-1}. Second, BUB-3 depletion resulted in a significant decrease in GFP-Mad3^{SAN-1} signal which suggests that the protein may be destabilized- such an effect is typically observed for proteins that are associated with each other. Taken together, these results suggest that a core Mad1^{MDF-1}-Mad2^{MDF-2} signaling mechanism, which involves conversion of the free “open” form of Mad2 (Mad2-O) to the Cdc20-inhibiting “closed” form (Mad2-C) by a kinetochore-bound Mad1-Mad2 complex (Fig. 2.6B; Musacchio and Salmon, 2007), cooperates with a Mad3^{SAN-1}/ BUB-3 dependent cytoplasmic mechanism to inhibit the APC/C (Fig. 2.6B); under normal conditions neither mechanism is sufficient to induce a cell cycle delay. Consistent with this idea, a Bub3-BubR1 complex has been purified from human cells and suggested to inhibit APC/C activity on its own in

a manner similar to Mad2 (Tang et al., 2001). The bypass we document here suggests that elevating Mad2 levels enhances Mad2-C formation to a point where the Mad1-Mad2 mechanism is sufficient to induce a kinetochore-dependent cell cycle delay in the absence of the BUB-3/Mad3^{SAN-1} branch (Fig. 2.6B). This result suggests that Mad2 levels are limiting for Mad2-C formation *in vivo* and may be tightly controlled to allow integration of the Mad2-C mechanism with Mad3/BUB-3.

In addition to functioning with Mad3^{SAN-1} in the cytoplasm, BUB-3 may also act at the kinetochore, since it does enrich there and its depletion reduces the ability of Mad2^{MDF-2} to enrich at kinetochores. Since both BUB-1 and Mad3 use a similar and mutually exclusive interaction mechanism to associate with BUB-3 (Larsen et al., 2007; Wang et al., 2001), it is tempting to speculate that there are two pools of BUB-3: a population that enriches at kinetochores complexed with BUB-1 and a population that associates with Mad3^{SAN-1} that acts cytoplasmically. It is unclear what effect there is, if any, of kinetochore cycling of BUB-3, presumably via its direct association with BUB-1. It is possible that kinetochore-cycled BUB-3 is modified to potentiate its association with Mad3^{SAN-1} in the cytoplasm, proving another kinetochore-dependent input.

It is interesting to speculate on why the checkpoint signaling pathway is organized into two interacting branches. One possibility is that synergy between the branches may confer a property to the checkpoint signaling circuit

that satisfies its difficult-to-reconcile requirements for potency and lability (Nasmyth, 2005). An attractive alternative possibility is that the Mad1-Mad2 and Mad3/BubR1 mechanisms provide independent inhibitory signals that are responsive to different states – lack of attachment for the Mad1-Mad2 mechanism and lack of tension for the Mad3/BubR1 mechanism. In support of the latter possibility, a Mad3 phosphorylation site targeted by the error correction kinase Aurora B was recently identified and shown to be specifically required for detecting a defect in tension but not in attachment in budding yeast (King et al., 2007a). The two branches may integrate these different inputs to control the stability of Cdc20, which is modulated by checkpoint activation (Pan and Chen, 2004). Further work on the relationship between the Mad1/Mad2 and Mad3/BUB-3 branches may help provide insight into the reasons for this bipartite architecture of the spindle checkpoint pathway.

2.5 Methods

2.5.1 Strains and culture conditions

All *C. elegans* strains were maintained at 20° C. Strain genotypes are listed in table 2.1. The strains OD108 (expressing a GFP fusion with MDF-2), OD109 (expressing a GFP fusion with SAN-1), and OD133 (expressing a GFP fusion with BUB-3), were all generated by cloning the coding (BUB-3, MDF-2) or genomic (SAN-1) sequences into the Spe1 site of pIC26 (Cheeseman et al., 2004) and integrating the constructs into DP38 (*unc-119 (ed3)*) by ballistic

bombardment (Praitis et al., 2001) with a PDS-1000/He Biolistic Particle Delivery System (Bio-Rad). Fluorescence intensity measurements in the nuclear region during early prometaphase (immediately following NEBD) in the AB cell indicate that the GFP::Mad3^{SAN-1} and GFP::BUB-3 proteins are expressed at similar levels (Mean±SD in arbitrary units: 100±16 (n=8) for GFP::Mad3^{SAN-1} and 81±22 (n=9) for GFP-BUB-3) and that the GFP::Mad2^{MDF-2} protein is expressed at a ~3-fold higher level relative to the other two (300±44 (n=16)). The strain RB1391 (*san-1(ok1580)* I; referred to as Mad3$^{san-1}\Delta$) was obtained from the CGC. The strain AG170 was a generous gift from the laboratory of Dr. A. Golden. 2-color strains were constructed by mating as described (Green et al., 2008).

2.5.2 RNA Interference

DsRNA was prepared as described (Oegema et al., 2001). Oligos used for dsRNA production are listed in table 2.2. L4 worms were injected with dsRNA and incubated for 45-48 h at 20°C. For double depletions, dsRNAs were mixed to obtain equal concentrations of >.75 mg/ml for each RNA. Western blots were performed as described previously (Desai et al., 2003).

2.5.3 Microscopy

All images for the timing assays and immunofluorescence were acquired on a DeltaVision deconvolution microscope (Applied Precision) equipped with a CoolSnap CCD camera (Roper Scientific) at 20°C. Z-sections

were acquired at 2-μm steps using a 100x, 1.3 NA Olympus U-Planapo objective with 2 x 2 binning and a 480 x 480 pixel area at 20-sec intervals, and each exposure was 100 msec. Z stacks were projected and imported into MetaMorph (Universal Imaging) to rotate and scale images. Immunofluorescence was performed as described previously (Desai et al., 2003; Oegema et al., 2001). Polyclonal antibodies against BUB-1, BUB-3 (amino acids 189-329), Zwilch^{ZWL-1} (amino acids 1-200) and Mad2^{MDF-2} (splice variant Y39A2AR.30A amino acids 2-203) were generated as described previously (Desai et al., 2003; Oegema et al., 2001). All images acquired using a specific strain or specific antibody were scaled identically.

For GFP::BUB-3, GFP::Mad3^{SAN-1} and GFP::Mad2^{MDF-2} localization, embryos were filmed using a spinning disk confocal mounted on an inverted microscope (Nikon TE2000-E; Nikon) equipped with a 60x 1.4 NA Plan Apochromat lens (Nikon), a krypton-argon 2.5-W water-cooled laser (Spectra-Physics) and an electron multiplication back-thinned charge-coupled device camera (iXon; Andor Technology). Acquisition parameters, shutters, and focus were controlled by MetaMorph software (MDS Analytical Technologies). 5 x 1 μm RFP/GFP z series with no binning and a single central reference DIC image with no binning were collected every 20 seconds. Exposures were 300 ms for both GFP and RFP, and 200 ms for DIC (laser power = 50%).

To specifically measure kinetochore-localized GFP::Mad2^{MDF-2}, a subtraction approach (Dammermann et al., 2008) was used. See Suppl. Fig. 2.3 legend for details.

2.6 Acknowledgements

We thank members of the Oegema and Desai labs for discussions and advice; Paul Maddox for help with imaging; Julien Espeut and Reto Gassmann for help with biochemistry; Andy Golden, Ann Rose and Pamela Padilla for strains and other reagents. This work was supported by the UCSD Genetics Training Grant (A.E.), a grant from the NIH to A.D. (GM074215) and by funding from the Ludwig Institute for Cancer Research to A.D. and K.O. This chapter has appeared in print under the following citation: *Mol. Biol. Cell*, 2009(4):1252-67, Essex A, Dammermann A, Lewellyn L, Oegema K, and Desai A. The dissertation author was the primary researcher and author of this paper.

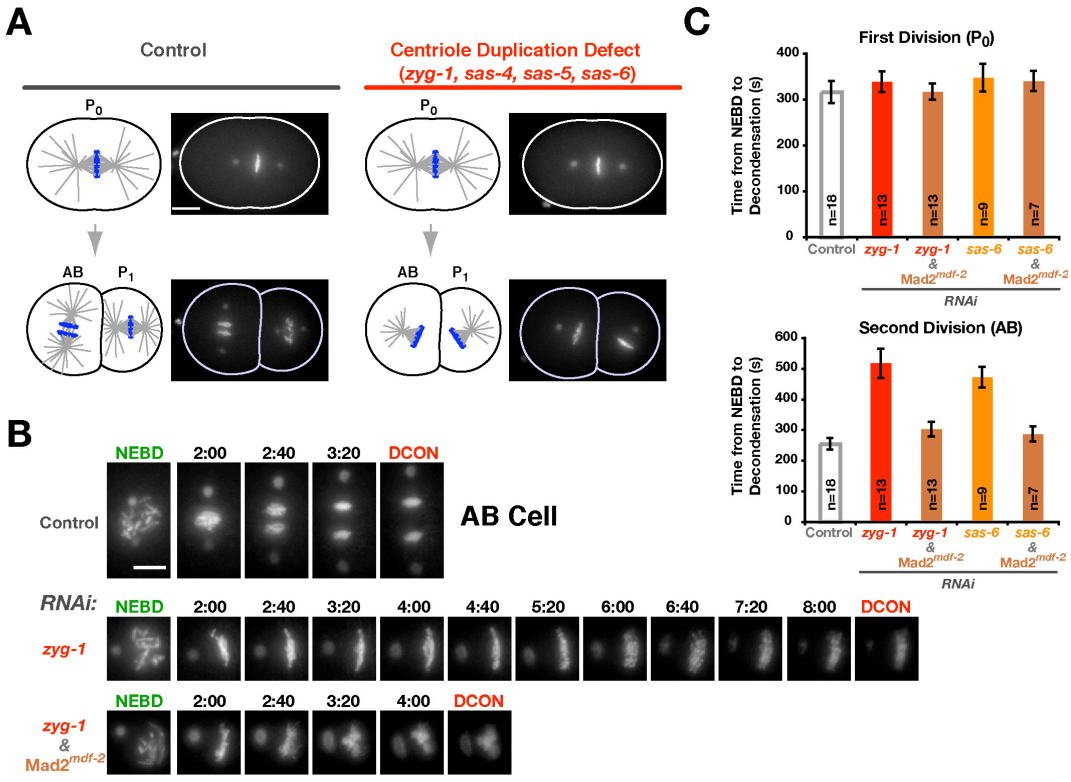

Figure 2.1 (A-C). Controlled monopolar spindle formation in *C. elegans* embryos results in a spindle checkpoint-mediated cell cycle delay

(A) Selected frames from time-lapse sequences of the first (P_0), second (AB), and third (P_1) divisions of embryos expressing GFP-histone H2B (*arrow*) and GFP-γ-tubulin (*arrowheads*), accompanied by schematics to the left of each image. Control embryos (***left***) have bipolar mitotic spindles in all divisions. In embryos depleted of proteins necessary for centriole duplication (***right***), the P_0 cell assembles a bipolar spindle (with one sperm-derived centriole at each spindle pole) but the subsequent AB and P_1 cells inherit only one centriole and assemble monopolar spindles. Scale bar = 10 μm. **(B)** Selected frames from time-lapse sequences of control, *zyg-1(RNAi)*, and *zyg-1+mdf-2 (RNAi)* embryos expressing GFP-histone H2B and GFP-gamma tubulin. Only the AB cell spindle region is shown. Numbers above panels indicate time after NEBD in min:sec; DCON indicates time of chromosome decondensation. Scale bar = 5 μm. **(C)** The mean NEBD to DCON interval for the indicated conditions is plotted for both the first (P_0, top) and second (AB, bottom) mitotic divisions.

D

	Embryonic RNAi Phenotype
Mad1 (MDF-1)	Viable
Mad2 (MDF-2)	Viable
Mad3 (SAN-1)	Viable
Bub1 (BUB-1)	Emb
Bub3 (BUB-3)	Viable
Rod (ROD-1)	Emb
Zwilch (ZWL-1)	Emb
Zw10 (CZW-1)	Ste

E

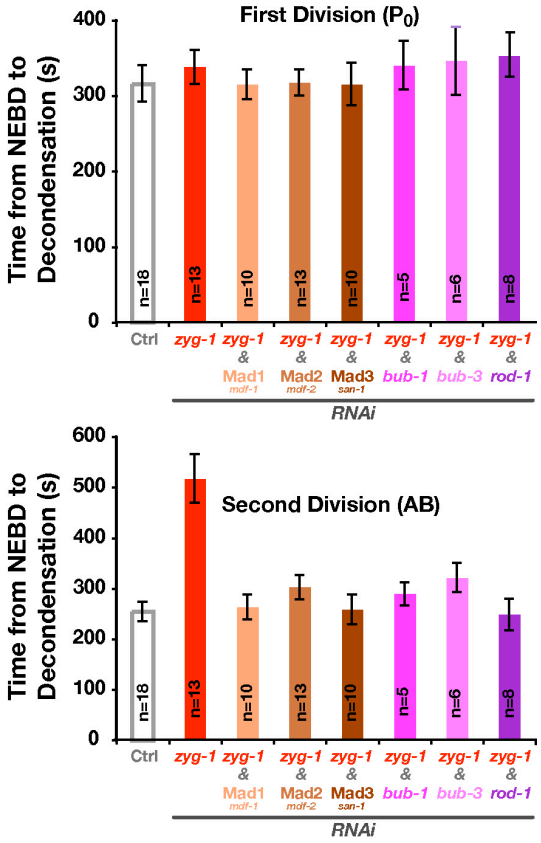

Figure 2.1 (D-E). Controlled monopolar spindle formation in *C. elegans* embryos results in a spindle checkpoint-mediated cell cycle delay

(D) Summary of the effect of depleting the *C. elegans* orthologs of spindle checkpoint proteins on embryo viability. L4 hermaphrodites were injected with dsRNAs and the consequences on embryo viability assessed 36-48 hours after injection. **(E)** The mean NEBD to DCON interval for the indicated conditions is plotted for both the first (P_0, ***top***) and second (AB, ***bottom***) mitotic divisions. Error bars are the 95 % confidence interval.

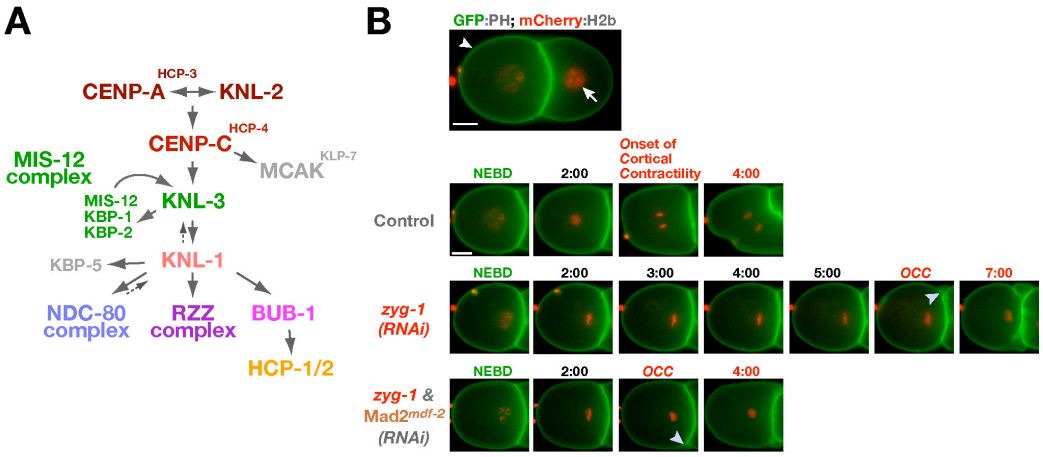

Figure 2.2 (A-B). Systematic analysis comparing the position of components in the kinetochore assembly hierarchy to their role in checkpoint activation.

(A) Summary of the kinetochore assembly pathway in *C. elegans* embryos. **(B)** Selected frames from time-lapse sequences of control, *zyg-1(RNAi)*, and *zyg-1*+Mad2^{mdf-2}*(RNAi)* embryos expressing GFP::PH and mCherry::Histone H2B to mark the plasma membrane and the chromosomes, respectively. The interval from NEBD to onset of cortical contractility (OCC, *arrowheads*) was measured. Scale bar = 10 µm.

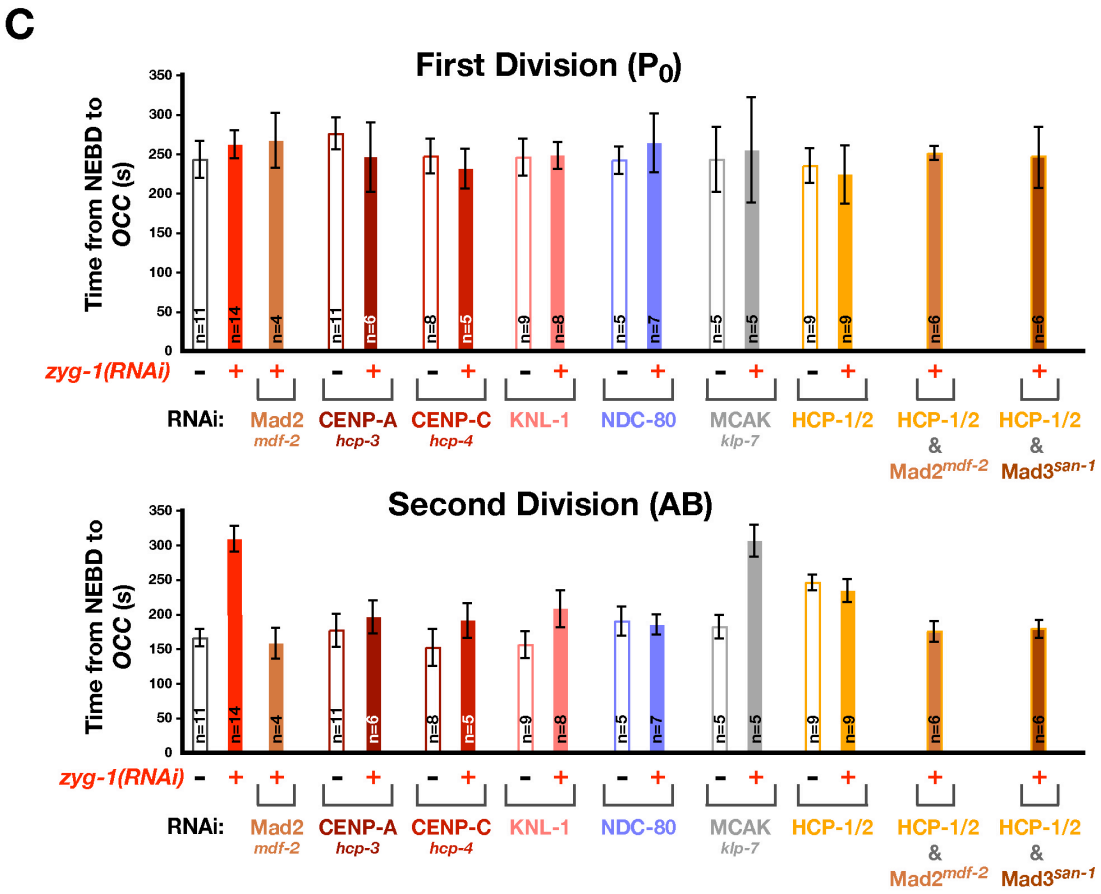

Figure 2.2 (C). Systematic analysis comparing the position of components in the kinetochore assembly hierarchy to their role in checkpoint activation.

(C) The mean NEBD to OCC interval for the indicated conditions is plotted for both the first (P_0, ***top***) and second (AB, ***bottom***) mitotic divisions. Error bars are the 95 % confidence interval.

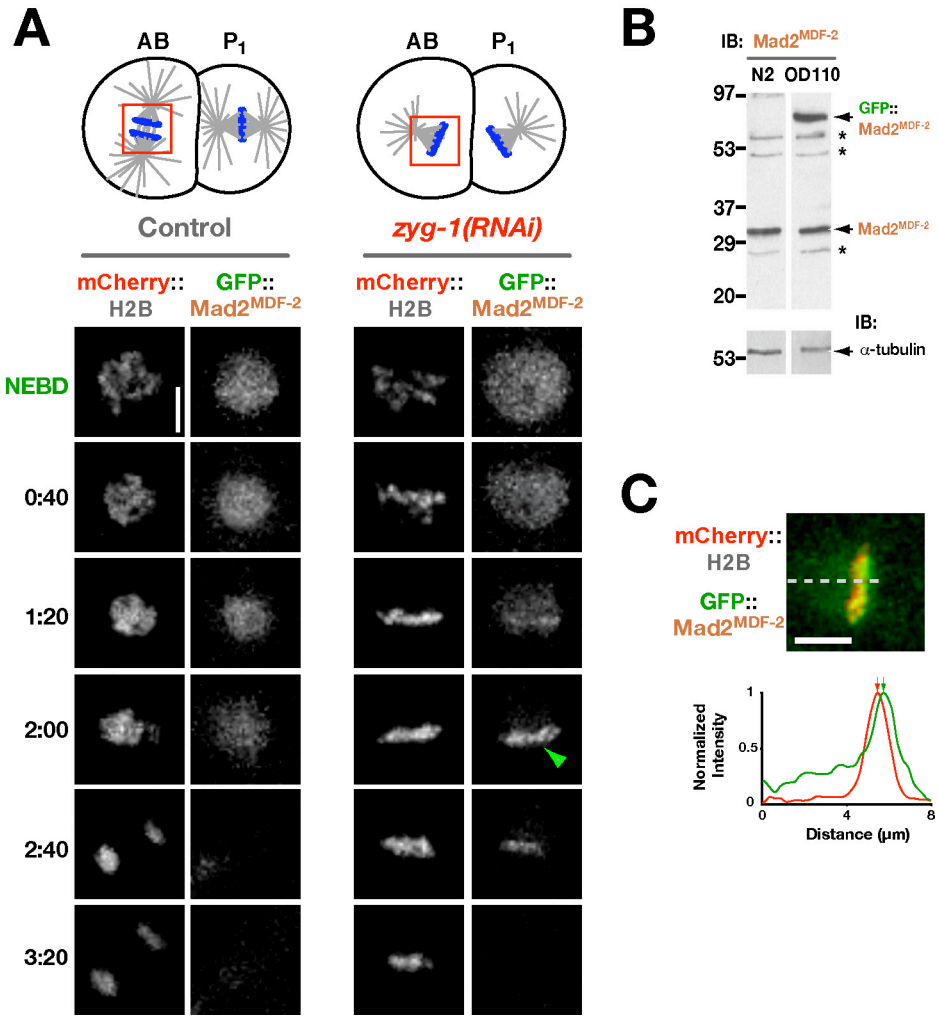

Figure 2.3 (A-C). The accumulation of GFP::Mad2^{MDF-2} on chromosomes associated with monopolar spindles correlates with checkpoint activation.

(A) Selected frames from time-lapse sequences of embryos expressing GFP::Mad2^{MDF-2} and mCherry::H2B that have normal bipolar spindles (control, left) or monopolar spindles (zyg-1(RNAi), right). Images correspond to boxed regions of the AB cell depicted in the schematics. GFP-MDF-2 $^{MDF-2}$ fluorescence accumulates on chromosomes associated with monopolar spindles (green arrowhead). Scale bar = 5 μm. **(B)** A western blot of N2 (wild-type) and OD110 (co-expressing mCherry::H2b and GFP::Mad2 $^{MDF-2}$) strains was probed with an anti::Mad2 $^{MDF-2}$ antibody. The Mad2 $^{MDF-2}$ and GFP::Mad2 $^{MDF-2}$ bands are indicated; asterisks mark non-specific bands that are not eliminated by Mad2 $^{MDF-2}$ RNAi. The blot was also probed with an antibody to α-tubulin as a loading control. **(C)** GFP::Mad-2 $^{MDF-2}$ accumulates asymmetrically on the chromosomal surface pointing away from the single spindle pole in monopolar spindles. The line scan (5-pixel wide; normalized relative to maximum intensity in each channel) illustrates the asymmetric distribution. Scale bar = 5 μm.

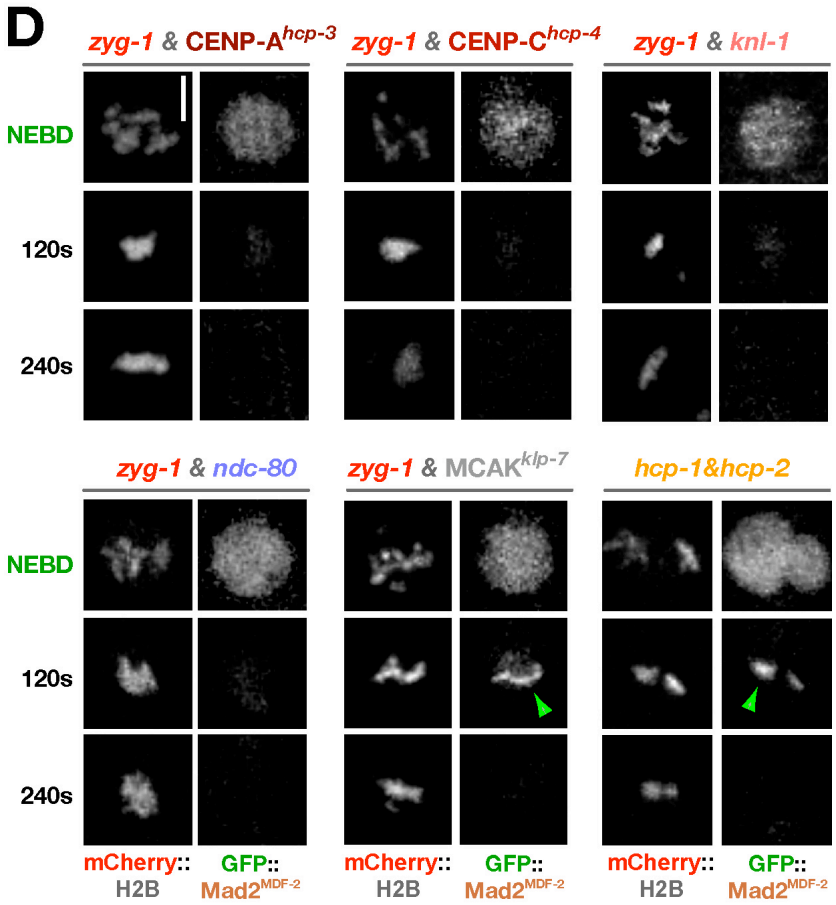

Figure 2.3 (D). The accumulation of GFP::Mad2MDF-2 on chromosomes associated with monopolar spindles correlates with checkpoint activation.

(D) Selected frames from time-lapse sequences of GFP::Mad2 $^{MDF-2}$;mCherry::H2B strain following the indicated perturbations of kinetochore proteins. Note GFP::Mad2 $^{MDF-2}$ accumulation at kinetochores (green arrowheads) in zyg-1+MCAK^{klp-7}(RNAi) and in hcp-1/2 (RNAi). Scale bar = 5 μm.

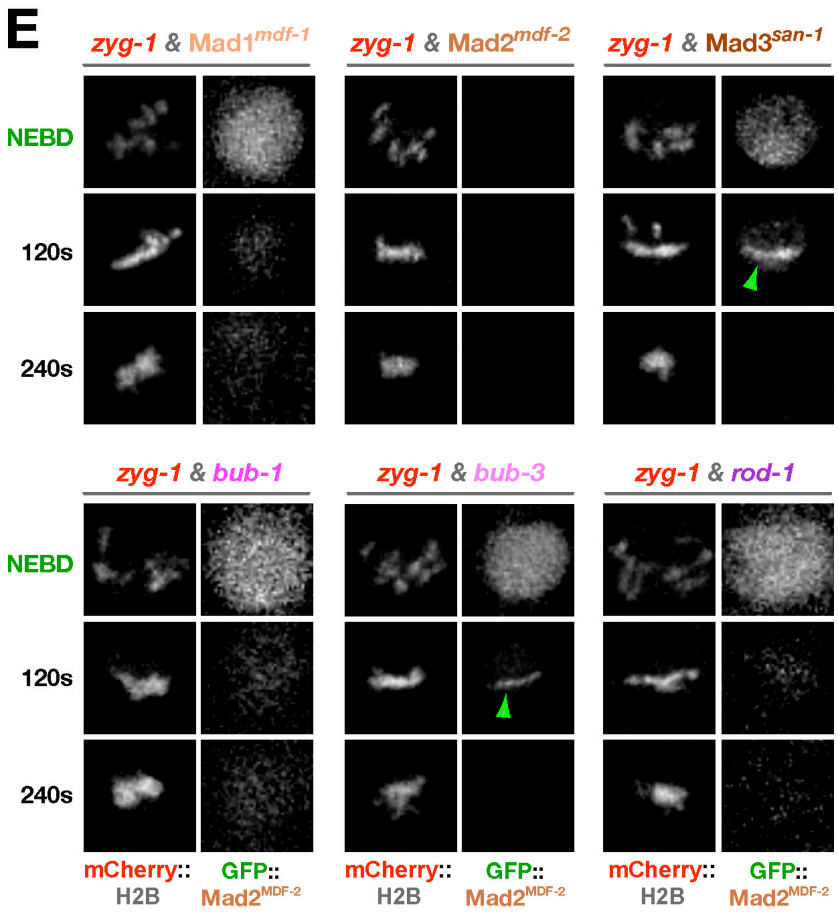

Figure 2.3 (E). The accumulation of GFP::Mad2^{MDF-2} on chromosomes associated with monopolar spindles correlates with checkpoint activation.

(E) Selected frames from time-lapse sequences of GFP::Mad2^{MDF-2};mCherry::H2B strain following the indicated perturbations of conserved checkpoint proteins. Note GFP::Mad2^{MDF-2} accumulation at kinetochores (*green arrowheads*) in *zyg-1*+Mad3^{san-1}*(RNAi)* and *zyg-1+bub-3(RNAi)*. Scale bar = 5 μm.

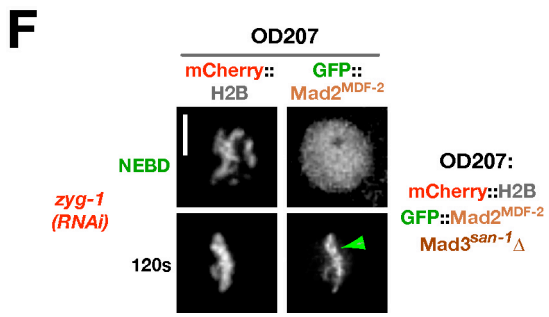

Figure 2.3 (F). The accumulation of GFP::Mad2^{MDF-2} on chromosomes associated with monopolar spindles correlates with checkpoint activation.

(F) Selected frames from a time-lapse sequence of a monopolar spindle (AB cell) in the Mad3$^{san-1\Delta}$ mutant strain into which the GFP::Mad2 $^{MDF-2}$ transgene was introduced by mating. Note accumulation of Mad2 $^{MDF-2}$ at kinetochores (green arrowhead). Scale bar = 5 μm.

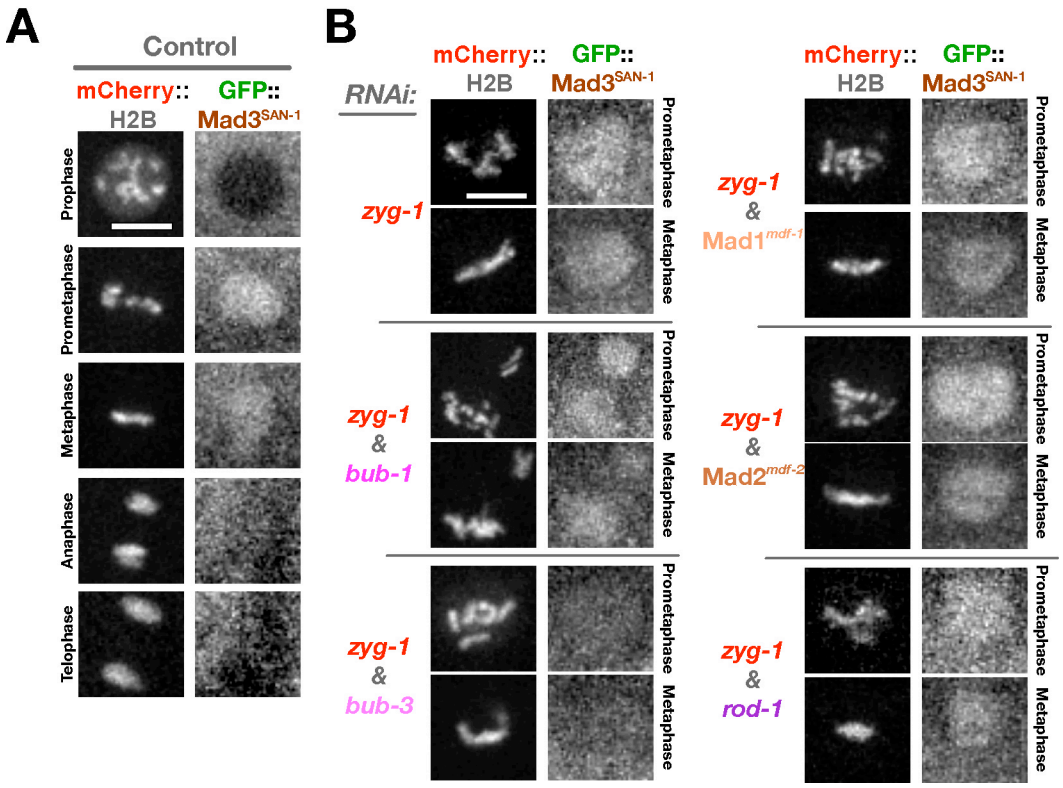

Figure 2.4 (A-B). Analysis of Mad3^{SAN-1} and BUB-3 localization in control and checkpoint-activated embryos.

(A, B) Selected frames from time-lapse sequences of embryos co-expressing mCherry::Histone H2b and GFP::Mad3^{SAN-1} are shown for the indicated conditions. GFP::Mad3^{SAN-1} is diffusely localized in the nuclear area in control embryos (A) but does not accumulate at unattached kinetochores of monopolar spindles (zyg-1(RNAi) in (B); in addition, fluorescence levels of GFP::Mad^{SAN-1} are significantly reduced by depletion of BUB-3 (compare with Mad3^{san-1}(RNAi) shown in Fig. S4B). Scale bars = 5 µm.

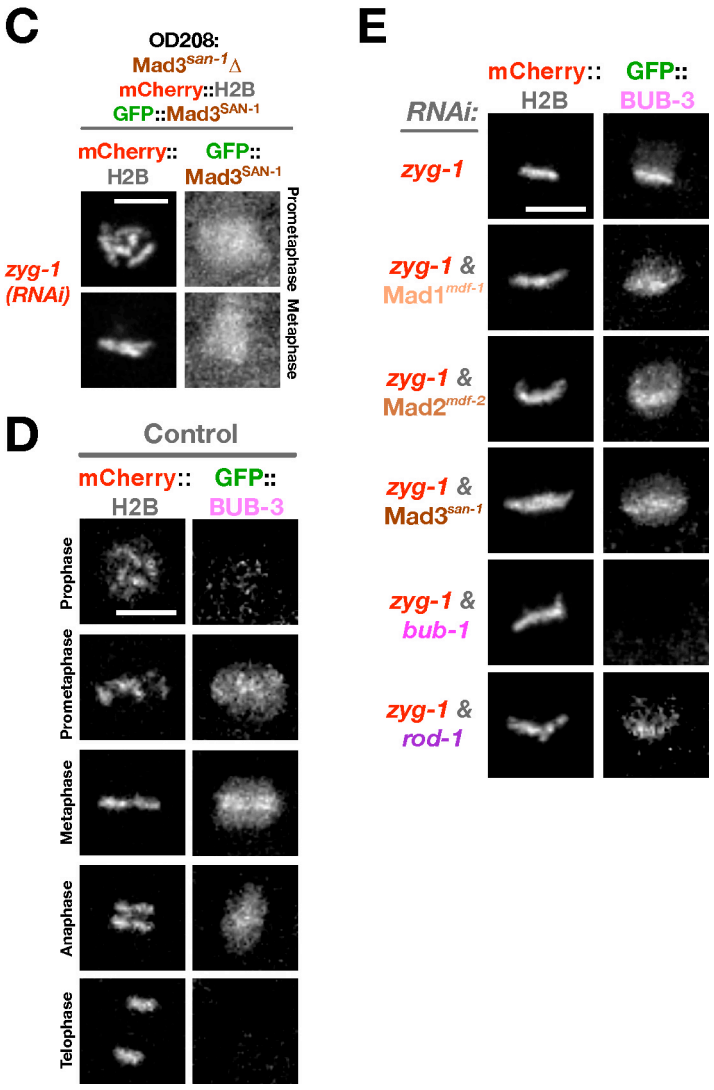

Figure 2.4 (C-E). Analysis of Mad3^{SAN-1} and BUB-3 localization in control and checkpoint-activated embryos.

(C) GFP::Mad3^{SAN-1} fails to accumulate at kinetochores of monopolar spindles even when endogenous Mad3^{SAN-1} is absent. Selected frames from a Mad3^{san-1}Δ mutant embryo into which the GFP::Mad3^{SAN-1} transgene was introduced by mating. Scale bar = 5 μm. **(D, E)** Selected frames from time-lapse sequences of embryos co-expressing mCherry::Histone H2b and GFP::BUB-3 are shown for the indicated conditions. Unlike GFP::Mad2^{MDF-2} and GFP::Mad3^{SAN-1}, GFP::BUB-3 is detected at kinetochores of bipolar spindles of control embryos. GFP::BUB-3 additionally accumulates on unattached kinetochores associated with monopolar spindles (*zyg-1(RNAi)* in *E*). GFP::BUB-3 localization to kinetochores depends on BUB-1 but is independent of Mad1^{MDF-1}, Mad2^{MDF-2} or Mad3^{SAN-1}; depletion of ROD-1, a subunit of the RZZ complex, reduces BUB-3 accumulation on unattached kinetochores. Scale bars = 5 μm.

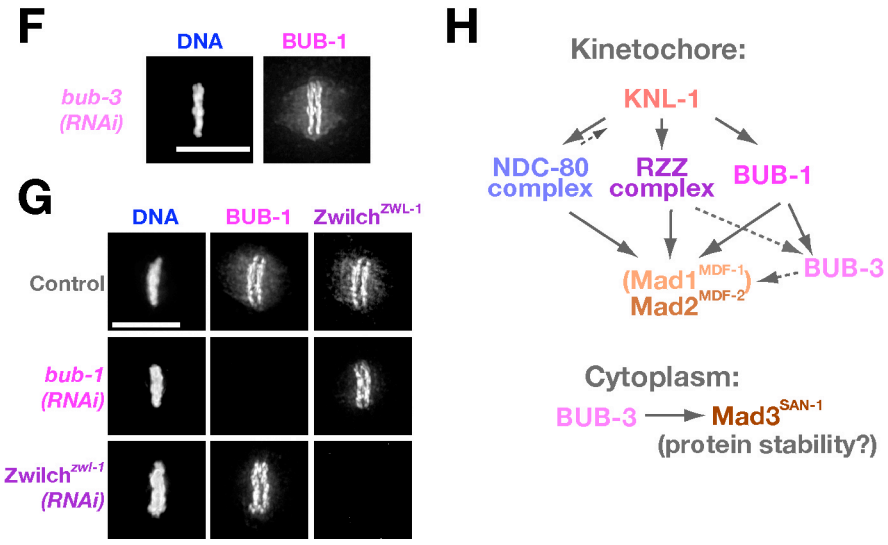

Figure 2.4 (F-H). Analysis of Mad3^{SAN-1} and BUB-3 localization in control and checkpoint-activated embryos.

(F) BUB-3 depletion does not perturb kinetochore localization of BUB-1. The efficacy of the BUB-3 depletion was established using immunofluorescence with an anti-BUB-3 antibody (Fig. S5). Scale bar = 10 μm. **(G)** BUB-1 and the RZZ Complex target independently of each other to the kinetochore. Scale bar=10 μm. (**H**) Summary of the relationships between outer kinetochore components and Mad2^{MDF-2} and BUB-3 localization at checkpoint-signaling kinetochores.

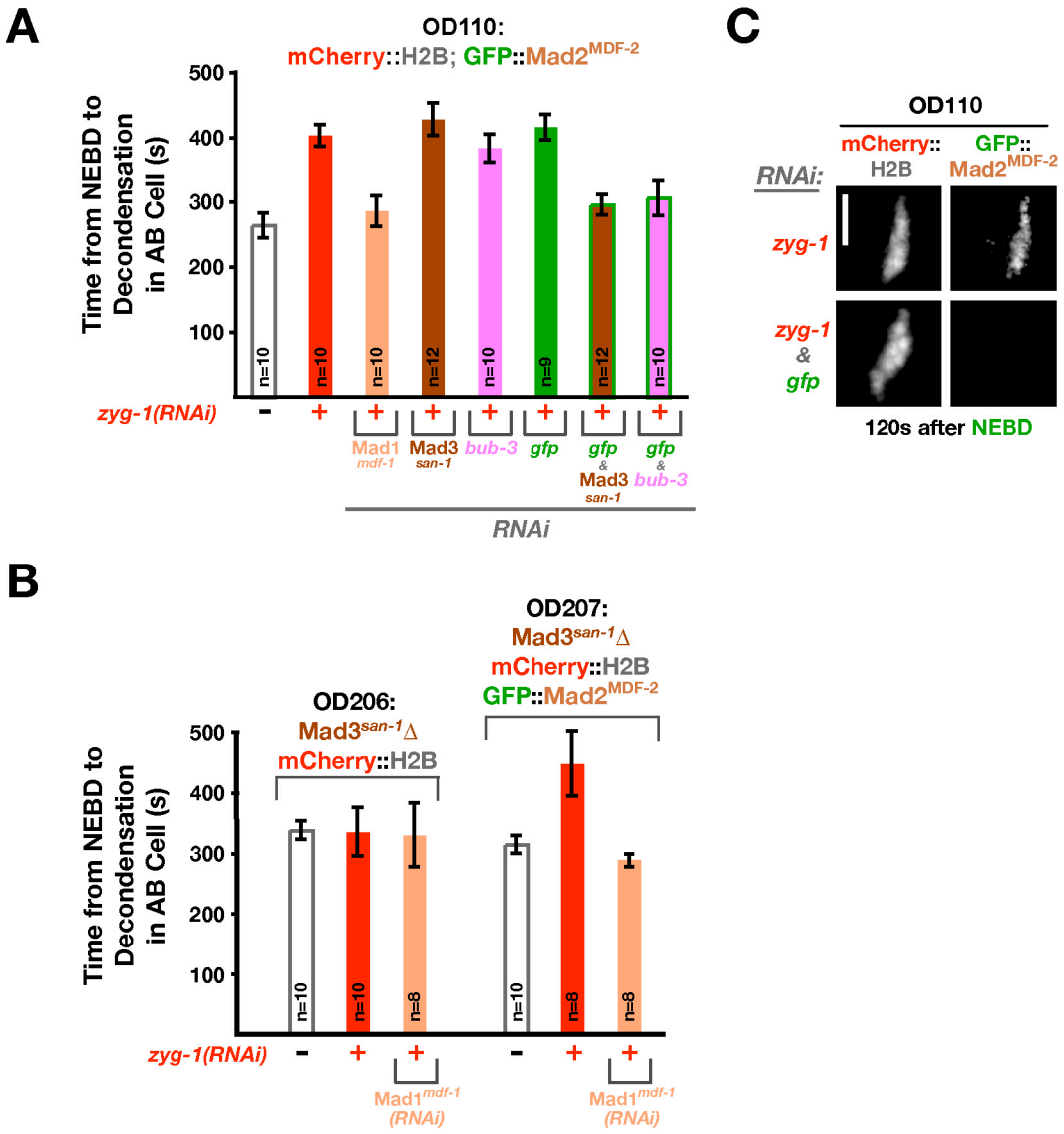

Figure 2.5. A subtle increase in Mad2^{MDF-2} levels bypasses the requirement for Mad3^{SAN-1} and BUB-3 in generating a monopolar spindle-induced cell cycle delay.

(A,B) The mean NEBD to DCON interval in the AB cell is plotted for the indicated conditions/strains. Error bars are the 95 % confidence interval. **(C)** A selected frame (120s after NEBD) from time-lapse sequences of the GFP::Mad2^{MDF-2} transgene-expressing strain injected with dsRNAs targeting *zyg-1* alone (*top row*) or GFP and *zyg-1* (*bottom row*). Scale bar = 5 µm.

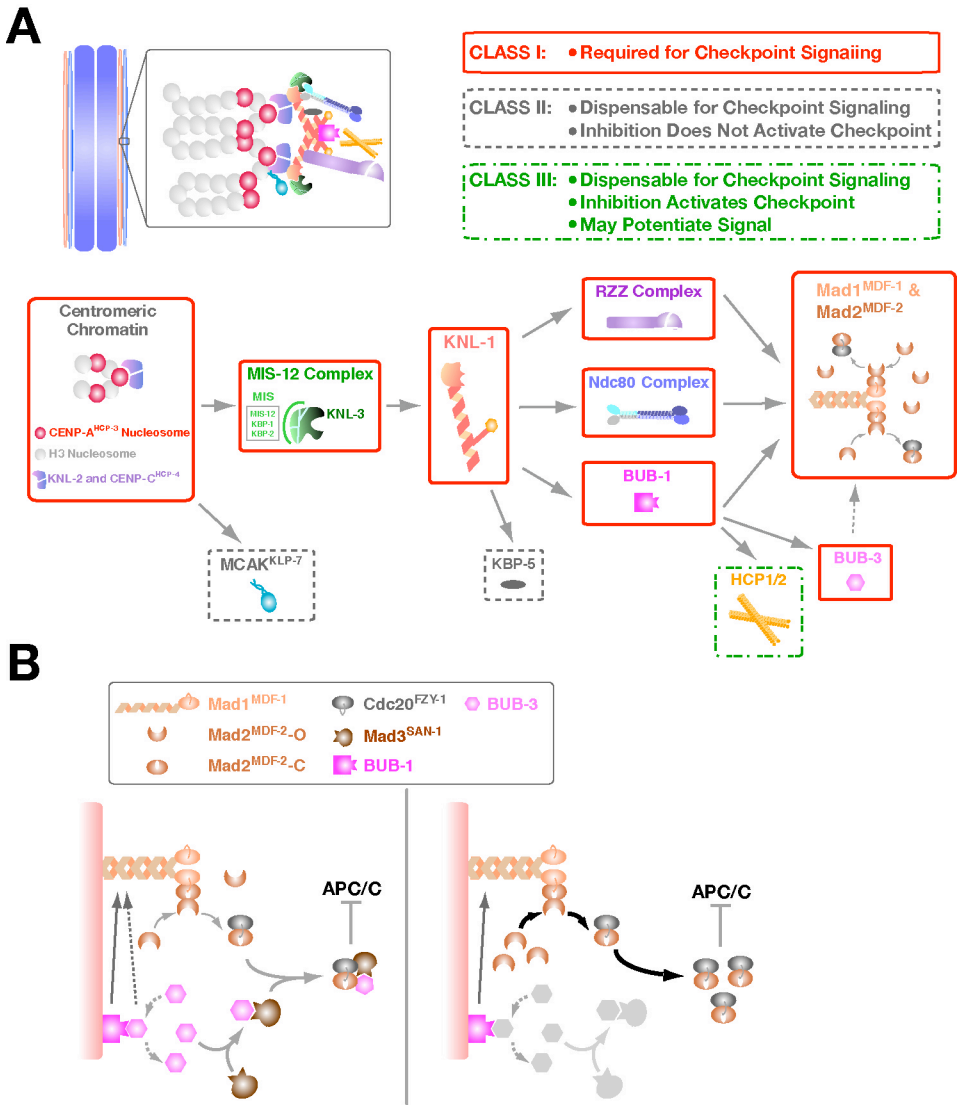

Figure 2.6. Summary of the systematic analysis and a model for the bypass of Mad3^{SAN-1} and BUB-3 by a subtle increase in Mad2^{MDF-2} levels.
(A) Summary of the requirements for checkpoint activation & GFP::Mad2^{MDF-2} accumulation at unattached kinetochores. Kinetochore components are placed into different functional groups based on prior *in vivo* and *in vitro* studies. The three classes of components, with respect to their role in checkpoint activation, are defined in the legend and are indicated by the colored boxes. **(B)** A model based on the Mad2 "template/conformational dimerization" model for why an increase in Mad2^{MDF-2} levels reduces the need for Mad3^{SAN-1} and BUB-3 to induce a kinetochore-dependent cell cycle delay. For simplicity, free Cdc20^{FZY-1} molecules are not drawn. In the left panel, the wild-type is depicted, in which Mad2-C generated at the kinetochore is integrated with cytoplasmic Mad3^{SAN-1}/BUB-3 to inhibit the APC/C. In the right panel, an increased flux of Mad2 results in higher levels of Mad2-C and bypasses the requirement for Mad3^{SAN-1}/BUB-3.

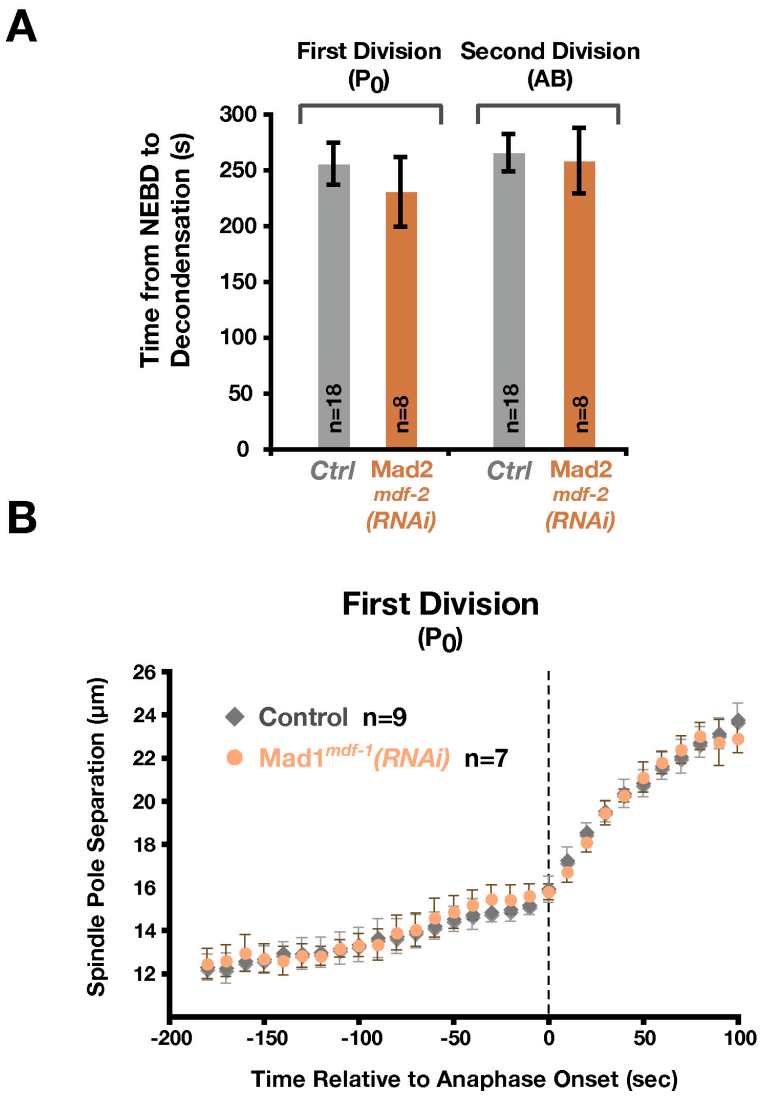

Figure S2.1. Mad2^{MDF-2} depletion does not affect the first mitotic division.
(A) The NEBD-DCON interval measured in the first (P_0) and second (AB) embryonic divisions for the indicated conditions in a strain expressing GFP-histone H2b and GFP-γ-tubulin. The number of control and Mad2^{MDF-2}-depleted embryos analyzed are indicated in the bars of the graph. Error bars represent the S.E.M. with a 95% confidence interval. The Control values shown for P_0 are the same as those in Figure 1. **(B)** Kinetochore-spindle microtubule interactions are unaffected by depletion of Mad1^{MDF-1}. Spindle pole positions were tracked at 10s intervals; different movies were time-aligned with respect to anaphase onset (t=0) and the average value plotted for each time point. Error bars represent the S.E.M. with a 95% confidence interval. Similar results were obtained in Mad2^{MDF-2}, Mad3^{SAN-1} and Mad2^{MDF-2} & Mad3^{SAN-1} co-depleted embryos.

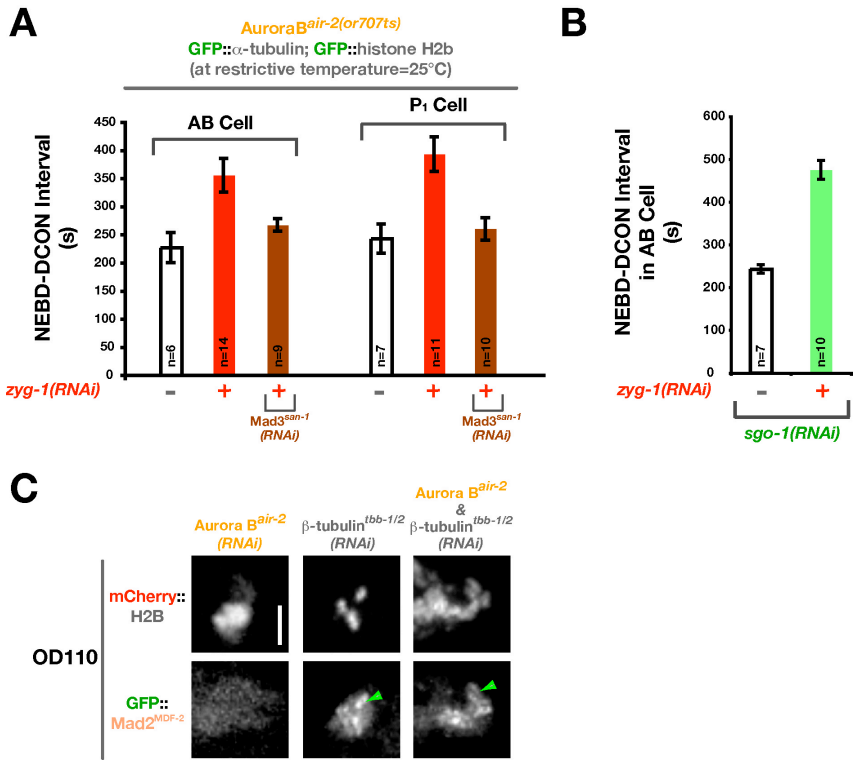

Figure S2.2. The checkpoint is independent of Aurora B^{AIR-2} and SGO-1. **(A)** Aurora B^{AIR-2} inhibition does not abrogate the monopolar spindle-induced delay. Aurora B^{AIR-2} (and the entire chromosomal passenger complex) is essential for meiotic chromosome disjunction and cytokinesis in *C. elegans* embryos (e.g. see Oegema et al., 2001). Consequently, Aurora B inhibition by RNAi results in a fertilized one-cell embryo with a highly aberrant genome (no polar bodies are formed) that does not undergo cytokinesis to form a 2-cell embryo (see supplementary movies for Oegema et al. 2001). This phenotype prevents use of the monopolar spindle assay that we developed to study checkpoint signaling. Aurora inhibitors do not work in *C. elegans;* inhibitor studies are also complicated by the embryo eggshell, which is impermeable. To overcome the above limitations we utilized a conditional mutation (*or707ts*) in Aurora B^{air-2} identified in a prior study (Severson et al., 2000 *Curr. Biol.* 10(19):1162-71). In this mutant, there is a Proline to Leucine substitution in subdomain XI of the kinase domain that leads to a temperature sensitive loss-of-function phenotype (see Severson et al. 2000 for a thorough characterization). We obtained this mutant and crossed it into a strain expressing GFP::alpha-tubulin and GFP::histone H2b. We then performed fast-acting temperature shifts on a microscope to analyze the consequences of reducing Aurora B activity *after* the first cell division was finished (we used cytokinesis failure, a consequence of Aurora B inhibition, as a means to assess efficacy of the temperature shift). We compared the indicated conditions at the restrictive temperature and quantified the NEBD-DCON interval in both AB & P_1 cell divisions. Inhibition of AuroraB^{AIR-2} did not abrogate the monopolar spindle induced delay – co-depletion of Mad3^{SAN-1} eliminated the delay. **(B)** *sgo-1(RNAi)* does not abrogate the monopolar spindle-induced delay. **(C)** GFP::Mad2^{MDF-2} enrichment at unattached kinetochores is not significantly affected by AuroraB^{AIR-2} RNAi. Unattached kinetochores were generated in the first division using a dsRNA targeting α-tubulin.

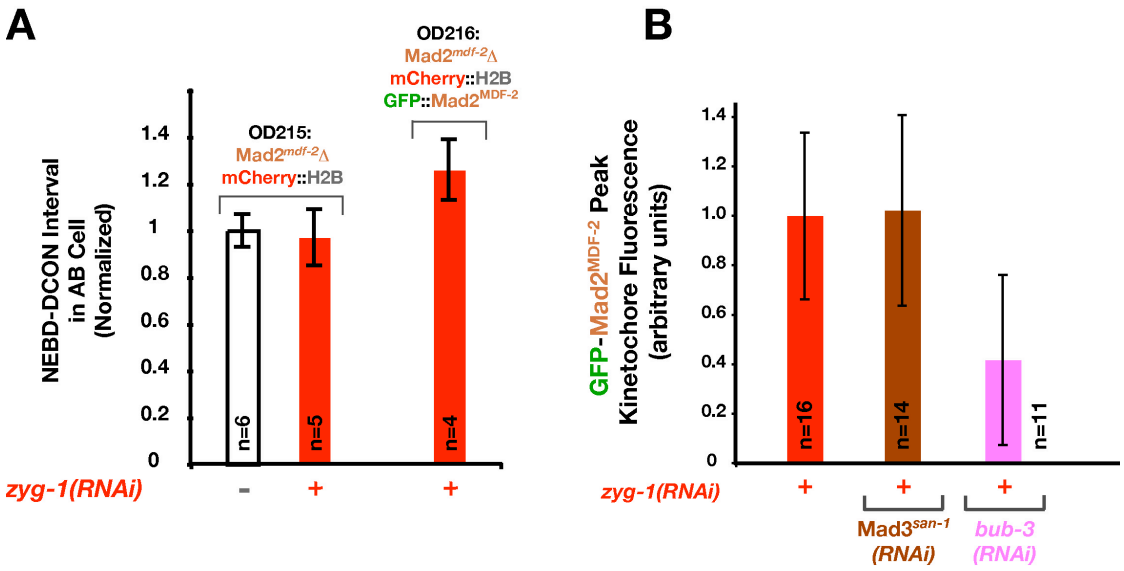

Figure S2.3. Analysis of the GFP::Mad2^{MDF-2} transgene.
(A) The GFP-Mad2^{MDF-2} transgene expressed under control of the *pie-1* promoter causes a monopolar spindle-induced delay in the second division of a strain in which endogenous Mad2^{MDF-2} is absent. The NEBD-DCON intervals measured in the two different strains (OD215 and OD216) and indicated conditions were normalized relative to the same interval measured in AB cells with bipolar spindles in the deletion mutant strain (OD215). The general sickness and very low brood size of the Mad2$^{mdf-2}\Delta$ strain, which is partially rescued by the GFP::Mad2^{MDF-2} transgene (*not shown*), limited analysis of the early embryonic divisions in these experiments. Error bars represent the 95% confidence interval – errors were propagated through the normalization using Graphpad (http://www.graphpad.com/quickcalcs/ErrorProp1.cfm?Format=SEM). **(B)** Effect of depleting Mad3^{SAN-1} or BUB-3 on peak kinetochore levels of GFP-Mad2^{MDF-2} in AB cells with monopolar spindles. To specifically measure kinetochore-localized GFP::Mad2^{MDF-2}, a subtraction approach, similar to Dammermann et al. (2008), was used. Total fluorescence in the nuclear region (measured by integrating fluorescence intensity in a box surrounding the nucleus after subtracting cytoplasmic background), which included kinetochore-localized fluorescence, was measured for each of the indicated conditions and also for *zyg-1+rod-1(RNAi)*, where kinetochore accumulation of Mad2^{MDF-2} is inhibited. Each sequence was normalized relative to the total fluorescence at NEBD and the values measured at each time point for the *zyg-1+rod-1(RNAi)* were subtracted from the same time points of the indicated conditions to specifically isolate kinetochore-specific GFP::Mad2^{MDF-2} fluorescence. The peak of GFP::Mad2^{MDF-2} accumulation was slightly earlier relative to NEBD in Mad3^{SAN-1} depletion, in comparison to the monopolar control, but the magnitude of the peak was indistinguishable from the monopolar control. BUB-3 depletion resulted in peak fluorescence approximately half that of the monopolar control. Errors were propagated throughout the analysis and the 95% confidence interval is plotted.

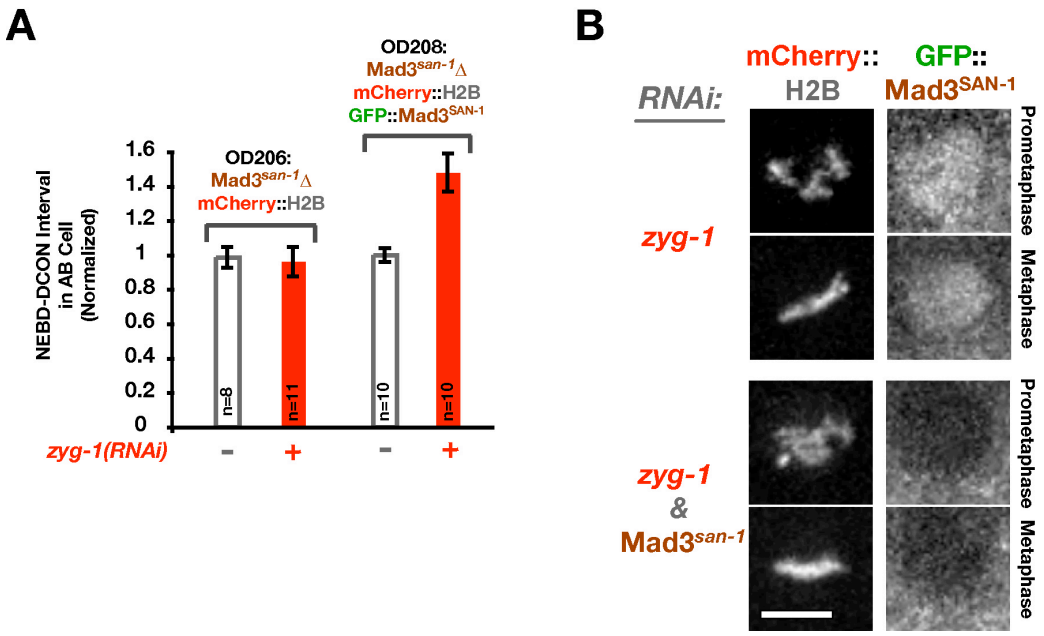

Figure S2.4. Analysis of the GFP::Mad3^{SAN-1} transgene.
(A) The GFP::Mad3^{SAN-1} transgene expressed under control of the *pie-1* promoter causes a monopolar spindle-induced delay in the second division of a strain in which endogenous Mad3^{SAN-1} is absent. The NEBD-DCON intervals measured after *zyg-1(RNAi)* were normalized relative to the same interval measured without *zyg-1(RNAi)* in each strain. Error bars represent the 95% confidence interval – errors were propagated through the normalization using Graphpad (http://www.graphpad.com/quickcalcs/ErrorProp1.cfm?Format=SEM).
(B) The diffuse nuclear region fluorescence of GFP::Mad3^{SAN-1} is eliminated by Mad3^{san-1}*(RNAi)*. Scale bar = 5 µm.

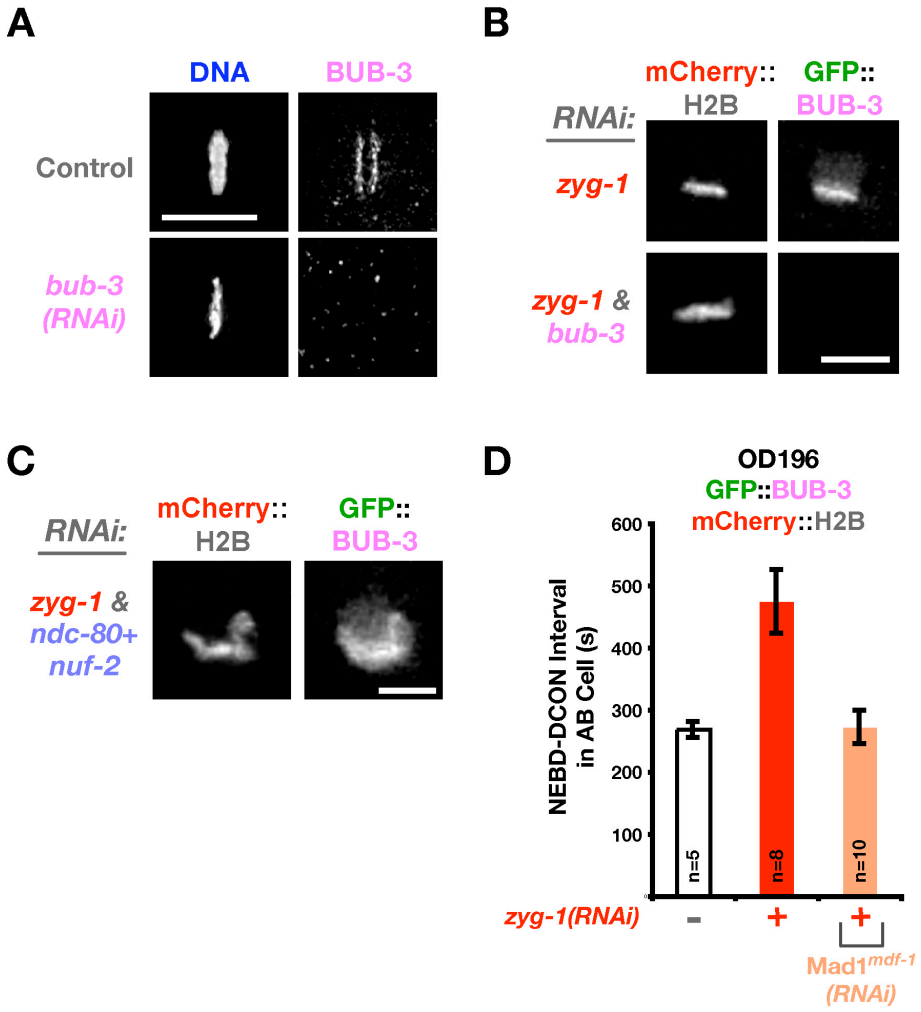

Figure S2.5. Analysis of endogenous and GFP::BUB-3.
(A) Localization of endogenous BUB-3 in a one-cell embryo with a bipolar spindle. *bub-3(RNAi)* eliminates the observed kinetochore localization. Scale bar = 10 μm. **(B)** Accumulation of GFP::BUB-3 at kinetochores on chromosomes associated with monopolar spindles is eliminated by *bub-3(RNAi)*. Scale bar = 5 μm. **(C)** GFP::BUB-3 kinetochore localization is independent of the NDC-80 complex. **(D)** Mad1^{MDF-1} is required for the monopolar spindle-induced delay in the GFP-BUB-3 strain.

Table 2.1. Worm strains used in this study.

Strain #	Genotype	Label in Figures & Movies
TH32	*unc-119(ed3) III; ruIs32 [pAZ132; pie-1/GFP::histone H2B] III; ddIs6 [GFP::tbg-1; unc-119(+)]*	GFP-histone H2b; GFP-γ-tubulin
OD56	*unc-119(ed3) III; ltIs37 [pAA64; pie-1/mCherry::his-58; unc-119 (+)] IV*	mCherry-histone H2b
OD95	*unc-119(ed3) III; ltIs37 [pAA64; pie-1/mCherry::his-58; unc-119 (+)] IV; ltIs38 [pAA1; pie-1/GFP::PH(PLC1delta1); unc-119(+)]*	mCherry-histone H2b; GFP-PH
OD108	*unc-119(ed3) III; ltIs52 [pOD379; pie-1/GFP::Y69A2AR.30; unc-119 (+)]*	GFP-Mad2^{MDF-2}
OD109	*unc-119(ed3) III; ltIs53 [pOD380; pie-1/GFP::ZC328.4; unc-119 (+)]*	GFP-Mad3^{SAN-1}
OD110	*unc-119(ed3) III; ltIs52 [pOD379; pie-1/GFP::Y69A2AR.30; unc-119 (+)]; ltIs37 [pAA64; pie-1/mCherry::his-58; unc-119 (+)] IV*	mCherry-histone H2b; GFP-Mad2^{MDF-2}
OD133	*unc-119(ed3) III; ltIs73 [pOD377; pie-1/GFP::Y54G9A.6; unc-119 (+)]*	GFP-BUB-3
OD196	*unc-119(ed3) III; ltIs73 [pOD377; pie-1/GFP::Y54G9A.6; unc-119 (+)], ltIs37 [pAA64; pie-1/mCherry::his-58; unc-119 (+)] IV*	mCherry-histone H2b; GFP-BUB-3
OD197	*unc-119(ed3) III; ltIs53 [pOD380; pie-1/GFP::ZC328.4; unc-119 (+)], ltIs37 [pAA64; pie-1/mCherry::his-58; unc-119 (+)] IV*	mCherry-histone H2b; GFP-Mad3^{SAN-1}
OD206	*unc-119(ed3) III; ltIs37 [pAA64; pie-1/mCherry::his-58; unc-119 (+)] IV; san-1(ok1580) I*	mCherry-histone H2b; *san-1*Δ
OD207	*unc-119(ed3) III; ltIs52 [pOD379; pie-1/GFP::Y69A2AR.30; unc-119 (+)], ltIs37 [pAA64; pie-1/mCherry::his-58; unc-119 (+)] IV, san-1(ok1580) I*	mCherry-histone H2b; GFP-Mad2^{MDF-2}; *san-1*Δ
OD208	*unc-119(ed3) III; ltIs53 [pOD380; pie-1/GFP::ZC328.4; unc-119 (+)], ltIs37 [pAA64; pie-1/mCherry::his-58; unc-119 (+)] IV, san-1(ok1580) I*	mCherry-histone H2b; GFP-Mad3^{SAN-1}; *san-1*Δ
OD215	*unc-119(ed3) III; ltIs37 [pAA64; pie-1/mCherry::his-58; unc-119 (+)] IV; mdf-2(tm2190)*	mCherry-histone H2b; *mdf-2*Δ

Table 2.1 (Continued). Worm strains used in this study.

Strain #	Genotype	Label in Figures & Movies
OD216	*unc-119(ed3) III; ltIs52 [pOD379; pie-1/GFP::Y69A2AR.30; unc-119 (+)], ltIs37 [pAA64; pie-1/mCHERRY::his-58; unc-119 (+)] IV, mdf-2(tm2190)*	mCherry-histone H2b; GFP-Mad2^{MDF-2}; *mdf-2*Δ
RB1391	*san-1(ok1580) I*	N/A – Source strain for *san-1*Δ
AG170	*mdf-2(tm2190)*	N/A – Source strain for *mdf-2*Δ

Table 2.2. Double-stranded RNAs used in this study.

RNA #	Gene #	Name	Conc. mg/ml	Oligo #1	Oligo #2	Template
2	Y69A2AR.30	*mdf-2*	3.2	TAATACGACTCACTATAGGgagaccacacggatgtaaagacacaaaacg	TAATACGACTCACTATAGGgagaccacgtgaactgacgtcgagaatgag	cDNA
3	F55G1.4	*rod-1*	2.1	TAATACGACTCACTATAGGgagaccactcgtatggaaagtatgccactg	TAATACGACTCACTATAGGgagaccacgttcatgcaaagcagtcaaatc	cDNA
5	F20D12.4	*czw-1*	2.0	TAATACGACTCACTATAGGgagaccactgattggacaattaccagaacg	TAATACGACTCACTATAGGgagaccacctgattgtcaccactagcctca	cDNA
29	T06E4.1	*hcp-2*	1.9	TAATACGACTCACTATAGGtctcggaaaggaatcgaaaa	AATTAACCCTCACTAAAGGtcgttgtctccaattccaca	genomic DNA
61	C02F5.1	*knl-1*	1.9	TAATACGACTCACTATAGGccgctgaaatggatacgagt	AATTAACCCTCACTAAAGGccatgctaatgtcttcacacg	genomic DNA
62	K11D9.1	*klp-7*	2.6	TAATACGACTCACTATAGGgtgcttctgccaacaaacg	AATTAACCCTCACTAAAGGtgatctggaatatggcgtga	genomic DNA
64	ZK1055.1	*hcp-1*	2.1	TAATACGACTCACTATAGGaaaccgagtcgccattttc	AATTAACCCTCACTAAAGGagatcgcgctgaagactttc	genomic DNA
84	W01B6.9	*ndc-80*	1.6	AATTAACCCTCACTAAAGGccccagtctgagtcaacctc	TAATACGACTCACTATAGGccaactcgctttgaatttcc	genomic DNA
93	T03F1.9	*hcp-4*	1.36	AATTAACCCTCACTAAAGGggaaatgtacggagcgaaaa	TAATACGACTCACTATAGGacattgttggtgggtccaat	genomic DNA

Table 2.2 (Continued). Double-stranded RNAs used in this study.

RNA #	Gene #	Name	Conc. mg/ml	Oligo #1	Oligo #2	Template
205	F59E12.2	*zyg-1*	1.4	AATTAACCCTCACTAAAGGtggacggaaattcaaacgat	TAATACGACTCACTATAGGaacgaaattcccttgagctg	cDNA
235	Y39G10AR.2	*zwl-1*	2.0	AATTAACCCTCACTAAAGGatgccactcaccatcgagcag	TAATACGACTCACTATAGGggatcagtgaagcgagatgactc	cDNA
263	C50F4.11	*mdf-1*	1.12	TAATACGACTCACTATAGGaagcgaagttggctgaaaaa	AATTAACCCTCACTAAAGGagcatcctcaagtcgttcgt	genomic DNA
264	Y54G9A.6	*bub-3*	.875	TAATACGACTCACTATAGGgacgctaaaacttgtcggat	AATTAACCCTCACTAAAGGttatgaagctgaataatacg	genomic DNA
265	ZC328.4	*san-1*	1.23	TAATACGACTCACTATAGGcgaagaacttcaaaacctgga	AATTAACCCTCACTAAAGGtttgtcggtccagatcctc	genomic DNA
327	Y45F10D.9	*sas-6*	3.7	AATTAACCCTCACTAAAGGtatggagctaatttgaactcggttacggtta	TAATACGACTCACTATAGGagcagagttttattttcaagtaaaggaagtaaagga	genomic DNA
358	F58A4.3	*hcp-3*	2.85	AATTAACCCTCACTAAAGGgccgatgacaccccaattat	TAATACGACTCACTATAGGccgtgggagtaatcgacaag	cDNA
365	R06C7.8	*bub-1*	3.4	AATTAACCCTCACTAAAGGtgccaaatggaaggacactt	TAATACGACTCACTATAGGtctgagattcttccggttcg	genomic DNA
374		*GFP*	1.1	TAATACGACTCACTA TAGGgtcagtggagagggtggaaggtg	AATTAACCCTCACTA AAGGcatgccatgtgtaa tcccagcagc	Plasmid pIC26

Chapter 3: A New Mechanism Controlling Kinetochore-Microtubule Interactions Revealed by Comparison of Two Dynein-Targeting Components: SPDL-1 and the Rod/Zwilch/Zw10 Complex

3.1 Summary

Chromosome segregation requires stable bipolar attachments of spindle microtubules to kinetochores. The dynein/dynactin motor complex localizes transiently to kinetochores and is implicated in chromosome segregation, but its role remains poorly understood. Here, we use the *C. elegans* embryo to investigate the function of kinetochore dynein by analyzing the Rod/Zwilch/Zw10 (RZZ) complex and the associated coiled-coil protein SPDL-1. Both components are essential for Mad2 targeting to kinetochores and spindle checkpoint activation. RZZ complex inhibition, which abolishes both SPDL-1 and dynein/dynactin targeting to kinetochores, slows but does not prevent the formation of load-bearing kinetochore-microtubule attachments and reduces the fidelity of chromosome segregation. Surprisingly, inhibition of SPDL-1, which abolishes dynein/dynactin targeting to kinetochores without perturbing RZZ complex localization, prevents the formation of load-bearing attachments during most of prometaphase and results in extensive chromosome mis-segregation. Co-inhibition of SPDL-1 along with the RZZ

complex reduces the phenotypic severity to that observed following RZZ complex inhibition alone. We propose that the RZZ complex can inhibit the formation of load-bearing attachments and that this activity of the RZZ complex is normally controlled by dynein/dynactin localized via SPDL-1. This mechanism could coordinate the hand-off from initial weak dynein-mediated lateral attachments, which help orient kinetochores and enhance their ability to capture microtubules, to strong end-coupled attachments that drive chromosome segregation.

3.2 Introduction

In higher eukaryotes, kinetochores are built on the centromere region of chromosomes to connect to the microtubules of the nascent mitotic spindle after nuclear envelope breakdown (NEBD). To avoid chromosome loss, kinetochores must be efficient at capturing microtubules emanating from the two spindle poles and at converting initial transient contacts into stable end-coupled attachments capable of resisting the forces that drive chromosome alignment (Nicklas, 1988). A safeguard is provided by the mitotic spindle checkpoint, which delays cell cycle progression by producing a diffusible inhibitor at kinetochores that have not yet captured microtubules (Musacchio and Salmon, 2007). Stable end-on attachments shut off production of the inhibitory signal, allowing the cell to exit mitosis.

The core microtubule attachment site at the kinetochores is formed by a set of conserved interacting proteins, collectively named KMN network after its

constituent components KNL-1, the Mis12 complex, and the Ndc80 complex (Cheeseman et al., 2004). The network contains two microtubule binding sites, one in KNL-1 and the other in the Ndc80 complex (Cheeseman et al., 2006; Wei et al., 2007). In eukaryotes ranging from yeast to human cells, compromising Ndc80 complex function *in vivo* leads to severe chromosome alignment defects correlated with an inability of kinetochores to form stable bipolar attachments (Kline-Smith et al., 2005).

Additional kinetochore-microtubule interactions are mediated by the microtubule minus end-directed motor cytoplasmic dynein and its cofactor dynactin. Because dynein/dynactin has multiple functions in the cell, insight into its kinetochore roles has primarily come from studies on the conserved Rod/Zwilch/Zw10 (RZZ) complex (Karess and Glover, 1989; Scaerou et al., 1999; Scaerou et al., 2001; Smith et al., 1985; Williams and Goldberg, 1994; Williams et al., 2003), which is essential for kinetochore recruitment of dynein/dynactin (Starr et al., 1998). Inhibitions of RZZ subunits (Li et al., 2007; Savoian et al., 2000; Yang et al., 2007) and direct disruption of dynein/dynactin (Vorozhko et al., 2008) have shown that the minus-end directed motility of kinetochore dynein contributes to transient poleward movement of chromosomes in early prometaphase (Rieder and Alexander, 1990). Inhibition of dynein/dynactin also affects the microtubule-based poleward transport of checkpoint proteins and RZZ subunits, which is thought

to constitute an important mechanism for silencing the spindle checkpoint (Howell et al., 2001; Wojcik et al., 2001).

Despite significant work over the past decade, the relevance of kinetochore dynein/dynactin for the process of chromosome alignment remains unclear. When dynein/dynactin is inhibited following bipolar spindle assembly, metaphase plate formation occurs normally (Howell et al., 2001; Vorozhko et al., 2008). Similarly, *D. melanogaster* null mutations in the *rod* and *zw10* genes were reported as having no obvious phenotype prior to anaphase in mitotic cells (Williams and Goldberg, 1994; Williams et al., 1992). In contrast, recent work in mammalian cells showed significant delays in chromosome alignment after depletion of Zw10 (Li et al., 2007; Yang et al., 2007). The dissection of RZZ complex function in chromosome alignment is complicated by its role in spindle checkpoint signaling. Analysis in *D. melanogaster* embryos, human cells, and Xenopus extracts demonstrated that the RZZ complex is essential for spindle checkpoint function (Basto et al., 2000; Chan et al., 2000; Kops et al., 2005) and for the localization to unattached kinetochores of two essential spindle checkpoint components, Mad1 and Mad2 (Buffin et al., 2005; Kops et al., 2005).

The detection of a two-hybrid interaction between Zw10 and the dynactin subunit dynamitin suggested that the RZZ complex is directly involved in recruiting dynein/dynactin (Starr et al., 1998). A recent study in *D. melanogaster* identified Spindly, a component acting downstream of the RZZ

complex, which is required for targeting dynein, but not dynactin, to kinetochores (Griffis et al., 2007). NudE and NudEL, two proteins that associate with dynein, have also been implicated in dynein targeting to kinetochores (Stehman et al., 2007; Vergnolle and Taylor, 2007).

We have developed the early *C. elegans* embryo as a system to identify proteins that play important roles in chromosome segregation and characterize their mechanism of action (Cheeseman et al., 2004; Desai et al., 2003; Oegema et al., 2001). Here, we use this system to study the function of the Rod/Zwilch/Zw10 (RZZ) complex and Spindly (SPDL-1), components of the outer kinetochore that are essential for spindle checkpoint function and constitute a module that targets the dynein/dynactin motor to the kinetochore during chromosome alignment. A comparative analysis of SPDL-1 and RZZ complex function revealed that, despite their equivalent requirement for dynein/dynactin recruitment, SPDL-1 inhibition results in a significantly more severe defect in chromosome segregation, which, until just prior to anaphase onset, closely mimics the lack of stable end-coupled attachments. This defect can be quantitatively reduced to match that of inhibiting the RZZ complex alone by co-inhibiting SPDL-1 and the RZZ complex. Thus, by uncoupling kinetochore localization of the RZZ complex from that of dynein/dynactin, we have uncovered a regulatory relationship between the RZZ complex and the formation of stable end-coupled attachments. We discuss the implications of these findings for dynein/dynactin function at the kinetochore.

3.3 Results

3.3.1 The *C. elegans* Spindly Homolog C06A8.5/SPDL-1 is Required for Chromosome Segregation

All *C. elegans* proteins essential for chromosome segregation are required for embryonic viability. Embryos individually depleted of each of the ~2000 gene products required for embryonic viability have been filmed using differential interference contrast (DIC) microscopy to identify genes whose inhibition results in the presence of extra nuclei (karyomeres) due to chromosome mis-segregation (Sonnichsen et al., 2005). However, since mis-segregation does not always lead to the formation of karyomeres and DIC does not directly visualize chromosomes, it is likely that chromosome segregation genes have been missed by this approach. To test this idea, we targeted using RNA-mediated interference (RNAi) 50 genes of unknown function required for embryonic viability but annotated as having no defects by DIC analysis in a strain co-expressing GFP:histone H2B and GFP:γ-tubulin to visualize chromosomes and spindle poles, respectively (O'Connell et al., 2001). This screen identified one previously uncharacterized gene, C06A8.5, whose depletion resulted in severe chromosome mis-segregation. C06A8.5 encodes a 479-amino acid protein that contains five predicted coiled-coil domains in its N-terminal 360 residues. Sequence searches identified potential homologues throughout the animal kingdom, including the previously characterized *D. melanogaster* Spindly (Griffis et al., 2007). Although

C06A8.5 shows low sequence identity with the other proteins, it shares a highly conserved motif located near a break in the coiled-coils (Fig. 3.1C and Supplementary Fig. 3.1). As our functional analysis supports the idea that C06A8.5 is a Spindly homolog, we named the *C. elegans* protein SPDL-1.

Embryos depleted of SPDL-1 exhibited defective chromosome alignment, premature spindle pole separation, and significant chromatin bridges in anaphase (Fig 3.1A; Supplementary Video 3.1). The onset of both sister chromatid separation and cytokinesis occurred with normal timing in *spdl-1(RNAi)* embryos, indicating that cell cycle progression was unaffected (Fig. 3.1B).

The chromosome mis-segregation observed in *spdl-1(RNAi)* embryos could be the result of compromised mitotic chromosome structure, an aberrant mitotic spindle, or a defect in kinetochore function. To distinguish between these possibilities, we imaged a worm strain expressing GFP:Spc24^{KBP-4}, a subunit of the outer kinetochore NDC-80 complex (Cheeseman et al., 2004). In *spdl-1(RNAi)* embryos, GFP:Spc24^{KBP-4} localized normally to paired diffuse kinetochores which maintained a rigid parallel conformation during prometaphase chromosome movements, demonstrating that centromere resolution and chromosome condensation were unaffected (Fig. 3.1D; Supplementary Video 3.2). Sister kinetochores remained paired until the onset of anaphase, when individual chromatids separated from each other (Fig. 3.1D, arrows), indicating proper regulation of sister chromatid cohesion.

All microtubule-dependent events in the early embryo (pronuclear migration, rotation of the centrosome-pronuclear complex, spindle assembly and asymmetric spindle positioning) were normal in *spdl-1(RNAi)* embryos. In particular, fixed and live analysis in a worm strain expressing GFP:b-tubulin showed that mitotic spindle formation in *spdl-1(RNAi)* embryos was not perturbed (Fig. 3.1E; Supplementary Video 3.3). We conclude that the severe chromosome segregation defect in embryos depleted of SPDL-1 does not result from problems with either the microtubule cytoskeleton, mitotic spindle formation, or chromosome structure.

Immunoblotting using affinity purified antibodies confirmed that our RNAi conditions resulted in penetrant depletion of SPDL-1 (Fig. 3.1F). Immunostaining revealed that SPDL-1 is recruited to kinetochores at NEBD and localizes there until the metaphase-anaphase transition, after which it is no longer detected (Fig. 3.1G and I). Imaging of a worm strain expressing GFP:SPDL-1 confirmed this transient localization pattern and also revealed a weak spindle pole localization (Fig. 3.1H; Supplementary Video 3.4). We conclude that SPDL-1 is a transiently kinetochore-localized protein that plays an essential role in chromosome segregation.

3.3.2 SPDL-1 is Recruited to Kinetochores by the RZZ Complex

To understand SPDL-1 function at kinetochores, we first sought to determine if it interacts with other known kinetochore components. We immunoprecipitated several inner and outer kinetochore proteins (CENP-A,

CENP-C, MCAK^{KLP-7}, KNL-1, BUB-1, Zwilch^{ZWL-1}, NDC-80, HCP-1, CLASP^{CLS-2}) and probed the precipitates for SPDL-1. Only affinity-purified antibodies to Zwilch^{ZWL-1} (Fig. 3.2C) co-precipitated a detectable amount of SPDL-1 (Fig. 3.2A and data not shown). Mass spectrometric analysis of the Zwilch^{ZWL-1} immunoprecipitate (Fig. 3.2B) confirmed the presence of SPDL-1 and identified the two other subunits of the RZZ complex, ROD-1 and Zw10^{CZW-1}. In contrast, a more stringent tandem purification of Zwilch^{ZWL-1} using the Localization and Affinity Purification (LAP) tag (Cheeseman et al., 2004) isolated only the three RZZ subunits, which could be readily visualized on a silver-stained gel (Fig. 3.2B), but not SPDL-1, suggesting that SPDL-1 is peripherally associated rather than a stable core subunit of the RZZ complex. Consistent with this idea, gel filtration experiments revealed that endogenous SPDL-1 exhibited the same fractionation profile as recombinant SPDL-1, and that this fractionation behavior was clearly distinct from that of endogenous Zwilch^{ZWL-1} (data not shown).

We next analyzed the localization dependencies between SPDL-1 and the RZZ complex. Immunofluorescence and live-imaging of GFP^{LAP} fusions to Zwilch^{ZWL-1} and Zw10^{CZW-1} showed that these two RZZ subunits localize transiently to kinetochores in a fashion essentially identical to SPDL-1 (Fig. 3.2D and E; Supplementary Videos 3.5 and 3.6). ROD-1 depletion abolished kinetochore localization of both and Zw10^{CZW-1} and Zwilch^{ZWL-1}, suggesting

that the three RZZ subunits are likely inter-dependent for kinetochore targeting (Fig. 3.2D and data not shown). Depletion of Zwilch^{ZWL-1} or ROD-1 abolished SPDL-1 targeting to kinetochores (Fig. 3.2D), whereas SPDL-1 depletion did not alter the kinetics of kinetochore localization for either RZZ subunit (Fig. 3.2E; Supplementary Videos 3.5 and 3.6). Specifically, rapid disappearance of Zwilch^{ZWL-1} and ROD-1 from kinetochores in early anaphase was observed in both control and *spdl-1(RNAi)* embryos. This loss occurred prior to mitotic kinetochore disassembly, monitored using the NDC-80 complex subunit Spc24^{KBP-4}, suggesting the existence of a regulatory step controlling RZZ complex removal from kinetochores that is not affected by SPDL-1 depletion. We conclude that SPDL-1 is recruited to kinetochores by the RZZ complex and that both the localization and cell cycle progression-dependent loss of the RZZ complex from kinetochores are independent of SPDL-1.

3.3.3 SPDL-1 and the RZZ Complex are Dispensable for Building the Core Kinetochore Microtubule Attachment Site

Next we positioned SPDL-1 and the RZZ complex within the established hierarchy for kinetochore assembly. SPDL-1 and RZZ complex localization was dependent on KNL-1 (Fig. 3.3A), which is required for the localization of multiple outer kinetochore proteins in *C. elegans* (Desai et al., 2003). Depletion of the CENP-F-like proteins HCP-1 and HCP-2 had no effect on SPDL-1 localization. An intermediate effect on SPDL-1 localization was

observed following depletion of NDC-80 or BUB-1; the effect of BUB-1 depletion was consistently more severe than that of NDC-80 depletion. RZZ complex targeting was not affected by any of these depletions (Fig. 3.3A and A. Essex and A. Desai, unpublished data).

Depletion of SPDL-1 and RZZ subunits had no effect on the localization of KNL-1, KNL-2, KNL-3, MIS-12, NDC-80, the NDC-80 complex subunit Spc25^{KBP-3}, BUB-1, HCP-1, or CLASP^{CLS-2} (Fig. 3.3B and data not shown). We conclude that outer kinetochore assembly, including formation of the core microtuble attachment site constituted by the KMN network, does not require either the RZZ complex or SPDL-1 (Fig. 3.3C).

3.3.4 SPDL-1, Like the RZZ Complex, is Required for a Functional Spindle Checkpoint and Mad2^{MDF-2} Recruitment to Unattached Kinetochores

Having established that SPDL-1 functions in close proximity to the RZZ complex, we sought to test if any of the roles ascribed to the RZZ complex require SPDL-1. Work in *D. melanogaster* and vertebrates has shown that the RZZ complex is required for a functional spindle checkpoint and for localization of the checkpoint protein Mad2 to kinetochores. To probe spindle checkpoint activation in the early *C. elegans* embryo, we used an assay based on controlled formation of monopolar spindles in the second embryonic division following inhibition of centriole duplication (Essex et al., 2009). These monopolar spindles elicit a checkpoint-mediated cell-cycle delay (Fig. 3.4B). Depletion of SPDL-1 in cells with monopolar spindles abrogated the delay,

demonstrating that the spindle checkpoint requires SPDL-1 (Fig. 3.4B). The same result was observed for depletions of the RZZ subunit ROD-1. The delay was correlated with transient enrichment of GFP:Mad2^{MDF-2} on the unattached kinetochores that are distal to the monopole (Fig. 3.4C; Supplementary Video 7). Depletion of SPDL-1 or ROD-1 abrogated GFP:Mad2^{MDF-2} localization to kinetochores of monopolar spindles. We conclude that SPDL-1, like the RZZ complex, is required for spindle checkpoint activation and kinetochore recruitment of GFP:Mad2^{MDF-2}.

3.3.5 SPDL-1 is Required for the Recruitment of Dynein and Dynactin to Unattached Kinetochores

Dynein/dynactin recruitment to kinetochores has been hypothesized to occur via the dynactin subunit p50/dynamitin, a two-hybrid interactor of Zw10 (Starr et al., 1998). *D. melanogaster* Spindly (DmSpindly) was reported to be required for dynein but not dynactin targeting to kinetochores, suggesting that dynactin-Zw10 and DmSpindly make independent contributions to dynein localization (Griffis et al., 2007). To test if this is the case in *C. elegans*, we generated worm strains stably co-expressing mCherry:histone H2B and GFP:fusions of cytoplasmic dynein heavy chain^{DHC-1} or dynamitin^{DNC-2}. Both fusion proteins localized diffusely to the spindle and the spindle poles in mitosis and significant enrichment at kinetochores over the spindle signal was not evident in unperturbed embryos (data not shown). However, in cells with

monopolar spindles, GFP:dynein heavy chain^{DHC-1} and GFP:dynamitin^{DNC-2} became prominently enriched at kinetochores (Fig. 3.5A; Supplementary Video 3.8). Both fusion proteins were excluded from the nucleus in interphase and localized to the nuclear periphery opposite the single spindle pole prior to NEBD. After NEBD, both proteins accumulated at kinetochores. This behavior was distinct from that of GFP:KNL-2, a centromeric chromatin protein (Maddox et al., 2007), whose levels at kinetochores did not appreciably change throughout monopolar mitosis (Fig. 3.5A). GFP:KNL-2 was also present on all sister kinetochores regardless of their orientation relative to the spindle pole . In contrast, the accumulation of both GFP:dynein heavy chain^{DHC-1} and GFP:dynamitin^{DNC-2} was restricted to kinetochores that were located on the distal, unattached side of the monopolar spindle. These results indicate that both dynein and dynactin accumulate at unattached kinetochores in *C. elegans*, as is the case in vertebrates.

We next investigated the role of SPDL-1 in the accumulation of dynein and dynactin on kinetochores of monopolar spindles. We found that both GFP:dynein heavy chain^{DHC-1} and GFP:dynamitin^{DNC-2} failed to localize to kinetochores of monopolar spindles in *spdl-1(RNAi)* embryos (Fig. 3.5B; Supplementary Videos 3.9 and 3.10). A similar result was observed following RZZ complex inhibition. In contrast, depletion of NDC-80 did not prevent kinetochore localization of either GFP:dynein heavy chain^{DHC-1} or GFP:dynamitin^{DNC-2}. Since both SPDL-1 and the RZZ complex are required

for the spindle checkpoint-mediated delay elicited by monopolar spindles, we used Mad2^{MDF-2} depletion to test whether the lack of dynein/dynactin localization was caused by accelerated cell cycle progression. Although their gradual accumulation was cut short by premature mitotic exit, both GFP:dynein heavy chain^{DHC-1} and GFP:dynamitin^{DNC-2} were visible at kinetochores in Mad2^{MDF-2}-depleted cells with monopolar spindles (Fig. 3.5C; Supplementary Videos 3.9 and 3.10). Of note, none of the perturbations affected the localization of GFP:dynein heavy chain^{DHC-1} or GFP:dynamitin^{DNC-2} to the nuclear periphery. We conclude that kinetochore localization of both dynein and dynactin is dependent on SPDL-1.

3.3.6 Depletion of SPDL-1 Results in a More Severe Defect in Kinetochore-Microtubule Attachments than Depletion of RZZ Complex Subunits

SPDL-1 localizes downstream of the RZZ complex and is required for all RZZ complex functions established to date: spindle checkpoint activation, kinetochore recruitment of Mad2, and kinetochore recruitment of dynein/dynactin. These findings predict that chromosome segregation defects in *spdl-1(RNAi)* embryos should be of similar or reduced severity than those observed in embryos depleted of RZZ subunits. We first tested whether depletion of the three RZZ subunits resulted in embryonic lethality, as is the case for depletion of SPDL-1. This analysis confirmed the results of functional

genomic studies (Sonnichsen et al., 2005) that the three RZZ subunits are not functionally equivalent. Depletion of Zw10^{CZW1} causes penetrant sterility of the injected worm, whereas depletion of ROD-1 or Zwilch^{ZWL-1} results in embryonic lethality of its progeny (Essex et al., 2009). This difference is explained by the requirement of Zw10^{CZW1}, but not ROD-1 or Zwilch^{ZWL-1}, for membrane trafficking in the gonad (Anjon Audhya, personal communication); defects in trafficking pathways prevent oocyte formation and cause sterility in *C. elegans*. Consequently, we focused on ROD-1 and Zwilch^{ZWL-1} to specifically analyze RZZ complex function at kinetochores.

We compared the consequences of SPDL-1 depletion to those of ROD-1 or Zwilch^{ZWL-1} depletions in a strain co-expressing GFP:histone H2B, which allowed visual inspection of chromosome alignment and separation, and GFP:γ tubulin, which facilitated spindle pole tracking (Fig. 3.6A). The latter assay is particularly useful in the one-cell *C. elegans* embryo, where kinetochore–spindle attachments counteract cortical forces pulling on astral microtubules anchored at the spindle poles; premature pole separation following perturbation of kinetochore-localized proteins is diagnostic of impairment in the formation of load-bearing kinetochore-microtubule attachments, and specific pole separation profiles have proven important in categorizing different types of defects (Cheeseman et al., 2004; Desai et al., 2003; Oegema et al., 2001).

Surprisingly, we observed that chromosome segregation and kinetochore-spindle microtubule interaction defects were significantly worse in SPDL-1-depleted embryos than in embryos depleted of RZZ subunits. In *spdl-1(RNAi)* embryos, which never congressed their chromosomes to a compact metaphase plate (Fig. 3.6B), the pole separation profile was identical to that of *knl-3(RNAi*) embryos in which outer kinetochore assembly was prevented (Cheeseman et al., 2004), except for a short period (~40 s) prior to sister chromatid separation (Fig. 3.6E). Although pole separation slowed during this period, suggesting engagement of spindle microtubules by kinetochores, spindles were significantly longer at the time of sister chromatid separation in *spdl-1(RNAi)* embryos (20±0.5 μm) compared to controls (16.2±0.5 μm). By comparison, the chromosome segregation and premature pole separation defects in *rod-1(RNAi)* or *zwl-1 (RNAi)* embryos were markedly less severe (Fig. 3.6B and F; Supplementary Video 3.11). Chromosomes were able to congress and form a metaphase plate, and sister chromatid separation appeared successful in the majority of embryos. A small amount of lagging anaphase chromatin was consistently observed in approximately 30 % of first divisions in RZZ subunit depletions (Fig. 3.6D), whereas SPDL-1 depletion resulted in massive chromatin bridges in every first division examined. Pole tracking analysis also revealed a significantly less severe defect in *rod-1* or *zwl-1(RNAi)* embryos compared to *spdl-1(RNAi)* embryos (Fig. 3.6F). In RZZ subunit depletions, initial premature pole separation was observed indicating a

defect in establishing load-bearing attachments. However, approximately 100 s prior to sister chromatid separation, kinetochores engaged spindle microtubules and spindle length at the time of sister chromatid separation (*zwl-1(RNAi)*, 16±0.3 μm; *rod-1(RNAi)*, 15.6±0.2 μm) was indistinguishable from controls (16.2±0.5 μm).

Both quantitative immunoblotting (Fig. 3.1F and 3.2C) and immunofluorescence (Fig. 3.2D and 3.3B) indicate that the difference in phenotypic severity described above is unlikely due to reduced depletion efficiency of RZZ subunits relative to SPDL-1. The identical qualitative and quantitative phenotypes of *rod-1(RNAi)* and *zwl-1(RNAi)* also argue against this trivial explanation. To further establish that the weaker RZZ inhibition phenotype is not due to partial depletion of the targeted subunits, we co-depleted ROD-1 and Zwilch^{ZWL-1}. The observed phenotypes in both assays were indistinguishable from single depletions of ROD-1 or Zwilch^{ZWL-1} (Fig. 3.6C; Supplementary Fig. 3.2 and Video 3.12).

Thus, RZZ complex inhibition slows but does not prevent formation of load-bearing kinetochore microtubule attachments and leads to an increase in anaphase lagging chromatin, which is indicative of incorrectly attached kinetochores. Depletion of SPDL-1 results in significantly more severe defects both in the formation of load-bearing kinetochore-microtubule attachments and chromosome segregation. Based on the pole-tracking analysis, the severity of

the SPDL-1 inhibition defects closely resembles loss of core microtubule attachment until just prior to anaphase onset.

3.3.7 Co-Inhibition of SPDL-1 with RZZ Subunits Results in the Less Severe RZZ Inhibition Phenotype

The greater phenotypic severity of SPDL-1 inhibitions noted above may reflect additional non-kinetochore functions of SPDL-1 that are not affected by its displacement from the kinetochore in RZZ subunit depletions. To test this possibility, we co-depleted ROD-1 or Zwilch^{ZWL-1} with SPDL-1. In all embryos analyzed (n = 32), the resulting phenotype was indistinguishable from the weaker RZZ subunit depletions (Fig. 3.6C and G; Supplementary Video 3.12). To control for reduced efficacy of RNAi in the double depletions, the SPDL-1 single depletions were repeated after appropriate dilution with control dsRNA. The reduction in phenotypic severity in the double depletions was evident in both the chromosome segregation profile (Fig. 3.6C) and in the quantitative analysis of spindle pole separation (Fig. 3.6G). These results are consistent with the assembly epistasis at kinetochores, which showed that SPDL-1 depends on the RZZ complex for localization (Fig. 3.2), and exclude the possibility that the additional defects observed in *spdl-1(RNAi)* embryos are due to non-kinetochore functions of SPDL-1. We conclude that the severe defects in SPDL-1-depleted embryos are derived from RZZ complex localized to kinetochores in the absence of associated SPDL-1 and/or dynein/dynactin.

3.3.8 Co-Depletion of SPDL-1 or RZZ Subunits with NDC-80 Synergistically Recapitulates the "Kinetochore Null" Phenotype

Two microtubule-binding entities are independently targeted to the *C. elegans* kinetochore via KNL-1: dynein/dynactin (via the RZZ complex and SPDL-1) and the NDC-80 complex, a component of the KMN network (Fig. 3.3C). In *spdl1(RNAi)* embryos, just prior to sister chromatid separation, pole separation slowed down significantly and severe chromosome missegregation was observed along the spindle axis (Fig. 3.1A and 3.6B). We hypothesized that the eventual slowing of pole separation in *spdl-1(RNAi)* embryos reflected belated load-bearing attachments made by the NDC-80 complex, while the residual chromosome movements in *ndc-80(RNAi)* embryos (Supplementary Video 3.13) were mediated by kinetochore dynein/dynactin. Co-depletion experiments confirmed this view (Fig. 3.7A and B). While embryos singly depleted of SPDL-1 and NDC-80 were partially successful at congressing their chromosomes to the spindle equator and at segregating sister chromatids in anaphase, double depletions resulted in a phenotype identical to that of *knl-3(RNAi)* embryos (Supplementary Video 3.13), in which outer kinetochore assembly is abolished (Cheeseman et al., 2004). A "kinetochore null"-like phenotype was also observed in co-depletions of NDC-80 with ROD-1 (Supplementary Video 3.14). We conclude that it is the absence of the two independently targeted microtubule-interacting components, dynein/dynactin and the NDC-80 complex, that accounts for the synergistic defect. These

results further indicate that the reduction in pole separation just prior to anaphase onset and the mis-segregation of chromosomes observed in SPDL-1-depleted embryos are attributable to the action of the NDC-80 complex.

3.4 Discussion

3.4.1 Kinetochore dynein/dynactin accelerates the formation of load-bearing attachments and provides an important fidelity mechanism

Our analysis of the RZZ complex and SPDL-1, kinetochore-localized components that are sequentially required for dynein/dynactin targeting, gives new insight into how this minus-end-directed motor complex contributes to chromosome segregation. Specifically, the results suggest that kinetochore dynein/dynactin accelerates the formation of load-bearing attachments and provides an important fidelity mechanism, which prevents inappropriate attachments in prometaphase and reduces the missegregation frequency after anaphase onset. This fidelity mechanism likely involves negative regulation of load-bearing kinetochore-microtubule attachments by the RZZ complex. We speculate below that this negative regulation is modulated by dynein/dynactin to ensure the orderly conversion of weak dynein/dynactin-mediated lateral attachments to load-bearing end-coupled attachments during prometaphase.

3.4.2 SPDL-1 Targets Dynein/Dynactin to Kinetochores and is Required to Activate the Spindle Checkpoint

SPDL-1 targets to the kinetochore immediately downstream of the RZZ complex and is not involved in the assembly of the core kinetochore-microtubule binding site constituted by the KMN network. Functional analysis showed that SPDL-1 is required for the recruitment of dynein/dynactin and $Mad2^{MDF-2}$ to unattached kinetochores. The requirement for $Mad2^{MDF-2}$ targeting explains why SPDL-1 is essential for spindle checkpoint activation. By contrast, *D. melanogaster* Spindly was shown to be essential for the recruitment of dynein, but not dynactin, to kinetochores, and was found to be dispensable for Mad2 accumulation and spindle checkpoint activation. We also did not observe any abnormalities in cell shape or microtubule organization in SPDL-1 depleted embryos that resembled the defects seen following RNAi of DmSpindly in interphase S2 cells. Preliminary work in human tissue culture cells indicates that human Spindly is similar to *C. elegans* SPDL-1 in that it is required to recruit both dynein and dynactin to kinetochores and its inhibition does not result in detectable defects in interphase microtubule organization or cell shape. However, like DmSpindly, the human homologue is not required for Mad2 localization or spindle checkpoint activation (R. Gassmann and A. Desai, unpublished data).

Previous studies have shown that cytoplasmic dynein as well as its accessory factors dynactin and LIS-1 are involved in multiple processes during

the first embryonic division of *C. elegans*, including pronuclear migration, centrosome separation, and bipolar spindle assembly (Cockell et al., 2004; Gonczy et al., 1999; O'Rourke et al., 2007; Schmidt et al., 2005). All of these processes are unaffected following SPDL-1 depletion, indicating that SPDL-1 does not globally control dynein function.

3.4.3 The *C. elegans* RZZ complex

The close relationship between SPDL-1 and the RZZ homologues led us to functionally characterize the RZZ complex in *C. elegans*. The RZZ complex has been studied primarily in *D. melanogaster* with recent contributions from vertebrate systems (Karess, 2005). Our results in *C. elegans* confirm that ROD-1, Zwilch^{ZWL-1} and Zw10^{CZW-1} function as a complex which localizes transiently to kinetochores from NEBD until the onset of anaphase. The RZZ complex localizes to the outer kinetochore downstream of KNL-1 and, like SPDL-1, is not required for kinetochore targeting of the NDC-80 complex. In vertebrates, the coiled-coil protein Zwint acts as an intermediary between KNL-1 and the RZZ complex, but Zwint-like molecules have not been identified in *C. elegans* or *D. melanogaster* (Cheeseman et al., 2004; Kops et al., 2005; Starr et al., 2000). The two known roles of the RZZ complex, recruitment of dynein/dynactin to unattached kinetochores and activation of the spindle checkpoint through kinetochore targeting of Mad2, are conserved in *C. elegans*.

RNAi in *C. elegans* suggests that Zw10^{CZW-1}, but not ROD-1 or Zwilch^{ZWL-1}, has an additional non-kinetochore function in membrane trafficking, as previously reported in vertebrates (Hirose et al., 2004). This difference between the RZZ subunits raises a cautionary note about interpreting Zw10 perturbations strictly in terms of kinetochore function, and we were careful to focus on ROD-1 and Zwilch^{ZWL-1} as targets to specifically inhibit RZZ complex activity at kinetochores.

3.4.4 Implications of *C. elegans* RZZ Complex Analysis for the Role of Dynein/Dynactin at the Kinetochore

Chromosome movement: Dynein/dynactin and the microtubule-binding NDC-80 complex are independently targeted to kinetochores downstream of KNL-1. While the NDC-80 complex is required to make load-bearing kinetochore-microtubule attachments, its inhibition does not result in a "kinetochore null" phenotype as clear residual chromosome movements are observed (Desai et al., 2003). Such Ndc80 complex-independent movements have also been described in vertebrate cells and dynein/dynactin has been implicated as their source (DeLuca et al., 2005; McCleland et al., 2004; Vorozhko et al., 2008). Our finding that double depletions of NDC-80 with either ROD-1 or SPDL-1 synergistically recapitulate the "kinetochore null" phenotype is consistent with the conclusion that both of these microtubule-

binding activities contribute to chromosome-spindle microtubule interactions downstream of KNL-1.

Kinetics of load-bearing attachment formation: In the absence of the NDC-80 complex, kinetochore-localized dynein/dynactin is insufficient to generate load-bearing attachments that can oppose the effects of aster-based cortical pulling forces during chromosome alignment. In RZZ complex-inhibited embryos, formation of load-bearing attachments occurs, but is delayed. This result suggests that kinetochore-localized dynein/dynactin accelerates the formation of NDC-80 complex dependent end-coupled attachments. We speculate that this kinetic acceleration is due to the ability of dynein/dynactin to efficiently collect microtubules that pass by the kinetochore. Such microtubules would remain laterally associated with the kinetochore until their dynamic plus ends are close enough to be integrated into the outer plate by the KMN network. Importantly, in RZZ complex-inhibited embryos, despite the kinetic defect in forming load-bearing attachments, spindles always reached wild-type length at anaphase onset and had a tightly aligned metaphase plate. Thus, kinetochore dynein/dynactin is dispensable for end-coupled load-bearing attachments, but it accelerates their formation in early prometaphase.

Attachment geometry: In addition to the kinetic effect on the formation of load-bearing attachments, RZZ complex inhibitions revealed an increased frequency of lagging chromatin during anaphase. Importantly, depletion of

either Mad1^{MDF-1} or Mad2^{MDF-2}, both essential components of the spindle checkpoint, does not have any deleterious effects on chromosome segregation in the first embryonic division (Essex et al., 2009). Thus, the lack of a spindle checkpoint-mediated cell cycle delay cannot explain the chromosome mis-segregation observed in RZZ complex inhibitions. This finding is similar to the situation in *D. melanogaster*, where *mad2* null mutants are reported to have little or no chromosome segregation defects, while the signature phenotype of *zw10* and *rod* null mutants is lagging anaphase chromatin (Buffin et al., 2007; Karess and Glover, 1989; Williams et al., 1992). Since RZZ complex-inhibited embryos have no noticeable defects in chromosome condensation, it is likely that the chromatin bridges in anaphase are caused by incorrect merotelic attachments, where a single kinetochore is connected to both poles (Cimini et al., 2003). We propose that a major role of kinetochore dynein/dynactin is to prevent the generation of such maloriented kinetochores in early prometaphase, when kinetochore-microtubule interactions are first established. When an unattached sister kinetochore binds laterally to an astral microtubule, the minus end-directed motility of dynein/dynactin would provide a force that orients the kinetochore towards the spindle pole at which that particular microtubule originates, thereby decreasing the probability that the same kinetochore captures a microtubule from the opposite pole. Thus, dynein/dynactin would ensure correct attachment geometry by forcing sister kinetochores to face opposite poles.

3.4.5 Transient Inhibition of Load-Bearing Kinetochore-Microtubule Attachments by the RZZ Complex: A Mechanism to Coordinate the Transition from Lateral to End-Coupled Attachments?

The RZZ complex and SPDL-1 are equivalently required for both dynein/dynactin targeting to kinetochores and spindle checkpoint activation. Yet, the consequences of their inhibition are strikingly different. Pole tracking analysis revealed that the consequences of inhibiting SPDL-1 are indistinguishable from complete loss of load-bearing attachments until just prior to anaphase onset. By contrast, in the RZZ complex inhibitions, after a slight delay, kinetochore-microtubule attachments eventually bear load equally well as those of unperturbed embryos, resulting in wild-type spindle length at anaphase onset.

This comparison reveals that following SPDL-1 inhibition there is a significant defect in formation of KMN network-mediated load-bearing attachments. The defect is attributable to the presence of the RZZ complex at kinetochores, as co-inhibition of SPDL-1 and the RZZ complex reduces the phenotypic severity to match that of inhibiting the RZZ complex alone. This observation indicates that the RZZ complex negatively regulates KMN network activity and that this negative regulation persists for most of prometaphase in the absence of SPDL-1 (Fig. 3.7C and D). The RZZ complex may inhibit the KMN network either directly or via other regulators of KMN network function. Aurora B kinase is known to negatively regulate the microtubule-binding

activity of the Ndc80 complex (Cheeseman et al., 2006; DeLuca et al., 2006). In preliminary work using a temperature-sensitive Aurora B^{AIR-2} mutant, co-inhibition of Aurora B did not reduce the severity of the chromosome segregation defect following SPDL-1 depletion (R. Gassmann and A. Desai, unpublished data), suggesting that the RZZ complex does not regulate the KMN network through Aurora B. In the absence of the RZZ complex from kinetochores, the mechanism for negatively regulating KMN network activity is no longer present, explaining why co-inhibition of SPDL-1 and the RZZ complex quantitatively reduces the phenotypic severity to match that of the RZZ complex alone (Fig. 3.7D).

We propose that the physiological function of the regulatory link between the RZZ complex and the KMN network is to ensure a coordinated transition from transient lateral attachments made by dynein, which accelerate formation of end-coupled attachments of correct geometry, to stable load-bearing end-coupled attachments that do the job of chromosome segregation. In this model, RZZ complex inhibition of the KMN network is modulated by the microtubule minus-end directed motility of dynein/dynactin, which is linked to the outer kinetochore via SPDL-1 and the RZZ complex (Fig. 3.7E). When dynein/dynactin is laterally attached to a microtubule that extends past the kinetochore, the RZZ complex is under low tension and negatively regulates the microtubule-binding activity of the KMN network. This prevents the KMN network from tightly binding to a microtubule extending past the kinetochore

that has been captured by dynein/dynactin. When dynein/dynactin translocation towards the microtubule minus end is met with resistance due to the microtubule plus end being embedded in the kinetochore outer plate, the RZZ complex is placed under tension and inhibition of the KMN network is relieved. We envision that such a feedback mechanism prevents premature lateral binding of the KMN network to microtubules, which would interfere with dynein-mediated kinetochore orientation and increase the likelihood of forming incorrect merotelic attachments.

In summary, our results reveal a new mechanism regulating kinetochore-microtubule attachments that involves the RZZ complex and is likely to be modulated by dynein/dynactin activity. We speculate on the underlying reason for why such a regulatory mechanism would be necessary for the fidelity of chromosome segregation. This mechanism is likely to be integrated with spindle checkpoint signaling that also requires the RZZ complex in all metazoans.

3.5 Methods

3.5.1 Worm Strains and Antibodies

Worm strains used in this study are listed in Supplementary Table 3.1. For worm GFP^{LAP} fusions of SPDL-1, ZWL-1, CZW-1, and MDF-2 the genomic locus was cloned into pIC26 (Cheeseman et al., 2004); the genomic locus of DNC-2 was cloned into pAZ132 (Praitis et al., 2001). For DHC-1, the

start codon was replaced with GFP by recombineering a full-length *dhc-1* fosmid clone (details will be described elsewhere). All constructs were integrated into the DP38 strain (*unc-119(ed3)*) using microparticle bombardment (Praitis et al., 2001) with a PDS-1000/He Biolistic Particle Delivery System (Bio-Rad), and mCherry:histone H2B was subsequently introduced by mating (Green et al., 2008). Affinity purified polyclonal antibodies against full-length SPDL-1 and Zwilch^{ZWL-1} were generated as described previously (Desai et al., 2003).

3.5.2 RNA-mediated Interference

L4 worms were injected with dsRNA (Supplementary Table 3.2) prepared as described previously (Oegema et al., 2001) and incubated for 48 h at 20 °C. For double depletions, dsRNAs were mixed to obtain equal concentrations of ≥ 0.75 mg/ml for each dsRNA.

3.5.3 Immunofluorescence

For stainings with the anti-SPDL-1 antibody, embryos were fixed for 5 min in 3 % paraformaldehyde as detailed previously (Howe et al., 2001). Immunofluorescence for other antibodies and microscopy was performed as described in (Oegema et al., 2001) and (Cheeseman et al., 2004), respectively. All antibodies used were directly labelled with fluorescent dyes (Cy2, Cy3, or Cy5; Amersham Biosciences).

3.5.4 Live-Imaging

Time-lapse movies of worm strain TH32 (co-expressing GFP:histone H2B and GFP:γ-tubulin) (Oegema et al., 2001) were acquired at 21 °C on a Nikon Eclipse E800 microscope using a charge-coupled device camera (Orca-ER; Hamamatsu Photonics) at 2 x 2 binning, and a 60x 1.4 NA Plan Apochromat objective. Acquisition parameters, shutters, and focus were controlled by MetaMorph software (MDS Analytical Technologies). Quantitative analysis of spindle pole elongation was performed using a MetaMorph algorithm (Desai et al., 2003). Movies of strain TH32 for the spindle checkpoint assay were recorded at 18 °C on a DeltaVision microscope (Applied Precision) equipped with a CoolSnap charge-coupled device camera (Roper Scientific) at 2 x 2 binning and a 100x NA 1.3 U-planApo objective (Olympus). Imaging of all other worm strains was performed at 21 °C on a spinning disc confocal head (McBain Instruments) mounted on an inverted Nikon TE2000e microscope equipped with a 60x 1.4 NA Plan Apochromat lens (Nikon), a krypton-argon 2.5 W water-cooled laser (Spectra-Physics) and a charge-coupled device camera (iXon; Andor Technology, or Orca-ER; Hamamatsu Photonics). Acquisition parameters, shutters, and focus were controlled by MetaMorph software. Imaging conditions for individual strains are listed in Supplementary Table 3.3. Spinning disc confocal imaging: For strains XA3501 and OD110, images were recorded with a charge-coupled device camera from Andor Technology (iXon) at 1 x 1 binning; for all other

strains, a Hamamatsu Photonics camera (Orca-ER) at was used at 2 x 2 binning. Laser power was ~ 1 W (40 %)

3.5.5 Immunoprecipitations, LAP purifications, and Mass Spectrometry

Immunoprecipitations were conducted on high-speed supernatant from adult worms as described previously (Cheeseman et al., 2004). For western blotting, proteins were eluted from the antibody-Protein A resin with sample buffer (50 mM Tris-HCl pH 6.8, 15 % (w/v) sucrose, 2 mM EDTA, 3 % SDS) at 70 °C for 15 min. For mass spectrometric analysis, the elution was performed with 8 M urea in 50 mM Tris-HCl pH 8.5. LAP purification of Zwilch^{ZWL-1} and mass spectrometry were conducted as described previously (Cheeseman et al., 2001; Cheeseman et al., 2004). Tandem mass spectra were searched against the most recent version of the predicted *C. elegans* proteins (Wormpep111).

3.6 Acknowledgements

We are grateful to Ana Carvalho, Andrew Holland, and Alex Dammermann for critical reading of the manuscript. This work was supported by a National Science Foundation of Switzerland fellowship (R.G.), the UCSD Genetics Training Grant (A.E.), a Leukemia and Lymphoma Society fellowship (S.O.), a Damon Runyon Cancer Research Foundation fellowship (P.M.), grants from the NIH to A.D. (GM074215) and to B.B (GM49869), by a Scholar Award from the Damon Runyon Cancer Research Foundation to A.D. (DRS

38-04) and by funding from the Ludwig Institute for Cancer Research to A.D. and K.O. This chapter has appeared in print under the following citation: *Genes Dev*., 2008 Sep. 1;22(17):2385-99, Gassmann R, Essex A, Hu JS, Maddox PS, Motegi F, Sugimoto A, O'Rourke SM, Bowerman B, McLeod I, Yates JR 3rd, Oegema K, Cheeseman IM, and Desai A. The dissertation author was co-second author of this paper and created figure 4, including performing the experiments and data analysis.

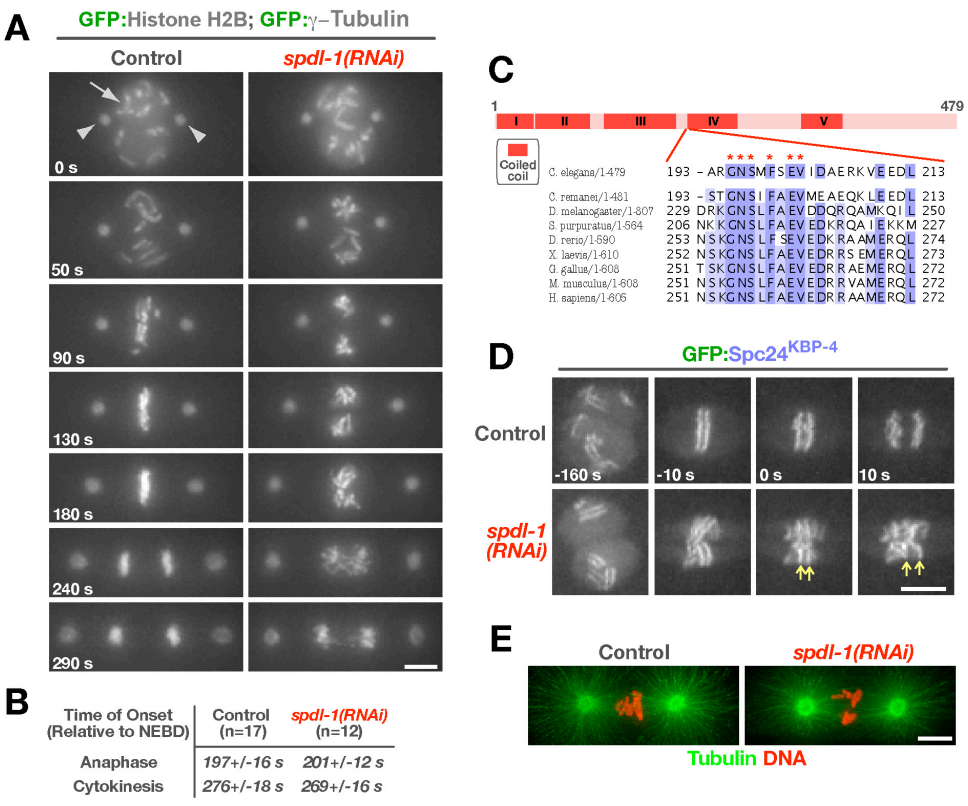

Figure 3.1 (A-E). SPDL-1 is a transient kinetochore component essential for chromosome segregation.

(A) Selected frames from a live-imaging sequence of the first division in unperturbed and *spdl-1(RNAi)* embryos expressing GFP:histone H2B and GFP:γ-tubulin, to simultaneously visualize chromosomes (arrow) and spindle poles (arrowheads), respectively (see also Supplementary Video 1). Images are time-aligned relative to NEBD (0 s). Scale bar, 5 um. **(B)** Timing of anaphase onset and cytokinesis onset in unperturbed and *spdl-1(RNAi)* embryos. Anaphase onset was defined as the first visible sister chromatid separation (GFP:histone H2B) and cytokinesis onset by the first visible ingression of the cleavage furrow in DIC images acquired in parallel. Values represent the S.E.M with a 95 % confidence interval. **(C)** Primary sequence features of SPDL-1 and related proteins. The highly conserved motif that defines this conserved coiled-coil protein family is depicted (see also Supplementary Fig. 1). **(D)** Chromosome condensation, sister centromere resolution, and the separation of sister chromatids at anaphase onset are normal in *spdl-1(RNAi)* embryos. Selected frames of a live-imaging sequence are shown (see also Supplementary Video 2). Kinetochores are marked by GFP:Spc24^{KBP-4}, a subunit of the NDC-80 complex. Arrows highlight separating sister kinetochores at anaphase onset (0 s) in *spdl-1(RNAi)* embryos. Scale bar, 5 um. **(E)** Mitotic spindle morphology in control and *spdl-1(RNAi)* embryos fixed and stained with a fluorescently-labeled antibody against β-tubulin (see also Supplementary Video 3). Scale bar, 5 um.

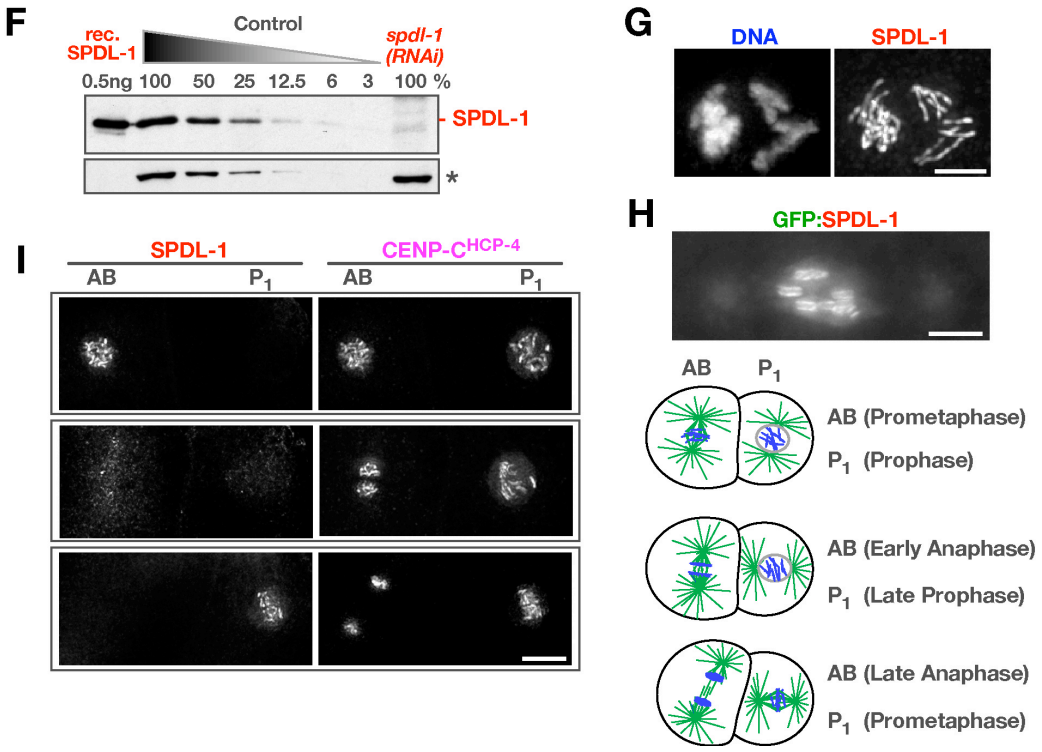

Figure 3.1 (F-I). SPDL-1 is a transient kinetochore component essential for chromosome segregation.

(F) Immunoblotting with an affinity-purified polyclonal antibody raised against SPDL-1 detects purified recombinant (rec.) SPDL-1 and a protein of equal size in wild-type (N2) worms, which is depleted > 95% by RNAi. The relative amount of worm extract loaded is indicated above each lane. A cross-reacting protein band (*) serves as the loading control.

(G) Immunofluorescence image of a one-cell embryo at prometaphase immunostained for SPDL-1. Scale bar, 2 um. **(H)** Snapshot of a one-cell embryo in prometaphase expressing GFP:SPDL-1. Scale bar, 5 um. **(I)** SPDL-1 localizes transiently to kinetochores from prometaphase to anaphase onset. Two-cell embryos at different stages are shown co-stained for CENP-C^{HCP-4}, which is present at kinetochores throughout mitosis, and SPDL-1. The natural difference in cell cycle timing of the AB and P_1 cells (with AB entering and exiting mitosis prior to P_1, as diagrammed on the right) defines the transient period of SPDL-1 kinetochore localization (see also Supplementary Video 4). Scale bar, 5 um.

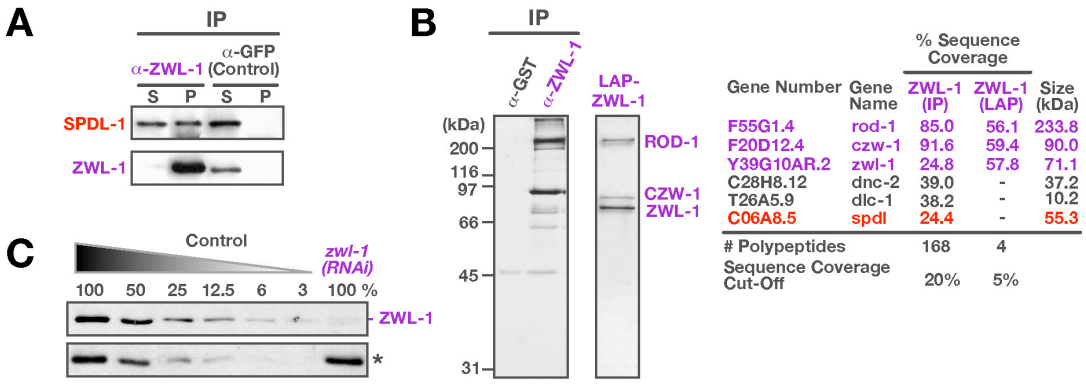

Gene Number	Gene Name	% Sequence Coverage ZWL-1 (IP)	% Sequence Coverage ZWL-1 (LAP)	Size (kDa)
F55G1.4	rod-1	85.0	56.1	233.8
F20D12.4	czw-1	91.6	59.4	90.0
Y39G10AR.2	zwl-1	24.8	57.8	71.1
C28H8.12	dnc-2	39.0	-	37.2
T26A5.9	dlc-1	38.2	-	10.2
C06A8.5	spdl	24.4	-	55.3
# Polypeptides		168	4	
Sequence Coverage Cut-Off		20%	5%	

Figure 3.2 (A-C). SPDL-1 is recruited to the kinetochore by the RZZ complex.

(A) SPDL-1 co-immunoprecipitates with Zwilch^{ZWL-1}. Worm extracts were depleted of Zwilch^{ZWL-1} using an affinity-purified polyclonal antibody, and the resulting supernatant (S) and pellet (P) was analyzed by immunoblot. Loading of pellet is 20 x relative to supernatant. An antibody against GFP was used in the control immunoprecipitation experiment.

(B) SPDL-1 associates with the RZZ complex but is not a core subunit. A one-step immunoprecipitation of Zwilch^{ZWL-1} and a stringent two-step isolation of GFP^{LAP}-tagged Zwilch^{ZWL-1} were visualized on a silver stained gel and analyzed by mass spectrometry as shown on the right. **(C)** Immunoblotting with the anti-Zwilch^{ZWL-1} antibody detects a 70-kD band, which is depleted > 95 % following RNAi. A cross-reacting protein band (*) serves as the loading control.

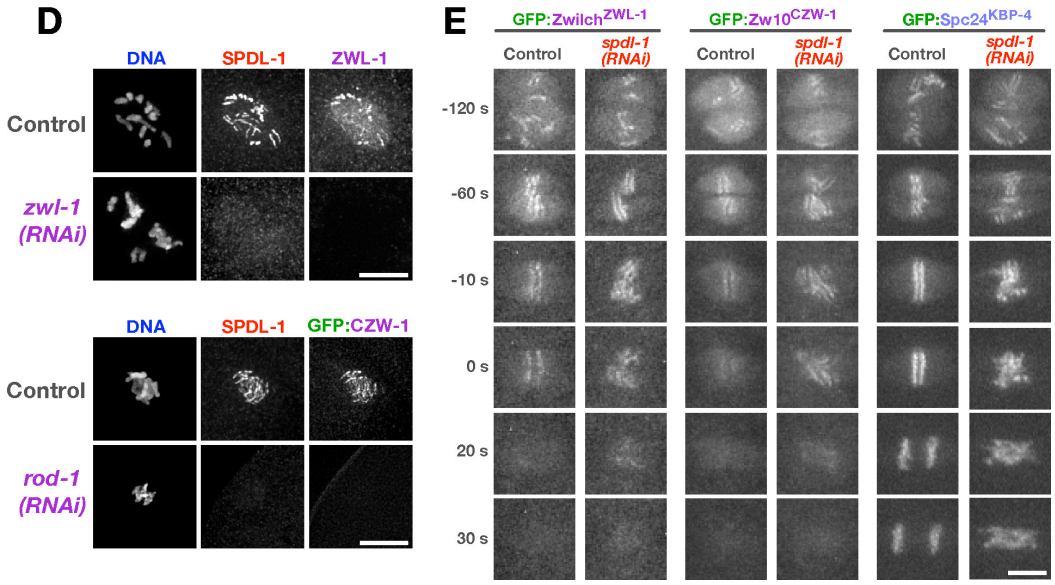

Figure 3.2 (D-E). SPDL-1 is recruited to the kinetochore by the RZZ complex.

(D) Immunofluorescence images of early embryos stained for SPDL-1 after depletion of Zwilch^{ZWL-1} or ROD-1. Scale bars, 5 um. **(E)** Depletion of SPDL-1 affects neither kinetochore targeting of RZZ subunits nor their rapid disappearance from kinetochores at anaphase onset. Selected frames from time-lapse sequences of embryos expressing GFP:Zwilch^{ZWL-1}, GFP:Zw10^{CZW-1}, and GFP:Spc24^{KBP-4} are shown (see also Supplementary Videos 5 and 6). Time is relative to the onset of sister chromatid separation. Scale bar, 5 um.

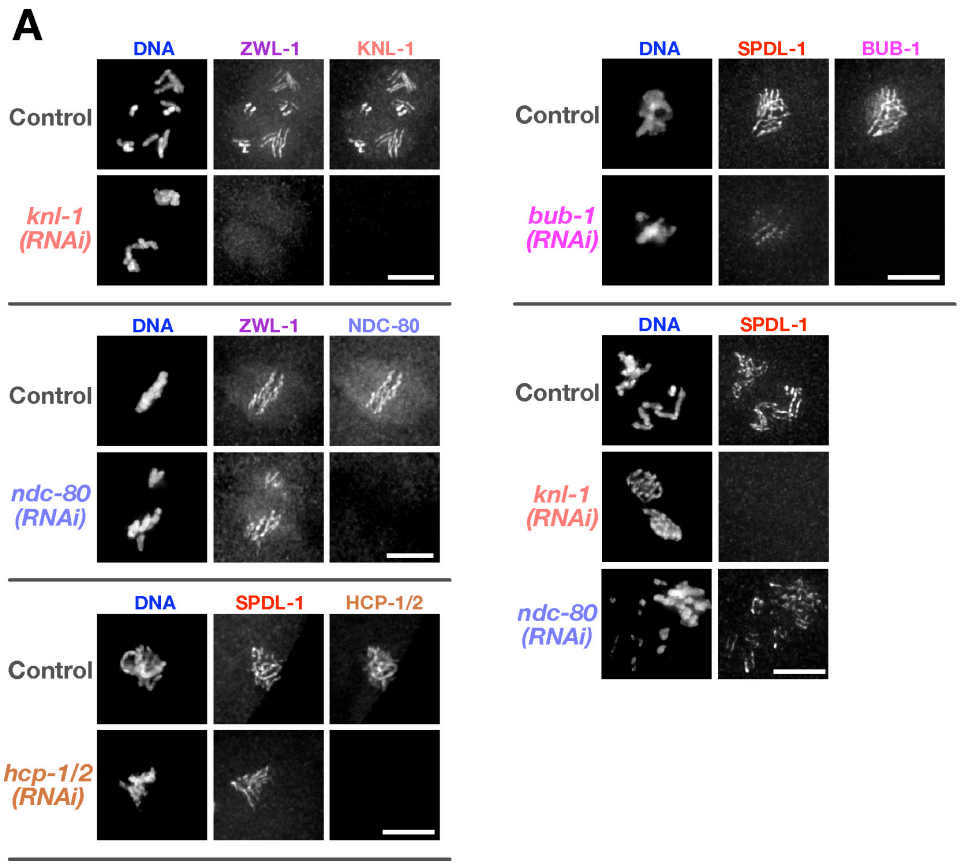

Figure 3.3 (A). SPDL-1 and the RZZ complex are dispensable for the formation of the core kinetochore microtubule attachment site.
(A) Consequences of outer kinetochore component depletion on the localization of SPDL-1 and Zwilch^{ZWL-1}, assayed by immunofluorescence. Scale bars, 5 um.

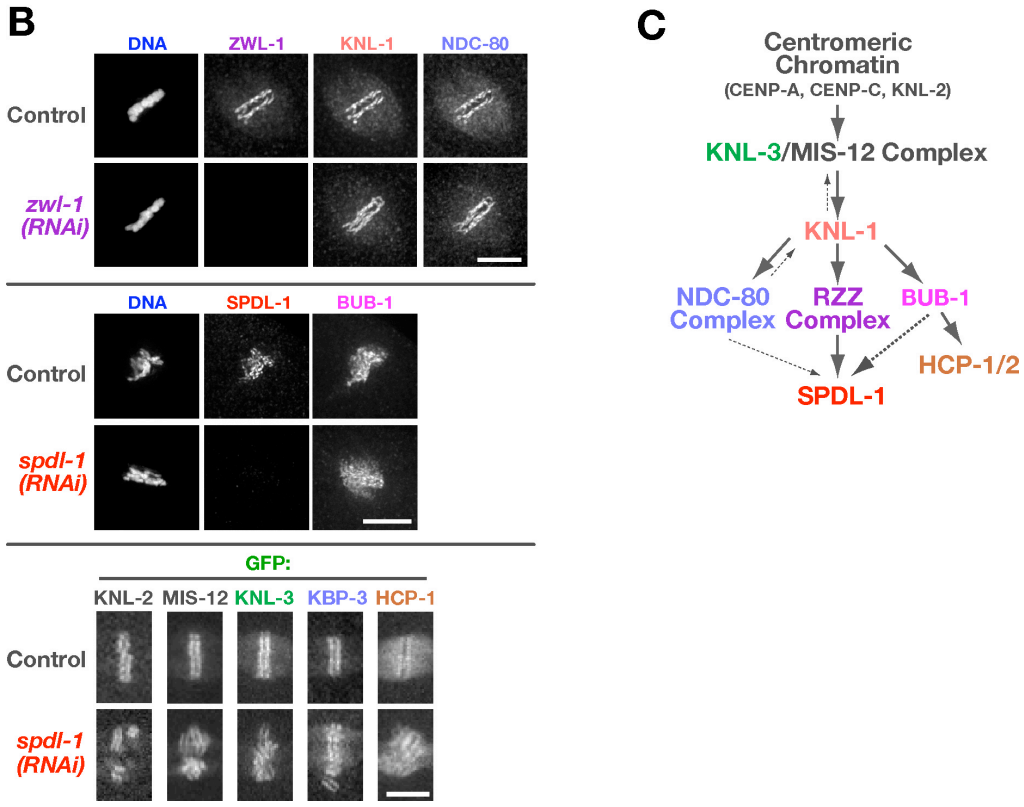

Figure 3.3 (B-C). SPDL-1 and the RZZ complex are dispensable for the formation of the core kinetochore microtubule attachment site.
(B) Normal localization of outer kinetochore components after depletion of SPDL-1 and Zwilch^{ZWL-1}, assayed by immunofluorescence or live-imaging of previously characterized GFP-fusions . Scale bars, 5 um. **(C)** Summary of the dependency analysis for kinetochore targeting of SPDL-1 and the RZZ complex. For each depletion-localization experiment, between 5 and 10 one- or two-cell embryos were examined.

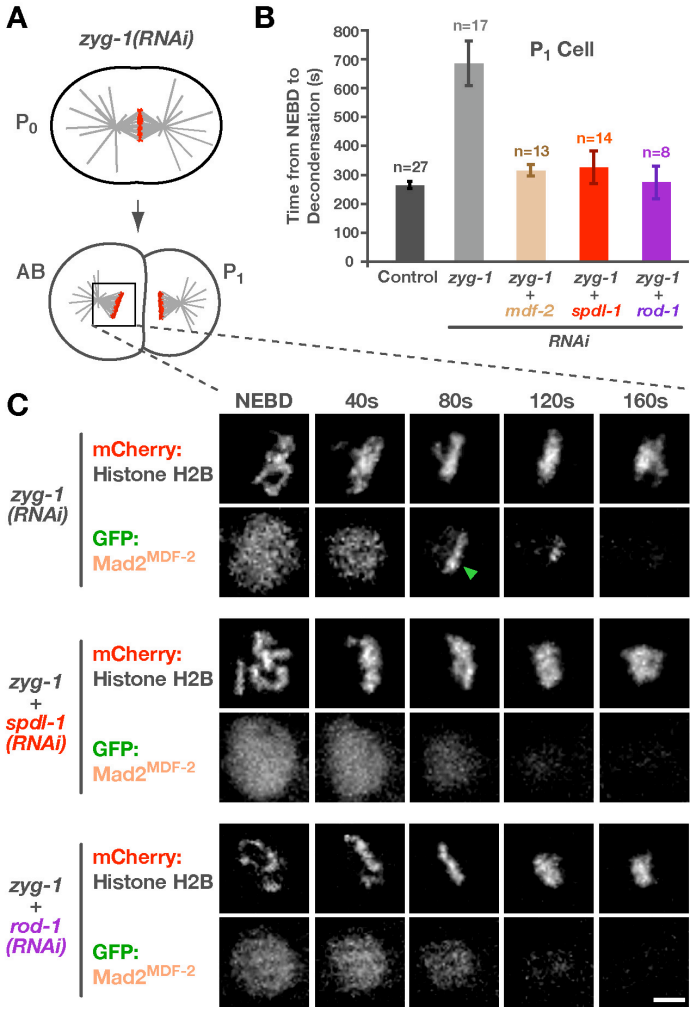

Figure 3.4. SPDL-1 is required for a functional spindle checkpoint and kinetochore localization of Mad2^{MDF-2}.

(A) Perturbation to generate monopolar spindles in the second division and trigger spindle checkpoint activation in *C. elegans* embryos. ZYG-1 is a kinase required for centriole duplication (O'Connell et al., 2001). In *zyg-1(RNAi)* embryos, the first division is normal, because two intact centrioles are contributed by sperm that is not affected by RNAi. These centrioles are unable to duplicate, however, resulting in a monopolar spindle in the subsequent division. **(B)** Average time from NEBD to chromosome decondensation in the P_1 cell of a worm strain expressing GFP:histone H2B. ZYG-1 single depletion results in a significant delay that depends on Mad2^{MDF-2}, SPDL-1, and ROD-1. Error bars represent the S.E.M. with a 95 % confidence interval. A similar result is observed in the AB cell (data not shown). **(C)** Stills from a time-lapse sequence of the AB cell monopolar division in a worm strain co-expressing GFP:Mad2^{MDF-2} and mCherry:histone H2B. In ZYG-1 single depletions, GFP:Mad2^{MDF-2} accumulates on kinetochores that are distal to the pole (arrow). Co-depletion of ZYG-1 with SPDL-1 or ROD-1 prevents kinetochore accumulation of GFP:Mad2^{MDF-2} (see also Supplementary Video 7). Scale bar, 5 um.

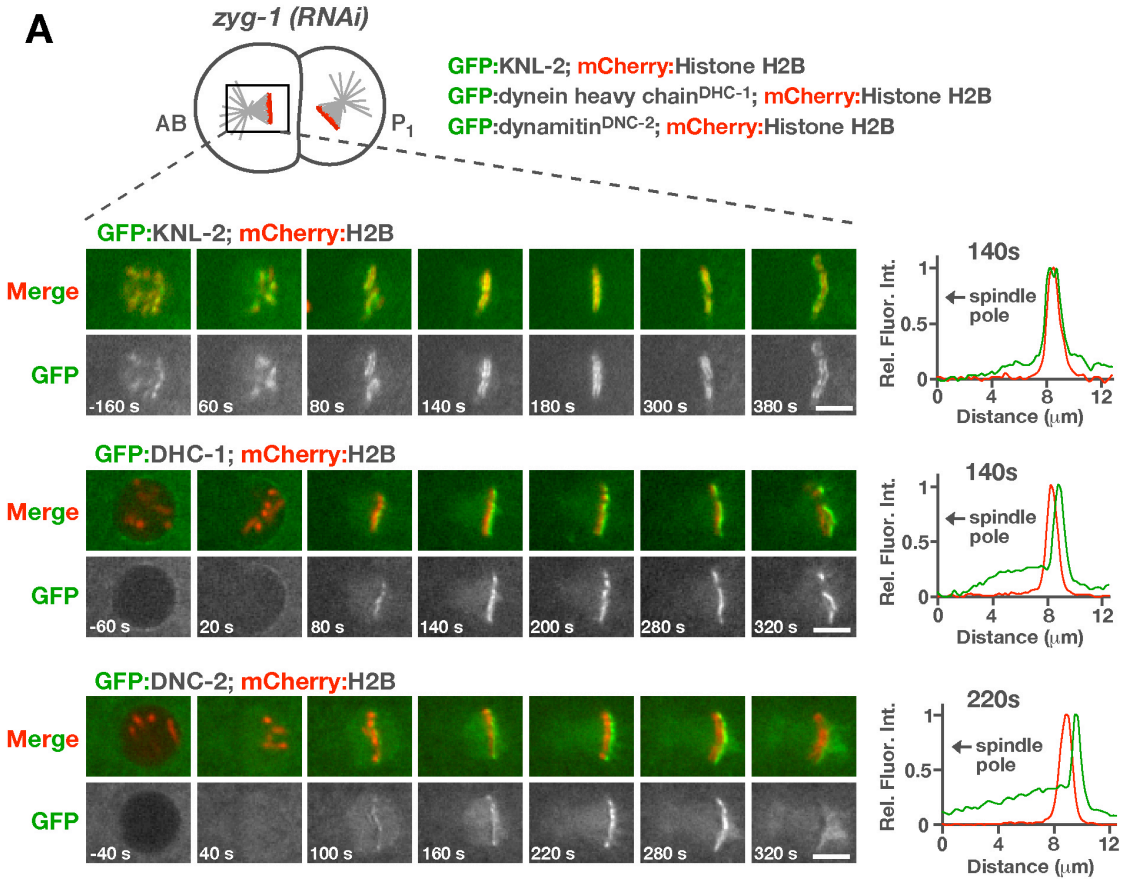

Figure 3.5 (A). Localization of dynein and dynactin to kinetochores requires SPDL-1.

(A) Unattached kinetochores on second division monopolar spindles accumulate dynein and dynactin. Strains stably co-expressing GFP:fusions of either KNL-2, full-length dynein heavy chain^{DHC-1}, or dynamitin^{DNC-2} with mCherry:histone H2B were used to monitor kinetochore localization (see also Supplementary Video 8). All images are of the AB cell and the single spindle pole is always to the left. Times are relative to NEBD. Line scans (5-pixel wide; normalized relative to maximum intensity in each channel) indicate the bilaterally symmetric distribution of KNL-2 relative to mCherry:histone H2B, which contrasts with the asymmetric enrichment of DHC-1 and DNC-2 on the chromosomal face pointing away from the single pole. Scale bars, 5 um.

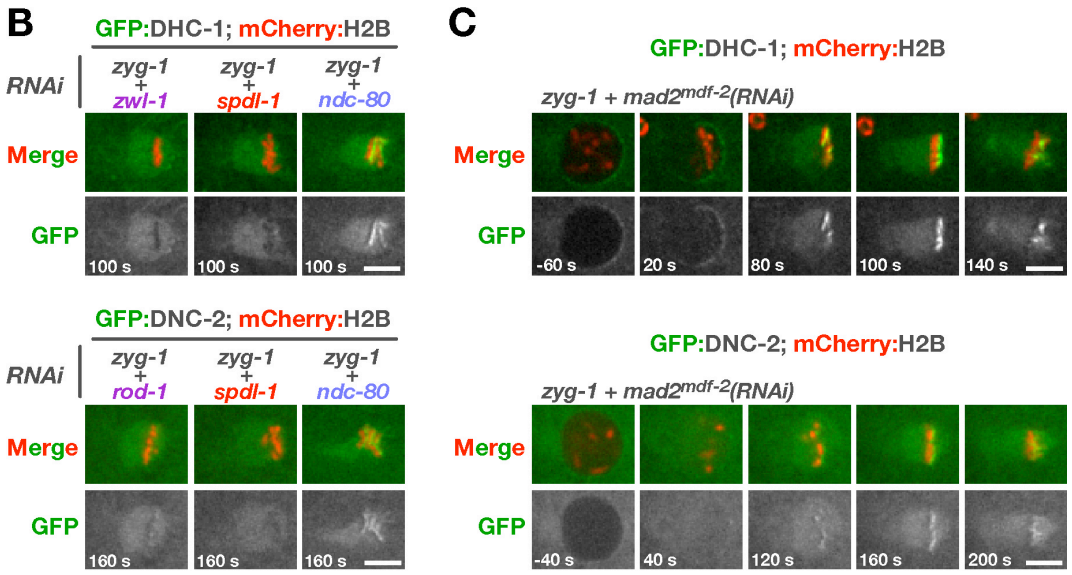

Figure 3.5 (B-C). Localization of dynein and dynactin to kinetochores requires SPDL-1.

(B) Kinetochore accumulation of GFP:dynein heavy chain^{DHC-1} and GFP:dynamitin^{DNC-2} requires SPDL-1 and the RZZ complex but not NDC-80. For brevity, a single frame is shown for each condition (see also Supplementary Videos 9 and 10). Scale bars, 5 um.

(C) Abrogating the spindle checkpoint by depleting Mad2^{MDF-2} does not prevent recruitment of GFP:dynein heavy chain^{DHC-1} or GFP:dynamitin^{DNC-2} to unattached kinetochores. However, accumulation of the GFP:fusion proteins is limited because of premature mitotic exit. Scale bars, 5 um.

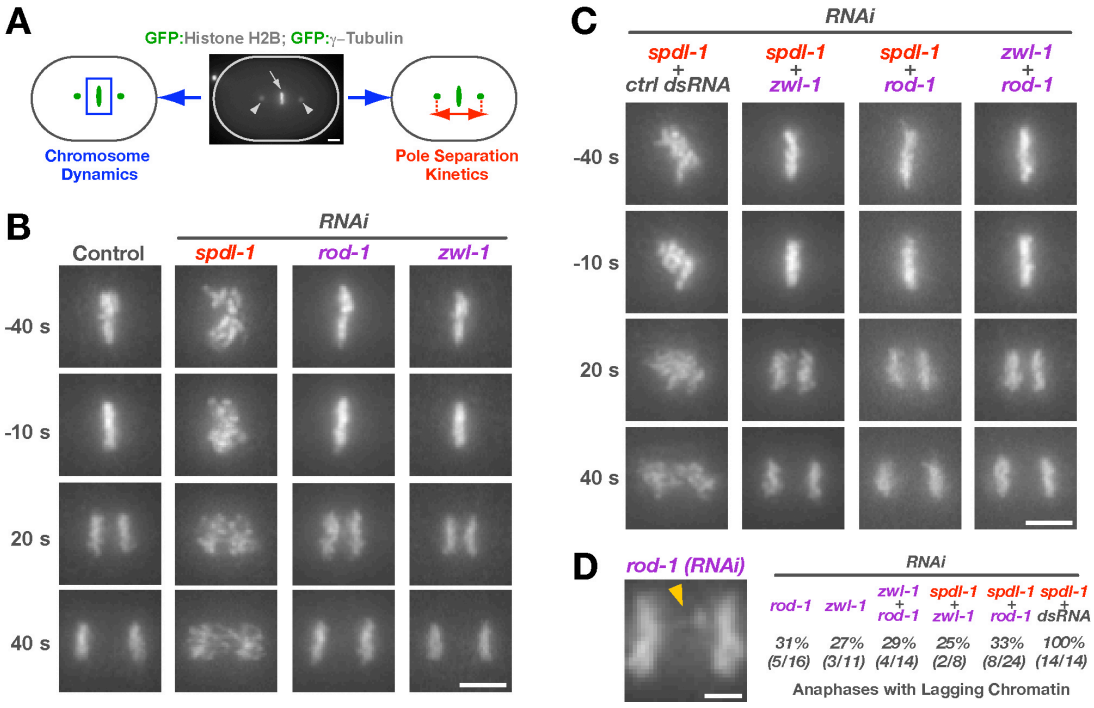

Figure 3.6 (A-D). Depletion of SPDL-1 results in a more severe chromosome segregation defect than depletion of ROD-1 or Zwilch^{ZWL-1}.
(A) Cartoon outlining the two parameters monitored in a strain expressing GFP:histone H2B and GFP:γ-tubulin: chromosome dynamics and kinetics of spindle pole separation.
(B) Frames from time-lapse sequences of the first embryonic division, highlighting the differences in chromosome dynamics after depletion of SPDL-1 and the RZZ complex subunits ROD-1 and Zwilch^{ZWL-1} (see also Supplementary Video 11). Time point 0 s denotes onset of sister chromatid separation. Scale bar, 5 um. **(C)** Selected frames from time-lapse sequences of embryos co-depleted of RZZ subunits and SPDL-1, which significantly reduces the severe chromosome missegregation phenotype of SPDL-1 single depletions to match that of RZZ subunit single depletions (see also Supplementary Video 12). Scale bar, 5 um.
(D) Representative image of anaphase with lagging chromatin in a *rod-1(RNAi)* one-cell embryo. The frequency of one-cell embryos with lagging anaphase chromatin is indicated for single and double inhibitions involving RZZ subunits and SPDL-1. Scale bar, 2 um.

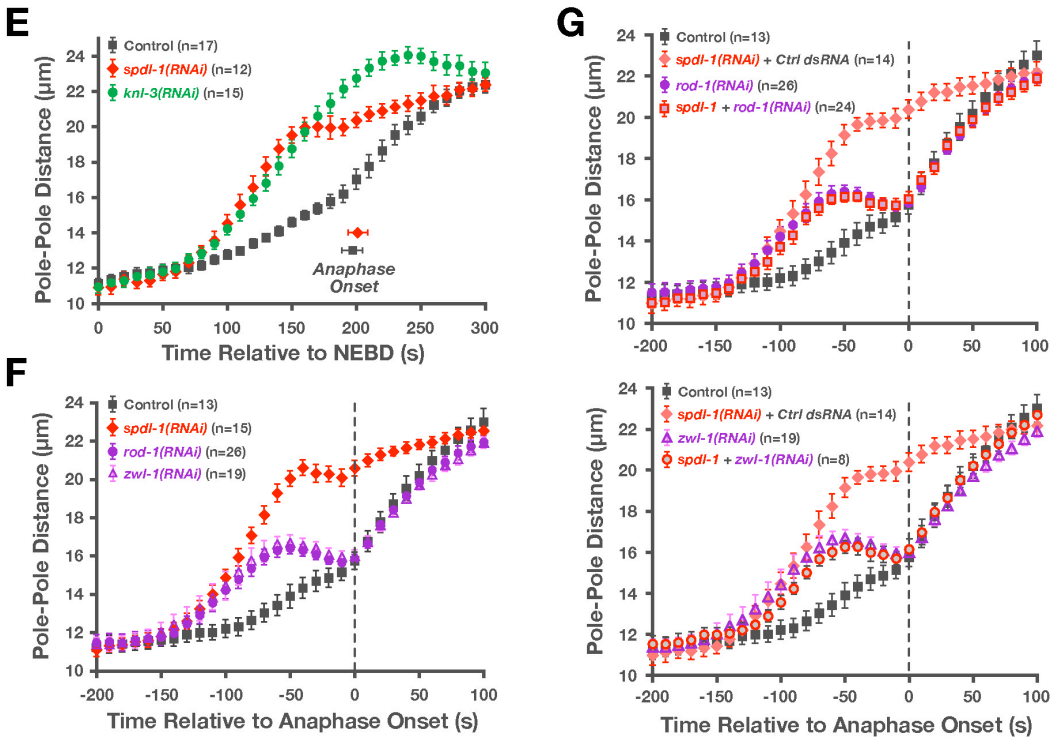

Figure 3.6 (E-H). Depletion of SPDL-1 results in a more severe chromosome segregation defect than depletion of ROD-1 or Zwilch^{ZWL-1}.
(E) Pole separation kinetics in wild type, *spdl-1(RNAi)*, and *knl-3(RNAi)* embryos. Images were acquired at 10 s intervals and sequences were time-aligned relative to NEBD. Pole-pole distances in the time-aligned sequences were measured, averaged for the indicated number (n) of embryos, and plotted against time. Error bars represent the S.E.M. with a 95 % confidence interval. **(F)** Pole separation kinetics of the perturbations shown in (B). Sequences were time-aligned relative to the onset of sister chromatid separation ("Anaphase Onset"). Error bars represent the S.E.M. with a 95 % confidence interval. **(G)** Pole separation kinetics of the perturbations shown in (C), demonstrating that double depletions of SPDL-1 and RZZ complex subunits result in a pole separation profile that is indistinguishable from RZZ subunit single depletions. For controls *spdl-1* dsRNA was diluted equally with dsRNA corresponding to the budding yeast gene *CTF13* or the *C. elegans* gene *sas-5*, which is not required for the first embryonic division (both conditions gave identical results). Error bars represent the S.E.M. with a 95 % confidence interval.

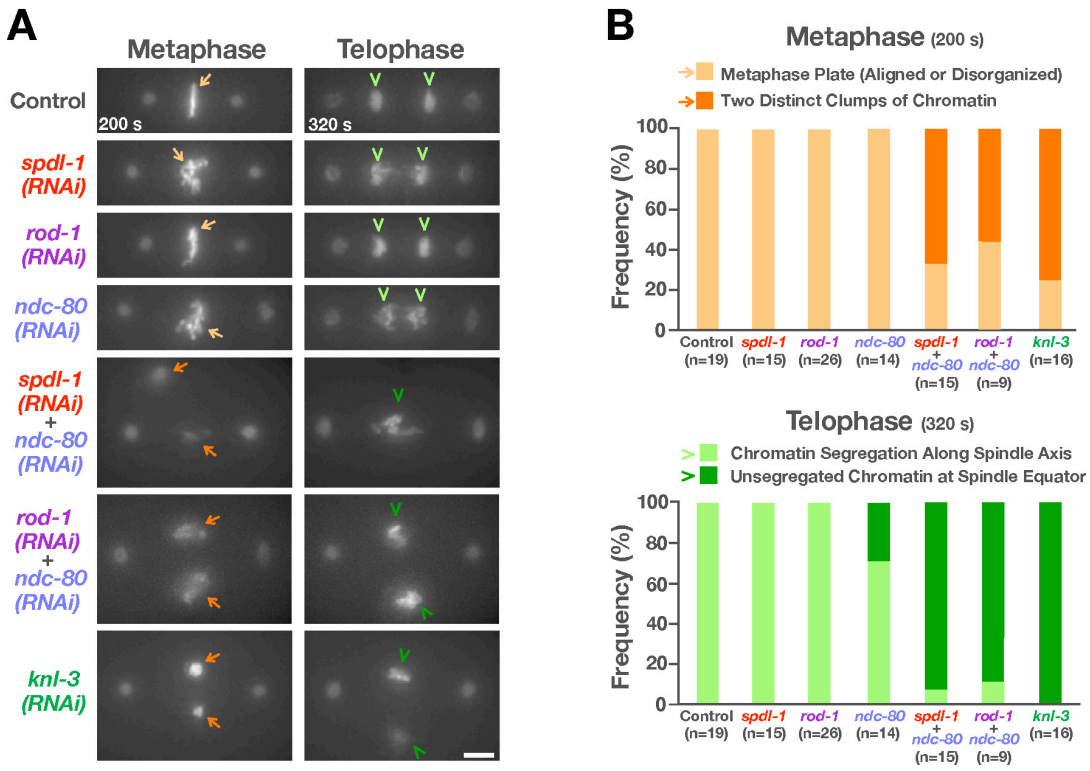

Figure 3.7 (A-B). Co-depletion of SPDL-1 or ROD-1 with NDC-80 recapitulates the "kinetochore null" phenotype.
(A) Frames from time-lapse sequences representing metaphase (200 s after NEBD) and telophase (320 s after NEBD). Co-depletion of SPDL-1 or ROD-1 with NDC-80 approximates the "kinetochore null" phenotype of *knl-3(RNAi)* embryos (see also Supplementary Videos 13 and 14), in which chromosomes of the two pronuclei are often visible as separate clumps at metaphase (arrows) and unsegregated chromatin remains at the spindle equator in telophase (arrowheads). Scale bar, 5 um. **(B)** Percentage of first divisions displaying the chromosome morphologies described in (A) at 200 s and 320 s after NEBD.

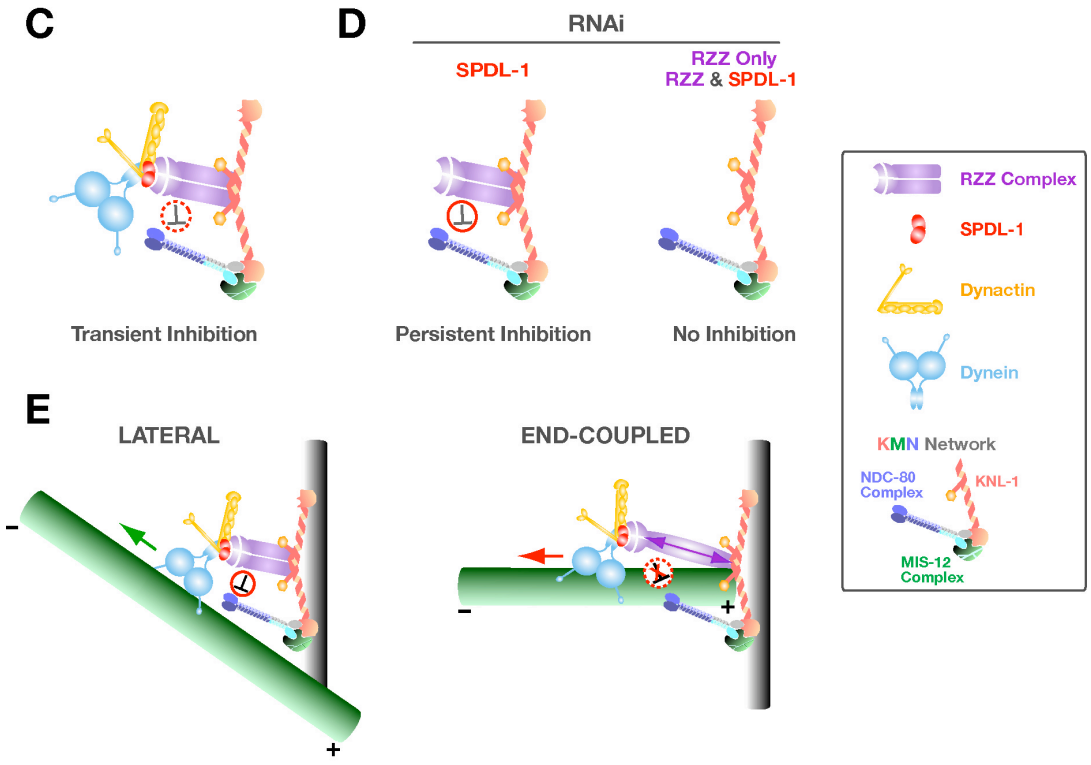

Figure 3.7 (C-E). Co-depletion of SPDL-1 or ROD-1 with NDC-80 recapitulates the "kinetochore null" phenotype.
(C) Schematic summary of the relationship between the RZZ complex, SPDL-1, dynein/dynactin, and the NDC-80 complex. The negative regulation of the KMN network by the RZZ complex, which is transient in the wild-type situation, may be either direct or indirect. **(D)** Model explaining the difference in phenotypic severity between SPDL-1 and RZZ complex inhibitions. Specifically, we propose that SPDL-1 depletion results in persistent RZZ complex-mediated inhibition of the KMN network (until just prior to anaphase onset), because RZZ complex localization to kinetochores is uncoupled from dynein/dynactin. In RZZ subunit depletions or co-depletions of SPDL-1 with RZZ subunits, the inhibitory mechanism is absent, resulting in the weaker phenotype, which reflects loss of dynein contribution to the establishment and orientation of load-bearing attachments. **(E)** A speculative model for the physiological role of a RZZ complex-mediated inhibition of the KMN network during prometaphase. Dynein/dynactin laterally captures microtubules to accelerate formation of end-coupled attachments of correct geometry. While a microtubule is laterally bound, dynein motility does not experience significant resistance (green arrow); consequently, there is low intra-kinetochore tension, and the RZZ complex inhibits the KMN network from binding prematurely to the microtubule, which would interfere with dynein-mediated kinetochore orientation. When the plus end of the microtubule becomes embedded into the outer plate (end-coupled attachment) and provides resistance to dynein/dynactin motility (red arrow), the increased intra-kinetochore tension turns off the inhibitory action of the RZZ complex, allowing formation of stable load-bearing attachments.

A

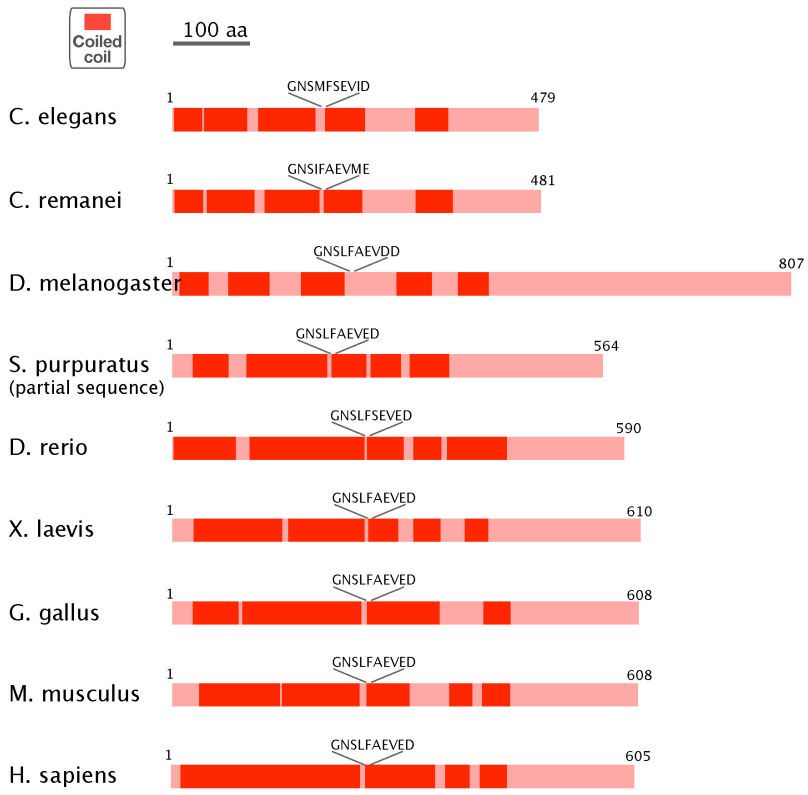

B

	Isoelectric Point	MW (kD)
C. elegans	5.78	55.3
C. remanei	5.59	55.8
D. melanogaster	5.90	91.4
S. purpuratus (partial)	6.63	64.7
D. rerio	5.57	68.9
X. laevis	5.38	70.8
G. gallus	5.73	71.2
M. musculus	5.75	70.2
H. sapiens	5.45	70.1

Figure S3.1. Sequence features of SPDL-1/Spindly related proteins.
(A) Coiled-coil regions are boxed in red. The position of the highly conserved GNS[I,L,M]F[S,A]EV motif is indicated. In all cases, this motif is positioned close to a predicted break in the coiled-coil. This motif is also present at a similar location, relative to the total number of amino acids in each protein, with the exception of the *D. melanogaster* protein that has an extended C-terminal region. **(B)** Predicted molecular weights and isolectric points of SPDL-1/Spindly-related proteins from different species. Accession numbers of the sequences used are: *C. elegans* (NP_495637); *D. melanogaster* (NP_608791); *S. purpuratus* (XP_794989); *D. rerio* (NP_001098412); *X. laevis* (NP_001084803); *G. gallus* (XP_414505); *M. musculus* (NP_081687); *H. sapiens* (Q96EA4).

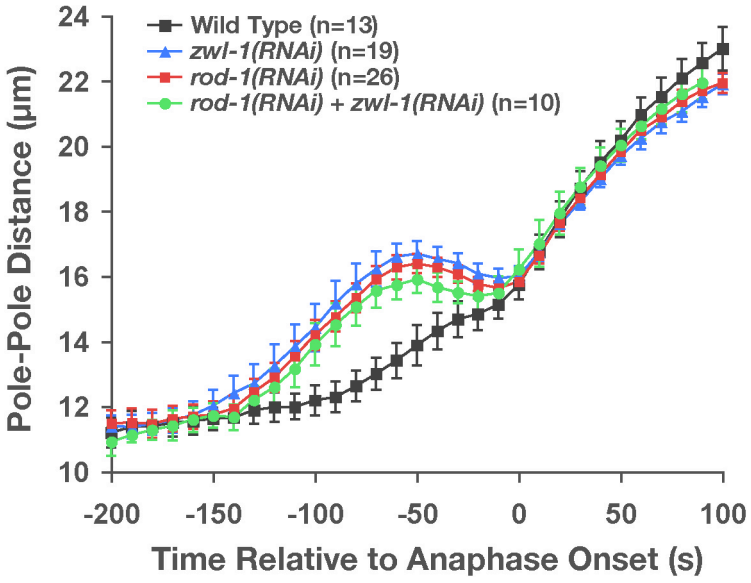

Figure S3.2. Co-depletion of ROD-1 with Zwilch^{ZWL-1} results in the same spindle pole separation profile as single depletion of ROD-1 or Zwilch^{ZWL-1}.

Images were acquired at 10 s intervals and sequences were time-aligned relative to anaphase onset. Pole-pole distances in the time-aligned sequences were measured, averaged for the indicated number (n) of embryos, and plotted against time. Error bars represent the S.E.M. with a 95 % confidence interval.

Table S3.1. Worm strains used in this study.

Strain #	Genotype
TH32	*unc-119(ed3) III; ruIs32 [pAZ132; pie-1/GFP::histone H2B] III; ddIs6 [GFP::tbg-1; unc-119(+)]*
XA3501	*unc 119(ed3) III; ruIs32 [pAZ132; pie-1/GFP::histone H2B] III; ruIs57 [pAZ147; pie-1/GFP::C36E8.5] V*
OD1	*unc-119(ed3) III; ltIs1 [pIC22; pie-1/GFP::knl-3; unc-119 (+)]*
OD7	*unc-119(ed3) III; ltIs3 [pIC31; pie-1/GFP-TEV-STag::hcp-1; unc-119 (+)]*
OD8	*unc-119(ed3) III; ltIs4 [pIC32; pie-1/GFP-TEV-STag::mis-12; unc-119 (+)]*
OD11	*unc-119(ed3) III; ltIs7 [pIC41; pie-1/GFP-TEV-STag::kbp-4; unc-119 (+)]/+*
OD13	*unc-119(ed3) III; ltIs9 [pIC34; pie-1/GFP-TEV-STag::kbp-3; unc-119 (+)]/+*
OD29	*unc-119(ed3) III; ltIs21 [pIC54; pie-1/GFP-TEV-STag::czw-1; unc-119 (+)]*
OD31	*unc-119(ed3) III; ltIs22 [pPM3; pie-1/GFP-TEV-STag::knl-2; unc-119 (+)]*
OD42	*unc-119(ed3) III; ltIs31 [pIC70; pie-1/GFP-TEV-STag::Y39G10AR.2; unc-119 (+)]/+*
OD110	*unc-119(ed3) III; ltIs52 [pOD379; pie-1/GFP-TEV-STag::Y69A2AR.30; unc-119 (+)]; ltIs37 [pAA64; pie-1/mCherry::his-58; unc-119 (+)] IV*
OD201	*unc-119(ed3) III; ltIs121 [pie-1/GFP-TEV-STag::C06A8.5; unc-119 (+)]*
OD202	*unc-119(ed3) III; ltIs22 [pPM3; pie-1/GFP-TEV-STag::knl-2; unc-119 (+)]; ltIs37 [pAA64; pie-1/mCherry::his-58; unc-119 (+)] IV*
OD203	*unc-119(ed3) III; orIs17 [dhc-1::GFP::dhc-1; unc-119(+)]; ltIs37 [pAA64; pie-1/mCherry::his-58; unc-119 (+)] IV*
OD204	*unc-199(ed3) III; tjIs11 [pie-1/GFP::dnc-2; unc-119 (+)]; ltIs122 [pAA64; pie-1/mCherry::his-58; unc-119 (+)]*

Table S3.2. Double-stranded RNAs used in this study.

RNA #	Gene #	Name	Conc. mg/ml	Oligo #1	Oligo #2	Template
2	Y69A2AR.30	*mdf-2*	3.2	TAATACGACTCACTATAGGgagaccacacggatgtaaagacacaaaacg	TAATACGACTCACTATAGGgagaccacgtgaactgacgtcgagaatgag	cDNA
3	F55G1.4	*rod-1*	2.1	TAATACGACTCACTATAGGgagaccactcgtatggaaagtatgccactg	TAATACGACTCACTATAGGgagaccacgttcatgcaaagcagtcaaatc	cDNA
5	F20D12.4	*czw-1*	2.0	TAATACGACTCACTATAGGgagaccactgattggacaattaccagaacg	TAATACGACTCACTATAGGgagaccacctgattgtcaccactagcctca	cDNA
29	T06E4.1	*hcp-2*	1.9	TAATACGACTCACTATAGGtctcggaaaggaatcgaaaa	AATTAACCCTCACTAAAGGtcgttgtctccaattccaca	genomic DNA
57	None (yeast gene)	*CTF13*	1.8	TAATACGACTCACTATAGGTGTGGAGCTTCCAGGAAAAC	AATTAACCCTCACTAAAGGCTCGATGTTCCACCACTTGA	genomic DNA
61	C02F5.1	*knl-1*	1.9	TAATACGACTCACTATAGGccgctgaaatggatacgagt	AATTAACCCTCACTAAAGGccatgctaatgtcttcacacg	genomic DNA
64	ZK1055.1	*hcp-1*	2.1	TAATACGACTCACTATAGGaaaccgagtcgccattttc	AATTAACCCTCACTAAAGGagatcgcgctgaagactttc	genomic DNA
84	W01B6.9	*ndc-80*	1.6	AATTAACCCTCACTAAAGGccccagtctgagtcaacctc	TAATACGACTCACTATAGGccaactcgcttgaatttcc	genomic DNA
166	F35B12.5	*sas-5*	3.8	AATTAACCCTCACTAAAGGAGGACAAACCCCCAGTACC	TAATACGACTCACTATAGGAGAAGCGAGTCCGTTGTCAT	genomic DNA
171	T10B5.6	*knl-3*	1.2	AATTAACCCTCACTAAAGGatgtctcaaaaatcaaacgacacc	TAATACGACTCACTATAGGgtcgagaaaacttccgtgaag	cDNA
205	F59E12.2	*zyg-1*	1.4	AATTAACCCTCACTAAAGGtggacggaaattcaaacgat	TAATACGACTCACTATAGGaacgaaattccttgagctg	cDNA
235	Y39G10AR.2	*zwl-1*	2.0	AATTAACCCTCACTAAAGGatgccactcaccatcgagcag	TAATACGACTCACTATAGGggatcagtgaagcgagatgactc	cDNA

Table S3.2 (Continued). Double-stranded RNAs used in this study.

RNA #	Gene #	Name	Conc. mg/ml	Oligo #1	Oligo #2	Template
365	R06C7.8	*Bub-1*	3.4	AATTAACCCTCACTAAAGGtgccaaatggaaggacactt	TAATACGACTCACTATAGGtctgagattcttccggttcg	cDNA
377	C06A8.5	*Spdl-1*	2.2	AATTAACCCTCACTAAAGGatcgagcactgaaagggatg	TAATACGACTCACTATAGGgcgtaacggcaatactggat	cDNA

Table S3.3. Live-Imaging conditions for worm strains

Strain #	Time-lapse	Z-stack	Exposure (Fluorophore)
TH32	10 s	5 x 2 μm	150 ms (GFP)
TH32 (Fig. 4)	20 s	6 x 2 μm	100 ms (GFP)
XA3501	2 s	none	150 ms (GFP)
OD1	10 s	4 x 2 μm	150 ms (GFP)
OD7	10 s	3 x 2 μm	1000 ms (GFP)
OD8	10 s	4 x 2 μm	150 ms (GFP)
OD11	10 s	3 x 2 μm	1000 ms (GFP)
OD13	15 s	3 x 2 μm	250 ms (GFP)
OD29	10 s	3 x 2 μm	1000 ms (GFP)
OD31	5 s	none	500 ms (GFP)
OD42	10 s	3 x 2 μm	1000 ms (GFP)
OD110	20 s	5 x 2 μm	300 ms (GFP); 300 ms (mCherry)
OD201	30 s	3 x 2 μm	250 ms (GFP)
OD202	20 s	none	1000 ms (GFP); 1000 ms (mCherry)
OD203	20 s	none	1000 ms GFP); 1000 (mCherry)
OD204	20 s	none	750 ms (GFP); 1000 ms (mCherry)

Chapter 4: Conclusions and Future Directions

4.1 Conclusions

My thesis work has comprehensively defined the requirements of conserved kinetochore proteins for checkpoint activation and signaling. That checkpoint activation requires three components (the NDC-80 complex, the RZZ complex, and BUB-1) independently targeted by the scaffold protein KNL-1 strongly suggests that in order to mount a checkpoint response, a kinetochore capable of making productive, force-transducing microtubule interactions is required. KNL-1 and the NDC-80 complex are two members of the KMN network, which likely accounts for the core microtubule binding activity of the kinetochore (Cheeseman et al., 2006). The RZZ complex is necessary for targeting dynein and SPDL-1 to the kinetochore, the latter appearing to modulate the activity of RZZ in a dynein-dependent manner while also being a requirement for the checkpoint. RZZ in turn negatively regulates the microtubule binding activity of the KMN network. Thus, the RZZ-dynein-SPDL-1 axis provides a third point of contact from kinetochores to microtubules, in addition to the NDC-80 complex and KNL-1.

Perhaps the most interesting finding from my thesis work is the bypass of the requirement of BUB-3 and $Mad3^{SAN-1}$ in kinetochore-dependent checkpoint activation upon subtle overexpression of $Mad2^{MDF-2}$. Conversely, BUB-3 targets to and becomes enriched at kinetochores in the absence of

Mad2^{MDF-2}, although in this case no checkpoint signal is generated, indicating that the bypass only works one-way. I have also demonstrated that although Mad3^{SAN-1} does not localize to kinetochores upon checkpoint activation, two lines of evidence support a functional link to BUB-3. First, BUB-3 was the only protein whose depletion had an effect on Mad3^{SAN-1} fluorescence levels. Second, the aforementioned overexpression of Mad2^{MDF-2} bypassed the depletion of both BUB-3 and Mad3^{SAN-1}. Although Bub3 is required for kinetochore localization of Bub1 in other model systems (Musacchio and Salmon, 2007), this is not the case in worms (my unpublished observations). This begs the question, what is the role of kinetochore localized BUB-3? A recent study using purified checkpoint components *in vitro* has suggested that for catalysis of APC/C inhibitory activity, chromosomes, Mad1 and dimerization-competent Mad2 must be present (Kulukian et al., 2009). This study also found that most Cdc20 was in a complex with BubR1 (orthologous to Mad3^{SAN-1}), not Mad2. In light of this data, I propose that in *C. elegans*, the role of kinetochore localized BUB-3 may be to become modified to potentiate its association with Mad3^{SAN-1}, which may in turn influence the affinity of Mad3^{SAN-1} for Cdc20.

My thesis project initially focused on the role of BUB-1 in regulating kinetochore assembly, as it was shown early on to be a bona-fide kinetochore protein, and its depletion resulted in embryonic lethality (Desai et al., 2003; Oegema et al., 2001). Specifically, I wanted to determine the role of the kinase

domain in regulating kinetochore formation and chromosome segregation, as BUB-1 is the only conserved checkpoint protein in this organism that possesses such a domain – no Mps1 orthologue has been identified, and Mad3, orthologous to vertebrate BubR1, lacks a kinase domain. However, these studies did not progress far, due to the fact that despite multiple attempts with many different constructs, I never generated a transgenic strain expressing a fluorescently tagged version of the protein. We inferred from these failures that BUB-1 expression levels may be tightly regulated, and the presence of an extra copy (or copies) in the genome was likely not well tolerated. Because of this hurdle, we decided to shift the focus of the project to determine the requirements of kinetochore proteins for checkpoint activation. Having first developed the cell cycle timing assay based on monopolar spindle formation, I determined the requirement of each of the conserved checkpoint proteins for the delays. Although each is required for cell cycle delays in the second division, the kinetics of the first division remain unchanged following depletions of Mad2^{MDF-2} or Mad3^{SAN-1} (figure 2.1E). This is in contrast to results from HeLa cells, where depletion of these (but not other) checkpoint proteins resulted in accelerated timing of mitosis relative to controls (Meraldi et al., 2004). The discrepancy between these results is interesting, and it is tempting to speculate what other factors could explain why the cell cycle could appear to be accelerated under such conditions. The hypothesis put forth by Meraldi et al., is essentially that in prometaphase, the

checkpoint exists in two phases; the first phase (kinetochore independent) relies on Mad2 and BubR1 to inhibit APC/C activity, as still-forming kinetochores are not yet capable of sensing and transducing the state of microtubule binding. The second phase, later in prometaphase, is then kinetochore-dependent, as more "mature" kinetochores produce the canonical APC/C inhibitory factors as necessary. While this is an interesting hypothesis, its interpretation is compounded by the fact that both Mad2 and BubR1 have been shown to directly bind Cdc20 (while Mad1, Bub3, and RZZ do not), and this binding may produce a transient inhibition of APC/C early in prometaphase that could account for the first phase inhibition proposed by Meraldi et al. I propose that several fundamental differences in the mechanisms of mitosis between humans and *C. elegans* may account for the lack of accelerated mitosis following Mad2^{MDF-2} or Mad3^{SAN-1} depletions in worm embryos. First, the overall duration of (unperturbed) mitosis is much longer in human cells, which may reflect reduced efficiency (or increased complexity) of formation of proper kinetochore-microtubule interactions. Humans have evolved a larger, more fragmented genome; 46 chromosomes instead of 12 in *C. elegans.* The consequences of losing a chromosome may be greater in vertebrates, as is suggested by the fact that homozygous deletions of checkpoint proteins are embryonic lethal (Baker et al., 2005), but this is not the case in worms, at least for Mad1^{MDF-1}, Mad2^{MDF-2}, or Mad3^{SAN-1}. Additionally, the mechanisms of chromosome alignment appear subtly

different between holocentrics and monocentrics. In worms, chromosomes in prometaphase are not observed to oscillate in a “tug-of-war” between centrosomes, migrating first to one pole and then the other before final alignment at the metaphase plate; rather, the chromosomes stay more tightly clustered between centrosomes from nuclear envelope breakdown to metaphase. This suggests that the initial interactions of kinetochores with spindle microtubules may be fundamentally different than those of human cells, possibly as a result of the holocentric architecture. In summary, additional levels of mitotic regulation may have evolved in vertebrates, perhaps to deal with the more serious consequences of chromosome missegregation and/or the potentially more error-prone process of chromosome-microtubule attachments.

4.2 Future Directions

The role of BUB-1 kinase activity in checkpoint signaling and chromosome segregation remains unclear. The early embryo of *C. elegans* is uniquely suited to study the role of BUB-1 kinase activity to chromosome segregation, since my earlier work has demonstrated that the early mitotic divisions can proceed in the absence of a checkpoint, as when Mad2^{MDF-2} is depleted by RNAi. Although work in mammalian cells suggests that an important function of BUB-1 is the targeting of the Shugoshin proteins, I have also shown in my thesis work that depletion of the only conserved Shugoshin family protein, SGO-1, has no checkpoint or chromosome segregation

phenotype. A new technique (MosSCI) now exists that allows for the single copy insertion of a transgene driven under its endogenous promoter, at a defined locus in the genome (Frokjaer-Jensen et al., 2008). I have already used this method to generate strains expressing both wild type HCP-3 and various HCP-3 mutants under control of the endogenous promoter and 3'-UTR. These constructs fully rescue the *hcp-3* deletion strain *vc1393* (my unpublished data), validating the efficacy this method for performing structure-function studies. I propose using this technique to generate strains expressing both wild-type and kinase-dead BUB-1 (K718R, abrogates kinase activity in yeast (Roberts et al., 1994)) under control of the endogenous promoter and 3'-UTR, and crossing these strains into the *bub-1* deletion strain *tm2815*. Strains expressing GFP-histone H2b and (separately) GFP:: Mad2^{MDF-2} can then be crossed into the MosSCI-BUB-1 strains, and the effects of the kinase domain on chromosome segregation and checkpoint function then quantified using the assays described in chapter 2 of this thesis. Additional known functions of BUB-1 such as kinetochore targeting of BUB-3, dynein/dynactin, HCP-1/2, Clasp^{CLS-2} (chapters 2, 3 and (Encalada et al., 2005)) will also be tested for their dependence on BUB-1 kinase activity. It is highly likely that the wild-type MosSCI-BUB-1 will fully rescue the deletion strain; it is possible that the kinase-dead version will fail to rescue, however. If it does not rescue, this in itself is strong evidence that the kinase domain is necessary for the chromosome segregation functions of BUB-1. Other variants of BUB-1 that

abrogate its kinase activity such as a C-terminal truncation fully excluding the kinase domain (starts at amino acid 689, KLH..) may also be useful alternatives to the point mutant and should be tested.

In chapter 2 of this thesis, the magnitude of the mitotic delay observed in the second and third embryonic divisions in the presence of monopolar spindles was modest, only extending the cell cycle twofold. The small magnitude of this delay may reflect the large cytoplasm-to-nuclear ratio at the two cell stage. To determine if the delay is greater when the cytoplasm-to-nuclear ration is smaller, I propose timing cell cycle progression at the four cell stage, both in the presence of bipolar spindles as controls and monopolar spindles as the experimental condition. To generate monopolar spindles at this stage, the fast-acting temperature-sensitive DH1 strain will be used, after crossing in GFP-histone H2b to facilitate timing nuclear envelope breakdown and chromosome decondensation. DH1 possesses a ts mutation in the zyg-1 gene, which is fast acting and should therefore induce monopolar spindle formation after shifting the temperature to 25 degrees C following completion of the third cell division.

References

Abrieu, A., Kahana, J. A., Wood, K. W., and Cleveland, D. W. (2000). CENP-E as an essential component of the mitotic checkpoint in vitro. Cell *102*, 817-826.

Abrieu, A., Magnaghi-Jaulin, L., Kahana, J. A., Peter, M., Castro, A., Vigneron, S., Lorca, T., Cleveland, D. W., and Labbe, J. C. (2001). Mps1 is a kinetochore-associated kinase essential for the vertebrate mitotic checkpoint. Cell *106*, 83-93.

Amor, D. J., and Choo, K. H. (2002). Neocentromeres: role in human disease, evolution, and centromere study. Am J Hum Genet *71*, 695-714.

Baker, D. J., Chen, J., and van Deursen, J. M. (2005). The mitotic checkpoint in cancer and aging: what have mice taught us? Curr Opin Cell Biol *17*, 583-589.

Basto, R., Gomes, R., and Karess, R. E. (2000). Rough deal and Zw10 are required for the metaphase checkpoint in Drosophila. Nat Cell Biol *2*, 939-943.

Bettencourt-Dias, M., and Glover, D. M. (2007). Centrosome biogenesis and function: centrosomics brings new understanding. Nat Rev Mol Cell Biol *8*, 451-463.

Biggins, S., and Murray, A. W. (2001). The budding yeast protein kinase Ipl1/Aurora allows the absence of tension to activate the spindle checkpoint. Genes Dev *15*, 3118-3129.

Blower, M. D., Daigle, T., Kaufman, T., and Karpen, G. H. (2006). Drosophila CENP-A mutations cause a BubR1-dependent early mitotic delay without normal localization of kinetochore components. PLoS Genet *2*, e110.

Blower, M. D., Sullivan, B. A., and Karpen, G. H. (2002). Conserved organization of centromeric chromatin in flies and humans. Dev Cell *2*, 319-330.

Bomont, P., Maddox, P., Shah, J. V., Desai, A. B., and Cleveland, D. W. (2005). Unstable microtubule capture at kinetochores depleted of the centromere-associated protein CENP-F. Embo J *24*, 3927-3939.

Boyarchuk, Y., Salic, A., Dasso, M., and Arnaoutov, A. (2007). Bub1 is essential for assembly of the functional inner centromere. J Cell Biol *176*, 919-928.

Brauchle, M., Baumer, K., and Gonczy, P. (2003). Differential activation of the DNA replication checkpoint contributes to asynchrony of cell division in C. elegans embryos. Curr Biol *13*, 819-827.

Brinkley, B. R., and Stubblefield, E. (1966). The fine structure of the kinetochore of a mammalian cell in vitro. Chromosoma *19*, 28-43.

Buchwitz, B. J., Ahmad, K., Moore, L. L., Roth, M. B., and Henikoff, S. (1999). A histone-H3-like protein in C. elegans. Nature *401*, 547-548.

Buffin, E., Emre, D., and Karess, R. E. (2007). Flies without a spindle checkpoint. Nat Cell Biol *9*, 565-572.

Buffin, E., Lefebvre, C., Huang, J., Gagou, M. E., and Karess, R. E. (2005). Recruitment of Mad2 to the kinetochore requires the Rod/Zw10 complex. Curr Biol *15*, 856-861.

Burton, J. L., and Solomon, M. J. (2007). Mad3p, a pseudosubstrate inhibitor of APCCdc20 in the spindle assembly checkpoint. Genes Dev *21*, 655-667.

Canman, J. C., Hoffman, D. B., and Salmon, E. D. (2000). The role of pre- and post-anaphase microtubules in the cytokinesis phase of the cell cycle. Curr Biol *10*, 611-614.

Chan, G. K., Jablonski, S. A., Starr, D. A., Goldberg, M. L., and Yen, T. J. (2000). Human Zw10 and ROD are mitotic checkpoint proteins that bind to kinetochores. Nat Cell Biol *2*, 944-947.

Chan, G. K., Jablonski, S. A., Sudakin, V., Hittle, J. C., and Yen, T. J. (1999). Human BUBR1 is a mitotic checkpoint kinase that monitors CENP-E functions at kinetochores and binds the cyclosome/APC. J Cell Biol *146*, 941-954.

Cheeseman, I. M., Brew, C., Wolyniak, M., Desai, A., Anderson, S., Muster, N., Yates, J. R., Huffaker, T. C., Drubin, D. G., and Barnes, G. (2001). Implication of a novel multiprotein Dam1p complex in outer kinetochore function. J Cell Biol *155*, 1137-1145.

Cheeseman, I. M., Chappie, J. S., Wilson-Kubalek, E. M., and Desai, A. (2006). The conserved KMN network constitutes the core microtubule-binding site of the kinetochore. Cell *127*, 983-997.

Cheeseman, I. M., and Desai, A. (2008). Molecular architecture of the kinetochore-microtubule interface. Nat Rev Mol Cell Biol *9*, 33-46.

Cheeseman, I. M., MacLeod, I., Yates, J. R., 3rd, Oegema, K., and Desai, A. (2005). The CENP-F-like proteins HCP-1 and HCP-2 target CLASP to kinetochores to mediate chromosome segregation. Curr Biol *15*, 771-777.

Cheeseman, I. M., Niessen, S., Anderson, S., Hyndman, F., Yates, J. R., 3rd, Oegema, K., and Desai, A. (2004). A conserved protein network controls assembly of the outer kinetochore and its ability to sustain tension. Genes Dev *18*, 2255-2268.

Chen, R. H., Shevchenko, A., Mann, M., and Murray, A. W. (1998). Spindle checkpoint protein Xmad1 recruits Xmad2 to unattached kinetochores. J Cell Biol *143*, 283-295.

Chen, R. H., Waters, J. C., Salmon, E. D., and Murray, A. W. (1996). Association of spindle assembly checkpoint component XMAD2 with unattached kinetochores. Science *274*, 242-246.

Ciferri, C., De Luca, J., Monzani, S., Ferrari, K. J., Ristic, D., Wyman, C., Stark, H., Kilmartin, J., Salmon, E. D., and Musacchio, A. (2005). Architecture of the human ndc80-hec1 complex, a critical constituent of the outer kinetochore. J Biol Chem *280*, 29088-29095.

Ciferri, C., Pasqualato, S., Screpanti, E., Varetti, G., Santaguida, S., Dos Reis, G., Maiolica, A., Polka, J., De Luca, J. G., De Wulf, P.*, et al.* (2008). Implications for kinetochore-microtubule attachment from the structure of an engineered Ndc80 complex. Cell *133*, 427-439.

Cimini, D., Moree, B., Canman, J. C., and Salmon, E. D. (2003). Merotelic kinetochore orientation occurs frequently during early mitosis in mammalian tissue cells and error correction is achieved by two different mechanisms. J Cell Sci *116*, 4213-4225.

Cleveland, D. W., Mao, Y., and Sullivan, K. F. (2003). Centromeres and kinetochores: from epigenetics to mitotic checkpoint signaling. Cell *112*, 407-421.

Cockell, M. M., Baumer, K., and Gonczy, P. (2004). lis-1 is required for dynein-dependent cell division processes in C. elegans embryos. J Cell Sci *117*, 4571-4582.

Collins, K. A., Castillo, A. R., Tatsutani, S. Y., and Biggins, S. (2005). De novo kinetochore assembly requires the centromeric histone H3 variant. Mol Biol Cell *16*, 5649-5660.

Dammermann, A., Maddox, P. S., Desai, A., and Oegema, K. (2008). SAS-4 is recruited to a dynamic structure in newly forming centrioles that is stabilized by the gamma-tubulin-mediated addition of centriolar microtubules. J Cell Biol *180*, 771-785.

De Antoni, A., Pearson, C. G., Cimini, D., Canman, J. C., Sala, V., Nezi, L., Mapelli, M., Sironi, L., Faretta, M., Salmon, E. D., and Musacchio, A. (2005). The Mad1/Mad2 complex as a template for Mad2 activation in the spindle assembly checkpoint. Curr Biol *15*, 214-225.

DeLuca, J. G., Dong, Y., Hergert, P., Strauss, J., Hickey, J. M., Salmon, E. D., and McEwen, B. F. (2005). Hec1 and nuf2 are core components of the kinetochore outer plate essential for organizing microtubule attachment sites. Mol Biol Cell *16*, 519-531.

DeLuca, J. G., Gall, W. E., Ciferri, C., Cimini, D., Musacchio, A., and Salmon, E. D. (2006). Kinetochore microtubule dynamics and attachment stability are regulated by Hec1. Cell *127*, 969-982.

Desai, A., Rybina, S., Muller-Reichert, T., Shevchenko, A., Hyman, A., and Oegema, K. (2003). KNL-1 directs assembly of the microtubule-binding interface of the kinetochore in C. elegans. Genes Dev *17*, 2421-2435.

Ditchfield, C., Johnson, V. L., Tighe, A., Ellston, R., Haworth, C., Johnson, T., Mortlock, A., Keen, N., and Taylor, S. S. (2003). Aurora B couples chromosome alignment with anaphase by targeting BubR1, Mad2, and Cenp-E to kinetochores. J Cell Biol *161*, 267-280.

Dong, Y., Vanden Beldt, K. J., Meng, X., Khodjakov, A., and McEwen, B. F. (2007). The outer plate in vertebrate kinetochores is a flexible network with multiple microtubule interactions. Nat Cell Biol *9*, 516-522.

Dujardin, D., Wacker, U. I., Moreau, A., Schroer, T. A., Rickard, J. E., and De Mey, J. R. (1998). Evidence for a role of CLIP-170 in the establishment of metaphase chromosome alignment. J Cell Biol *141*, 849-862.

Encalada, S. E., Willis, J., Lyczak, R., and Bowerman, B. (2005). A spindle checkpoint functions during mitosis in the early Caenorhabditis elegans embryo. Mol Biol Cell *16*, 1056-1070.

Essex, A., Dammermann, A., Lewellyn, L., Oegema, K., and Desai, A. (2009). Systematic analysis in Caenorhabditis elegans reveals that the spindle checkpoint is composed of two largely independent branches. Mol Biol Cell *20*, 1252-1267.

Fang, G. (2002). Checkpoint protein BubR1 acts synergistically with Mad2 to inhibit anaphase-promoting complex. Mol Biol Cell *13*, 755-766.

Fang, G., Yu, H., and Kirschner, M. W. (1998). The checkpoint protein MAD2 and the mitotic regulator CDC20 form a ternary complex with the anaphase-promoting complex to control anaphase initiation. Genes Dev *12*, 1871-1883.

Feng, J., Huang, H., and Yen, T. J. (2006). CENP-F is a novel microtubule-binding protein that is essential for kinetochore attachments and affects the duration of the mitotic checkpoint delay. Chromosoma *115*, 320-329.

Flemming, W. (1965). Historical Paper. Contributions to the Knowledge of the Cell and Its Vital Processes. J Cell Biol *25*, SUPPL:1-69.

Fraschini, R., Beretta, A., Sironi, L., Musacchio, A., Lucchini, G., and Piatti, S. (2001). Bub3 interaction with Mad2, Mad3 and Cdc20 is mediated by WD40 repeats and does not require intact kinetochores. Embo J *20*, 6648-6659.

Frokjaer-Jensen, C., Davis, M. W., Hopkins, C. E., Newman, B. J., Thummel, J. M., Olesen, S. P., Grunnet, M., and Jorgensen, E. M. (2008). Single-copy insertion of transgenes in Caenorhabditis elegans. Nat Genet *40*, 1375-1383.

Fujita, Y., Hayashi, T., Kiyomitsu, T., Toyoda, Y., Kokubu, A., Obuse, C., and Yanagida, M. (2007). Priming of centromere for CENP-A recruitment by human hMis18alpha, hMis18beta, and M18BP1. Dev Cell *12*, 17-30.

Gaitanos, T. N., Santamaria, A., Jeyaprakash, A. A., Wang, B., Conti, E., and Nigg, E. A. (2009). Stable kinetochore-microtubule interactions depend on the Ska complex and its new component Ska3/C13Orf3. Embo J *28*, 1442-1452.

Gassmann, R., Essex, A., Hu, J. S., Maddox, P. S., Motegi, F., Sugimoto, A., O'Rourke, S. M., Bowerman, B., McLeod, I., Yates, J. R., 3rd*, et al.* (2008). A new mechanism controlling kinetochore-microtubule interactions revealed by comparison of two dynein-targeting components: SPDL-1 and the Rod/Zwilch/Zw10 complex. Genes Dev *22*, 2385-2399.

Gillett, E. S., Espelin, C. W., and Sorger, P. K. (2004). Spindle checkpoint proteins and chromosome-microtubule attachment in budding yeast. J Cell Biol *164*, 535-546.

Gonczy, P., Pichler, S., Kirkham, M., and Hyman, A. A. (1999). Cytoplasmic dynein is required for distinct aspects of MTOC positioning, including centrosome separation, in the one cell stage Caenorhabditis elegans embryo. J Cell Biol *147*, 135-150.

Green, R. A., Audhya, A., Pozniakovsky, A., Dammermann, A., Pemble, H., Monen, J., Portier, N., Hyman, A., Desai, A., and Oegema, K. (2008). Expression and imaging of fluorescent proteins in the C. elegans gonad and early embryo. Methods Cell Biol *85*, 179-218.

Griffis, E. R., Stuurman, N., and Vale, R. D. (2007). Spindly, a novel protein essential for silencing the spindle assembly checkpoint, recruits dynein to the kinetochore. J Cell Biol *177*, 1005-1015.

Guimaraes, G. J., Dong, Y., McEwen, B. F., and Deluca, J. G. (2008). Kinetochore-microtubule attachment relies on the disordered N-terminal tail domain of Hec1. Curr Biol *18*, 1778-1784.

Hajeri, V. A., Stewart, A. M., Moore, L. L., and Padilla, P. A. (2008). Genetic analysis of the spindle checkpoint genes san-1, mdf-2, bub-3 and the CENP-F homologues hcp-1 and hcp-2 in Caenorhabditis elegans. Cell Div *3*, 6.

Hanisch, A., Sillje, H. H., and Nigg, E. A. (2006). Timely anaphase onset requires a novel spindle and kinetochore complex comprising Ska1 and Ska2. Embo J *25*, 5504-5515.

Hardwick, K. G., Johnston, R. C., Smith, D. L., and Murray, A. W. (2000). MAD3 encodes a novel component of the spindle checkpoint which interacts with Bub3p, Cdc20p, and Mad2p. J Cell Biol *148*, 871-882.

Hauf, S., Cole, R. W., LaTerra, S., Zimmer, C., Schnapp, G., Walter, R., Heckel, A., van Meel, J., Rieder, C. L., and Peters, J. M. (2003). The small molecule Hesperadin reveals a role for Aurora B in correcting kinetochore-microtubule attachment and in maintaining the spindle assembly checkpoint. J Cell Biol *161*, 281-294.

Hayashi, T., Fujita, Y., Iwasaki, O., Adachi, Y., Takahashi, K., and Yanagida, M. (2004). Mis16 and Mis18 are required for CENP-A loading and histone deacetylation at centromeres. Cell *118*, 715-729.

Herzog, F., Primorac, I., Dube, P., Lenart, P., Sander, B., Mechtler, K., Stark, H., and Peters, J. M. (2009). Structure of the anaphase-promoting

complex/cyclosome interacting with a mitotic checkpoint complex. Science *323*, 1477-1481.

Hirose, H., Arasaki, K., Dohmae, N., Takio, K., Hatsuzawa, K., Nagahama, M., Tani, K., Yamamoto, A., Tohyama, M., and Tagaya, M. (2004). Implication of ZW10 in membrane trafficking between the endoplasmic reticulum and Golgi. Embo J *23*, 1267-1278.

Holt, S. V., Vergnolle, M. A., Hussein, D., Wozniak, M. J., Allan, V. J., and Taylor, S. S. (2005). Silencing Cenp-F weakens centromeric cohesion, prevents chromosome alignment and activates the spindle checkpoint. J Cell Sci *118*, 4889-4900.

Howe, M., McDonald, K. L., Albertson, D. G., and Meyer, B. J. (2001). HIM-10 is required for kinetochore structure and function on Caenorhabditis elegans holocentric chromosomes. J Cell Biol *153*, 1227-1238.

Howell, B. J., Hoffman, D. B., Fang, G., Murray, A. W., and Salmon, E. D. (2000). Visualization of Mad2 dynamics at kinetochores, along spindle fibers, and at spindle poles in living cells. J Cell Biol *150*, 1233-1250.

Howell, B. J., McEwen, B. F., Canman, J. C., Hoffman, D. B., Farrar, E. M., Rieder, C. L., and Salmon, E. D. (2001). Cytoplasmic dynein/dynactin drives kinetochore protein transport to the spindle poles and has a role in mitotic spindle checkpoint inactivation. J Cell Biol *155*, 1159-1172.

Howman, E. V., Fowler, K. J., Newson, A. J., Redward, S., MacDonald, A. C., Kalitsis, P., and Choo, K. H. (2000). Early disruption of centromeric chromatin organization in centromere protein A (Cenpa) null mice. Proc Natl Acad Sci U S A *97*, 1148-1153.

Hoyt, M. A., Totis, L., and Roberts, B. T. (1991). S. cerevisiae genes required for cell cycle arrest in response to loss of microtubule function. Cell *66*, 507-517.

Hwang, L. H., Lau, L. F., Smith, D. L., Mistrot, C. A., Hardwick, K. G., Hwang, E. S., Amon, A., and Murray, A. W. (1998). Budding yeast Cdc20: a target of the spindle checkpoint. Science *279*, 1041-1044.

Johnson, V. L., Scott, M. I., Holt, S. V., Hussein, D., and Taylor, S. S. (2004). Bub1 is required for kinetochore localization of BubR1, Cenp-E, Cenp-F and Mad2, and chromosome congression. J Cell Sci *117*, 1577-1589.

Kalitsis, P., MacDonald, A. C., Newson, A. J., Hudson, D. F., and Choo, K. H. (1998). Gene structure and sequence analysis of mouse centromere proteins A and C. Genomics *47*, 108-114.

Kapoor, T. M., Mayer, T. U., Coughlin, M. L., and Mitchison, T. J. (2000). Probing spindle assembly mechanisms with monastrol, a small molecule inhibitor of the mitotic kinesin, Eg5. J Cell Biol *150*, 975-988.

Karess, R. (2005). Rod-Zw10-Zwilch: a key player in the spindle checkpoint. Trends Cell Biol *15*, 386-392.

Karess, R. E., and Glover, D. M. (1989). rough deal: a gene required for proper mitotic segregation in Drosophila. J Cell Biol *109*, 2951-2961.

Kim, S. H., Lin, D. P., Matsumoto, S., Kitazono, A., and Matsumoto, T. (1998). Fission yeast Slp1: an effector of the Mad2-dependent spindle checkpoint. Science *279*, 1045-1047.

King, E. M., Rachidi, N., Morrice, N., Hardwick, K. G., and Stark, M. J. (2007a). Ipl1p-dependent phosphorylation of Mad3p is required for the spindle checkpoint response to lack of tension at kinetochores. Genes Dev *21*, 1163-1168.

King, E. M., van der Sar, S. J., and Hardwick, K. G. (2007b). Mad3 KEN boxes mediate both Cdc20 and Mad3 turnover, and are critical for the spindle checkpoint. PLoS ONE *2*, e342.

Kitagawa, R., and Rose, A. M. (1999). Components of the spindle-assembly checkpoint are essential in Caenorhabditis elegans. Nat Cell Biol *1*, 514-521.

Kitajima, T. S., Hauf, S., Ohsugi, M., Yamamoto, T., and Watanabe, Y. (2005). Human Bub1 defines the persistent cohesion site along the mitotic chromosome by affecting Shugoshin localization. Curr Biol *15*, 353-359.

Kittler, R., Pelletier, L., Heninger, A. K., Slabicki, M., Theis, M., Miroslaw, L., Poser, I., Lawo, S., Grabner, H., Kozak, K.*, et al.* (2007). Genome-scale RNAi profiling of cell division in human tissue culture cells. Nat Cell Biol *9*, 1401-1412.

Kiyomitsu, T., Obuse, C., and Yanagida, M. (2007). Human Blinkin/AF15q14 is required for chromosome alignment and the mitotic checkpoint through direct interaction with Bub1 and BubR1. Dev Cell *13*, 663-676.

Kline-Smith, S. L., Sandall, S., and Desai, A. (2005). Kinetochore-spindle microtubule interactions during mitosis. Curr Opin Cell Biol *17*, 35-46.

Kops, G. J., Kim, Y., Weaver, B. A., Mao, Y., McLeod, I., Yates, J. R., 3rd, Tagaya, M., and Cleveland, D. W. (2005). ZW10 links mitotic checkpoint signaling to the structural kinetochore. J Cell Biol *169*, 49-60.

Kulukian, A., Han, J. S., and Cleveland, D. W. (2009). Unattached kinetochores catalyze production of an anaphase inhibitor that requires a Mad2 template to prime Cdc20 for BubR1 binding. Dev Cell *16*, 105-117.

Kurz, T., Pintard, L., Willis, J. H., Hamill, D. R., Gonczy, P., Peter, M., and Bowerman, B. (2002). Cytoskeletal regulation by the Nedd8 ubiquitin-like protein modification pathway. Science *295*, 1294-1298.

Lampson, M. A., and Kapoor, T. M. (2005). The human mitotic checkpoint protein BubR1 regulates chromosome-spindle attachments. Nat Cell Biol *7*, 93-98.

Lampson, M. A., Renduchitala, K., Khodjakov, A., and Kapoor, T. M. (2004). Correcting improper chromosome-spindle attachments during cell division. Nat Cell Biol *6*, 232-237.

Larsen, N. A., Al-Bassam, J., Wei, R. R., and Harrison, S. C. (2007). Structural analysis of Bub3 interactions in the mitotic spindle checkpoint. Proc Natl Acad Sci U S A *104*, 1201-1206.

Li, R., and Murray, A. W. (1991). Feedback control of mitosis in budding yeast. Cell *66*, 519-531.

Li, X., and Nicklas, R. B. (1995). Mitotic forces control a cell-cycle checkpoint. Nature *373*, 630-632.

Li, Y., and Benezra, R. (1996). Identification of a human mitotic checkpoint gene: hsMAD2. Science *274*, 246-248.

Li, Y., Gorbea, C., Mahaffey, D., Rechsteiner, M., and Benezra, R. (1997). MAD2 associates with the cyclosome/anaphase-promoting complex and inhibits its activity. Proc Natl Acad Sci U S A *94*, 12431-12436.

Li, Y., Yu, W., Liang, Y., and Zhu, X. (2007). Kinetochore dynein generates a poleward pulling force to facilitate congression and full chromosome alignment. Cell Res *17*, 701-712.

Luo, X., Tang, Z., Rizo, J., and Yu, H. (2002). The Mad2 spindle checkpoint protein undergoes similar major conformational changes upon binding to either Mad1 or Cdc20. Mol Cell *9*, 59-71.

Luo, X., Tang, Z., Xia, G., Wassmann, K., Matsumoto, T., Rizo, J., and Yu, H. (2004). The Mad2 spindle checkpoint protein has two distinct natively folded states. Nat Struct Mol Biol *11*, 338-345.

Maddox, P. S., Hyndman, F., Monen, J., Oegema, K., and Desai, A. (2007). Functional genomics identifies a Myb domain-containing protein family required for assembly of CENP-A chromatin. J Cell Biol *176*, 757-763.

Maddox, P. S., Oegema, K., Desai, A., and Cheeseman, I. M. (2004). "Holo"er than thou: chromosome segregation and kinetochore function in C. elegans. Chromosome Res *12*, 641-653.

Malureanu, L. A., Jeganathan, K. B., Hamada, M., Wasilewski, L., Davenport, J., and van Deursen, J. M. (2009). BubR1 N terminus acts as a soluble inhibitor of cyclin B degradation by APC/C(Cdc20) in interphase. Dev Cell *16*, 118-131.

Manning, A. L., Ganem, N. J., Bakhoum, S. F., Wagenbach, M., Wordeman, L., and Compton, D. A. (2007). The kinesin-13 proteins Kif2a, Kif2b, and

Kif2c/MCAK have distinct roles during mitosis in human cells. Mol Biol Cell *18*, 2970-2979.

Mao, Y., Desai, A., and Cleveland, D. W. (2005). Microtubule capture by CENP-E silences BubR1-dependent mitotic checkpoint signaling. J Cell Biol *170*, 873-880.

Mapelli, M., Filipp, F. V., Rancati, G., Massimiliano, L., Nezi, L., Stier, G., Hagan, R. S., Confalonieri, S., Piatti, S., Sattler, M., and Musacchio, A. (2006). Determinants of conformational dimerization of Mad2 and its inhibition by p31comet. Embo J *25*, 1273-1284.

Mapelli, M., Massimiliano, L., Santaguida, S., and Musacchio, A. (2007). The Mad2 conformational dimer: structure and implications for the spindle assembly checkpoint. Cell *131*, 730-743.

Maresca, T. J., and Salmon, E. D. (2009). Intrakinetochore stretch is associated with changes in kinetochore phosphorylation and spindle assembly checkpoint activity. J Cell Biol *184*, 373-381.

McCleland, M. L., Gardner, R. D., Kallio, M. J., Daum, J. R., Gorbsky, G. J., Burke, D. J., and Stukenberg, P. T. (2003). The highly conserved Ndc80 complex is required for kinetochore assembly, chromosome congression, and spindle checkpoint activity. Genes Dev *17*, 101-114.

McCleland, M. L., Kallio, M. J., Barrett-Wilt, G. A., Kestner, C. A., Shabanowitz, J., Hunt, D. F., Gorbsky, G. J., and Stukenberg, P. T. (2004). The vertebrate Ndc80 complex contains Spc24 and Spc25 homologs, which are required to establish and maintain kinetochore-microtubule attachment. Curr Biol *14*, 131-137.

McEwen, B. F., Chan, G. K., Zubrowski, B., Savoian, M. S., Sauer, M. T., and Yen, T. J. (2001). CENP-E is essential for reliable bioriented spindle attachment, but chromosome alignment can be achieved via redundant mechanisms in mammalian cells. Mol Biol Cell *12*, 2776-2789.

McEwen, B. F., Dong, Y., and VandenBeldt, K. J. (2007). Using electron microscopy to understand functional mechanisms of chromosome alignment on the mitotic spindle. Methods Cell Biol *79*, 259-293.

McIntosh, J. R., Grishchuk, E. L., Morphew, M. K., Efremov, A. K., Zhudenkov, K., Volkov, V. A., Cheeseman, I. M., Desai, A., Mastronarde, D. N., and Ataullakhanov, F. I. (2008). Fibrils connect microtubule tips with kinetochores: a mechanism to couple tubulin dynamics to chromosome motion. Cell *135*, 322-333.

Meluh, P. B., Yang, P., Glowczewski, L., Koshland, D., and Smith, M. M. (1998). Cse4p is a component of the core centromere of Saccharomyces cerevisiae. Cell *94*, 607-613.

Meraldi, P., Draviam, V. M., and Sorger, P. K. (2004). Timing and checkpoints in the regulation of mitotic progression. Dev Cell *7*, 45-60.

Millband, D. N., and Hardwick, K. G. (2002). Fission yeast Mad3p is required for Mad2p to inhibit the anaphase-promoting complex and localizes to kinetochores in a Bub1p-, Bub3p-, and Mph1p-dependent manner. Mol Cell Biol *22*, 2728-2742.

Miller, S. A., Johnson, M. L., and Stukenberg, P. T. (2008). Kinetochore attachments require an interaction between unstructured tails on microtubules and Ndc80(Hec1). Curr Biol *18*, 1785-1791.

Minshull, J., Sun, H., Tonks, N. K., and Murray, A. W. (1994). A MAP kinase-dependent spindle assembly checkpoint in Xenopus egg extracts. Cell *79*, 475-486.

Moore, L. L., Morrison, M., and Roth, M. B. (1999). HCP-1, a protein involved in chromosome segregation, is localized to the centromere of mitotic chromosomes in Caenorhabditis elegans. J Cell Biol *147*, 471-480.

Moore, L. L., and Roth, M. B. (2001). HCP-4, a CENP-C-like protein in Caenorhabditis elegans, is required for resolution of sister centromeres. J Cell Biol *153*, 1199-1208.

Morrow, C. J., Tighe, A., Johnson, V. L., Scott, M. I., Ditchfield, C., and Taylor, S. S. (2005). Bub1 and aurora B cooperate to maintain BubR1-mediated inhibition of APC/CCdc20. J Cell Sci *118*, 3639-3652.

Murray, A. W., and Marks, D. (2001). Can sequencing shed light on cell cycling? Nature *409*, 844-846.

Musacchio, A., and Salmon, E. D. (2007). The spindle-assembly checkpoint in space and time. Nat Rev Mol Cell Biol *8*, 379-393.

Nasmyth, K. (2005). How do so few control so many? Cell *120*, 739-746.

Nicklas, R. B. (1988). The forces that move chromosomes in mitosis. Annu Rev Biophys Biophys Chem *17*, 431-449.

Nilsson, J., Yekezare, M., Minshull, J., and Pines, J. (2008). The APC/C maintains the spindle assembly checkpoint by targeting Cdc20 for destruction. Nat Cell Biol *10*, 1411-1420.

Nystul, T. G., Goldmark, J. P., Padilla, P. A., and Roth, M. B. (2003). Suspended animation in C. elegans requires the spindle checkpoint. Science *302*, 1038-1041.

O'Connell, K. F., Caron, C., Kopish, K. R., Hurd, D. D., Kemphues, K. J., Li, Y., and White, J. G. (2001). The C. elegans zyg-1 gene encodes a regulator of centrosome duplication with distinct maternal and paternal roles in the embryo. Cell *105*, 547-558.

O'Rourke, S. M., Dorfman, M. D., Carter, J. C., and Bowerman, B. (2007). Dynein modifiers in C. elegans: light chains suppress conditional heavy chain mutants. PLoS Genet *3*, e128.

Oegema, K., Desai, A., Rybina, S., Kirkham, M., and Hyman, A. A. (2001). Functional analysis of kinetochore assembly in Caenorhabditis elegans. J Cell Biol *153*, 1209-1226.

Oegema, K., and Hyman, A. A. (2006). Cell division. WormBook, 1-40.

Palmer, D. K., O'Day, K., Trong, H. L., Charbonneau, H., and Margolis, R. L. (1991). Purification of the centromere-specific protein CENP-A and demonstration that it is a distinctive histone. Proc Natl Acad Sci U S A *88*, 3734-3738.

Pan, J., and Chen, R. H. (2004). Spindle checkpoint regulates Cdc20p stability in Saccharomyces cerevisiae. Genes Dev *18*, 1439-1451.

Peters, J. M. (2002). The anaphase-promoting complex: proteolysis in mitosis and beyond. Mol Cell *9*, 931-943.

Pimpinelli, S., and Goday, C. (1989). Unusual kinetochores and chromatin diminution in Parascaris. Trends Genet *5*, 310-315.

Pinsky, B. A., and Biggins, S. (2005). The spindle checkpoint: tension versus attachment. Trends Cell Biol *15*, 486-493.

Powers, A. F., Franck, A. D., Gestaut, D. R., Cooper, J., Gracyzk, B., Wei, R. R., Wordeman, L., Davis, T. N., and Asbury, C. L. (2009). The Ndc80 kinetochore complex forms load-bearing attachments to dynamic microtubule tips via biased diffusion. Cell *136*, 865-875.

Praitis, V., Casey, E., Collar, D., and Austin, J. (2001). Creation of low-copy integrated transgenic lines in Caenorhabditis elegans. Genetics *157*, 1217-1226.

Putkey, F. R., Cramer, T., Morphew, M. K., Silk, A. D., Johnson, R. S., McIntosh, J. R., and Cleveland, D. W. (2002). Unstable kinetochore-microtubule capture and chromosomal instability following deletion of CENP-E. Dev Cell *3*, 351-365.

Rajagopalan, H., and Lengauer, C. (2004). Aneuploidy and cancer. Nature *432*, 338-341.

Regnier, V., Vagnarelli, P., Fukagawa, T., Zerjal, T., Burns, E., Trouche, D., Earnshaw, W., and Brown, W. (2005). CENP-A is required for accurate chromosome segregation and sustained kinetochore association of BubR1. Mol Cell Biol *25*, 3967-3981.

Rieder, C. L., and Alexander, S. P. (1990). Kinetochores are transported poleward along a single astral microtubule during chromosome attachment to the spindle in newt lung cells. J Cell Biol *110*, 81-95.

Rieder, C. L., Cole, R. W., Khodjakov, A., and Sluder, G. (1995). The checkpoint delaying anaphase in response to chromosome monoorientation is mediated by an inhibitory signal produced by unattached kinetochores. J Cell Biol *130*, 941-948.

Rieder, C. L., Schultz, A., Cole, R., and Sluder, G. (1994). Anaphase onset in vertebrate somatic cells is controlled by a checkpoint that monitors sister kinetochore attachment to the spindle. J Cell Biol *127*, 1301-1310.

Rischitor, P. E., May, K. M., and Hardwick, K. G. (2007). Bub1 is a fission yeast kinetochore scaffold protein, and is sufficient to recruit other spindle checkpoint proteins to ectopic sites on chromosomes. PLoS ONE *2*, e1342.

Roberts, B. T., Farr, K. A., and Hoyt, M. A. (1994). The Saccharomyces cerevisiae checkpoint gene BUB1 encodes a novel protein kinase. Mol Cell Biol *14*, 8282-8291.

Sandall, S., Severin, F., McLeod, I. X., Yates, J. R., 3rd, Oegema, K., Hyman, A., and Desai, A. (2006). A Bir1-Sli15 complex connects centromeres to microtubules and is required to sense kinetochore tension. Cell *127*, 1179-1191.

Savoian, M. S., Goldberg, M. L., and Rieder, C. L. (2000). The rate of poleward chromosome motion is attenuated in Drosophila zw10 and rod mutants. Nat Cell Biol *2*, 948-952.

Scaerou, F., Aguilera, I., Saunders, R., Kane, N., Blottiere, L., and Karess, R. (1999). The rough deal protein is a new kinetochore component required for accurate chromosome segregation in Drosophila. J Cell Sci *112 (Pt 21)*, 3757-3768.

Scaerou, F., Starr, D. A., Piano, F., Papoulas, O., Karess, R. E., and Goldberg, M. L. (2001). The ZW10 and Rough Deal checkpoint proteins

function together in a large, evolutionarily conserved complex targeted to the kinetochore. J Cell Sci *114*, 3103-3114.

Schmidt, D. J., Rose, D. J., Saxton, W. M., and Strome, S. (2005). Functional analysis of cytoplasmic dynein heavy chain in Caenorhabditis elegans with fast-acting temperature-sensitive mutations. Mol Biol Cell *16*, 1200-1212.

Severson, A. F., Hamill, D. R., Carter, J. C., Schumacher, J., and Bowerman, B. (2000). The aurora-related kinase AIR-2 recruits ZEN-4/CeMKLP1 to the mitotic spindle at metaphase and is required for cytokinesis. Curr Biol *10*, 1162-1171.

Shah, J. V., Botvinick, E., Bonday, Z., Furnari, F., Berns, M., and Cleveland, D. W. (2004). Dynamics of centromere and kinetochore proteins; implications for checkpoint signaling and silencing. Curr Biol *14*, 942-952.

Sharp-Baker, H., and Chen, R. H. (2001). Spindle checkpoint protein Bub1 is required for kinetochore localization of Mad1, Mad2, Bub3, and CENP-E, independently of its kinase activity. J Cell Biol *153*, 1239-1250.

Shonn, M. A., Murray, A. L., and Murray, A. W. (2003). Spindle checkpoint component Mad2 contributes to biorientation of homologous chromosomes. Curr Biol *13*, 1979-1984.

Simonetta, M., Manzoni, R., Mosca, R., Mapelli, M., Massimiliano, L., Vink, M., Novak, B., Musacchio, A., and Ciliberto, A. (2009). The influence of catalysis on mad2 activation dynamics. PLoS Biol *7*, e10.

Sironi, L., Mapelli, M., Knapp, S., De Antoni, A., Jeang, K. T., and Musacchio, A. (2002). Crystal structure of the tetrameric Mad1-Mad2 core complex: implications of a 'safety belt' binding mechanism for the spindle checkpoint. Embo J *21*, 2496-2506.

Smith, D. A., Baker, B. S., and Gatti, M. (1985). Mutations in genes encoding essential mitotic functions in Drosophila melanogaster. Genetics *110*, 647-670.

Sonnichsen, B., Koski, L. B., Walsh, A., Marschall, P., Neumann, B., Brehm, M., Alleaume, A. M., Artelt, J., Bettencourt, P., Cassin, E.*, et al.* (2005). Full-

genome RNAi profiling of early embryogenesis in Caenorhabditis elegans. Nature *434*, 462-469.

Starr, D. A., Saffery, R., Li, Z., Simpson, A. E., Choo, K. H., Yen, T. J., and Goldberg, M. L. (2000). HZwint-1, a novel human kinetochore component that interacts with HZW10. J Cell Sci *113 (Pt 11)*, 1939-1950.

Starr, D. A., Williams, B. C., Hays, T. S., and Goldberg, M. L. (1998). ZW10 helps recruit dynactin and dynein to the kinetochore. J Cell Biol *142*, 763-774.

Stehman, S. A., Chen, Y., McKenney, R. J., and Vallee, R. B. (2007). NudE and NudEL are required for mitotic progression and are involved in dynein recruitment to kinetochores. J Cell Biol *178*, 583-594.

Stein, K. K., Davis, E. S., Hays, T., and Golden, A. (2007). Components of the spindle assembly checkpoint regulate the anaphase-promoting complex during meiosis in Caenorhabditis elegans. Genetics *175*, 107-123.

Sudakin, V., Chan, G. K., and Yen, T. J. (2001). Checkpoint inhibition of the APC/C in HeLa cells is mediated by a complex of BUBR1, BUB3, CDC20, and MAD2. J Cell Biol *154*, 925-936.

Sullivan, B. A., Blower, M. D., and Karpen, G. H. (2001). Determining centromere identity: cyclical stories and forking paths. Nat Rev Genet *2*, 584-596.

Sullivan, K. F., Hechenberger, M., and Masri, K. (1994). Human CENP-A contains a histone H3 related histone fold domain that is required for targeting to the centromere. J Cell Biol *127*, 581-592.

Takahashi, K., Chen, E. S., and Yanagida, M. (2000). Requirement of Mis6 centromere connector for localizing a CENP-A-like protein in fission yeast. Science *288*, 2215-2219.

Tanaka, T., Cosma, M. P., Wirth, K., and Nasmyth, K. (1999). Identification of cohesin association sites at centromeres and along chromosome arms. Cell *98*, 847-858.

Tanaka, T. U., Rachidi, N., Janke, C., Pereira, G., Galova, M., Schiebel, E., Stark, M. J., and Nasmyth, K. (2002). Evidence that the Ipl1-Sli15 (Aurora kinase-INCENP) complex promotes chromosome bi-orientation by altering kinetochore-spindle pole connections. Cell *108*, 317-329.

Tanenbaum, M. E., Galjart, N., van Vugt, M. A., and Medema, R. H. (2006). CLIP-170 facilitates the formation of kinetochore-microtubule attachments. Embo J *25*, 45-57.

Tang, Z., Bharadwaj, R., Li, B., and Yu, H. (2001). Mad2-Independent inhibition of APCCdc20 by the mitotic checkpoint protein BubR1. Dev Cell *1*, 227-237.

Tang, Z., Shu, H., Oncel, D., Chen, S., and Yu, H. (2004a). Phosphorylation of Cdc20 by Bub1 provides a catalytic mechanism for APC/C inhibition by the spindle checkpoint. Mol Cell *16*, 387-397.

Tang, Z., Sun, Y., Harley, S. E., Zou, H., and Yu, H. (2004b). Human Bub1 protects centromeric sister-chromatid cohesion through Shugoshin during mitosis. Proc Natl Acad Sci U S A *101*, 18012-18017.

Tarailo, M., Tarailo, S., and Rose, A. M. (2007). Synthetic lethal interactions identify phenotypic "interologs" of the spindle assembly checkpoint components. Genetics *177*, 2525-2530.

Taylor, S. S., Ha, E., and McKeon, F. (1998). The human homologue of Bub3 is required for kinetochore localization of Bub1 and a Mad3/Bub1-related protein kinase. J Cell Biol *142*, 1-11.

Taylor, S. S., and McKeon, F. (1997). Kinetochore localization of murine Bub1 is required for normal mitotic timing and checkpoint response to spindle damage. Cell *89*, 727-735.

Uchida, K. S., Takagaki, K., Kumada, K., Hirayama, Y., Noda, T., and Hirota, T. (2009). Kinetochore stretching inactivates the spindle assembly checkpoint. J Cell Biol *184*, 383-390.

Vanoosthuyse, V., Valsdottir, R., Javerzat, J. P., and Hardwick, K. G. (2004). Kinetochore targeting of fission yeast Mad and Bub proteins is essential for spindle checkpoint function but not for all chromosome segregation roles of Bub1p. Mol Cell Biol *24*, 9786-9801.

Vaur, S., Cubizolles, F., Plane, G., Genier, S., Rabitsch, P. K., Gregan, J., Nasmyth, K., Vanoosthuyse, V., Hardwick, K. G., and Javerzat, J. P. (2005). Control of Shugoshin function during fission-yeast meiosis. Curr Biol *15*, 2263-2270.

Vergnolle, M. A., and Taylor, S. S. (2007). Cenp-F links kinetochores to Ndel1/Nde1/Lis1/dynein microtubule motor complexes. Curr Biol *17*, 1173-1179.

Vink, M., Simonetta, M., Transidico, P., Ferrari, K., Mapelli, M., De Antoni, A., Massimiliano, L., Ciliberto, A., Faretta, M., Salmon, E. D., and Musacchio, A. (2006). In vitro FRAP identifies the minimal requirements for Mad2 kinetochore dynamics. Curr Biol *16*, 755-766.

Vorozhko, V. V., Emanuele, M. J., Kallio, M. J., Stukenberg, P. T., and Gorbsky, G. J. (2008). Multiple mechanisms of chromosome movement in vertebrate cells mediated through the Ndc80 complex and dynein/dynactin. Chromosoma *117*, 169-179.

Wan, X., O'Quinn, R. P., Pierce, H. L., Joglekar, A. P., Gall, W. E., DeLuca, J. G., Carroll, C. W., Liu, S. T., Yen, T. J., McEwen, B. F.*, et al.* (2009). Protein architecture of the human kinetochore microtubule attachment site. Cell *137*, 672-684.

Wang, X., Babu, J. R., Harden, J. M., Jablonski, S. A., Gazi, M. H., Lingle, W. L., de Groen, P. C., Yen, T. J., and van Deursen, J. M. (2001). The mitotic checkpoint protein hBUB3 and the mRNA export factor hRAE1 interact with GLE2p-binding sequence (GLEBS)-containing proteins. J Biol Chem *276*, 26559-26567.

Warren, C. D., Brady, D. M., Johnston, R. C., Hanna, J. S., Hardwick, K. G., and Spencer, F. A. (2002). Distinct chromosome segregation roles for spindle checkpoint proteins. Mol Biol Cell *13*, 3029-3041.

Watanabe, S., Yamamoto, T. G., and Kitagawa, R. (2008). Spindle assembly checkpoint gene mdf-1 regulates germ cell proliferation in response to nutrition signals in C. elegans. Embo J *27*, 1085-1096.

Wei, R. R., Al-Bassam, J., and Harrison, S. C. (2007). The Ndc80/HEC1 complex is a contact point for kinetochore-microtubule attachment. Nat Struct Mol Biol *14*, 54-59.

Wei, R. R., Sorger, P. K., and Harrison, S. C. (2005). Molecular organization of the Ndc80 complex, an essential kinetochore component. Proc Natl Acad Sci U S A *102*, 5363-5367.

Weiss, E., and Winey, M. (1996). The Saccharomyces cerevisiae spindle pole body duplication gene MPS1 is part of a mitotic checkpoint. J Cell Biol *132*, 111-123.

Welburn, J. P., Grishchuk, E. L., Backer, C. B., Wilson-Kubalek, E. M., Yates, J. R., 3rd, and Cheeseman, I. M. (2009). The human kinetochore Ska1 complex facilitates microtubule depolymerization-coupled motility. Dev Cell *16*, 374-385.

Williams, B. C., and Goldberg, M. L. (1994). Determinants of Drosophila zw10 protein localization and function. J Cell Sci *107 (Pt 4)*, 785-798.

Williams, B. C., Karr, T. L., Montgomery, J. M., and Goldberg, M. L. (1992). The Drosophila l(1)zw10 gene product, required for accurate mitotic chromosome segregation, is redistributed at anaphase onset. J Cell Biol *118*, 759-773.

Williams, B. C., Li, Z., Liu, S., Williams, E. V., Leung, G., Yen, T. J., and Goldberg, M. L. (2003). Zwilch, a new component of the ZW10/ROD complex required for kinetochore functions. Mol Biol Cell *14*, 1379-1391.

Wilson-Kubalek, E. M., Cheeseman, I. M., Yoshioka, C., Desai, A., and Milligan, R. A. (2008). Orientation and structure of the Ndc80 complex on the microtubule lattice. J Cell Biol *182*, 1055-1061.

Wojcik, E., Basto, R., Serr, M., Scaerou, F., Karess, R., and Hays, T. (2001). Kinetochore dynein: its dynamics and role in the transport of the Rough deal checkpoint protein. Nat Cell Biol *3*, 1001-1007.

Xia, G., Luo, X., Habu, T., Rizo, J., Matsumoto, T., and Yu, H. (2004). Conformation-specific binding of p31(comet) antagonizes the function of Mad2 in the spindle checkpoint. Embo J *23*, 3133-3143.

Yang, M., Li, B., Liu, C. J., Tomchick, D. R., Machius, M., Rizo, J., Yu, H., and Luo, X. (2008). Insights into mad2 regulation in the spindle checkpoint revealed by the crystal structure of the symmetric mad2 dimer. PLoS Biol *6*, e50.

Yang, Z., Tulu, U. S., Wadsworth, P., and Rieder, C. L. (2007). Kinetochore dynein is required for chromosome motion and congression independent of the spindle checkpoint. Curr Biol *17*, 973-980.

Yu, H. (2002). Regulation of APC-Cdc20 by the spindle checkpoint. Curr Opin Cell Biol *14*, 706-714.

Yu, H. (2007). Cdc20: a WD40 activator for a cell cycle degradation machine. Mol Cell *27*, 3-16.